MULTILEAD ECG DATA ANALYSIS USING SVD AND HIGHER-ORDER SVD

A

Thesis submitted

for the award of the degree of

DOCTOR OF PHILOSOPHY

By

Sibasankar Padhy

DEPARTMENT OF ELECTRONICS AND ELECTRICAL ENGINEERING

INDIAN INSTITUTE OF TECHNOLOGY GUWAHATI

GUWAHATI - 781 039, ASSAM, INDIA

MARCH 2017

Certificate

This is to certify that the thesis entitled "**Multilead ECG Data Analysis using SVD and Higher-order SVD**", submitted by **Sibasankar Padhy** (11610236), a research scholar in the *Department of Electronics and Electrical Engineering, Indian Institute of Technology Guwahati*, for the award of the degree of **Doctor of Philosophy**, is a record of an original research work carried out by him under my supervision and guidance. The thesis has fulfilled all requirements as per the regulations of the Institute and in our opinion has reached the standard needed for submission. The results embodied in this thesis have not been submitted to any other University or Institute for the award of any degree or diploma.

Dr. S. Dandapat
Professor

Dated:
Place: IIT Guwahati

Department of Electronics and Electrical Engineering
Indian Institute of Technology Guwahati
Guwahati - 781 039, India.

To my Parents

Mr. Laxmi Narayan Padhy & **Mrs. Jhunurani Padhy**

for their blessings, support and encouragement

and

To my wife

Anjali

for her love and support

and

To my brother

Bhabani

for his encouragement

and

To **The Almighty**

for his blessings.

Acknowledgments

What a journey this has been! I would not have made it here without the help, guidance, and support of many people. To all of them, I extend my most sincere and heartfelt thanks.

To Prof. Samarendra Dandapat, my PhD supervisor. I am profoundly grateful for his constant support, his patient guidance, and his brilliant ideas. Working with him has been a great opportunity to grow scientifically and personally, and it has also been a lot of thanks to his cheerful disposition. Looking back at the last five years, I can say I've been very fortunate to have him as my supervisor.

To my doctoral committee members, Prof. H. B. Nemade, Prof. S. R. M. Prasanna and Prof. R. Sinha for their support, encouragement and suggestions rendered during my research work. They have always provided me with detailed feedback on my work and have offered me sound advice on multiple occasions. Their contagious energy and enthusiasm for research have been great help along the way.

To the Head-of-the-Department (HOD), Prof. C. Mahanta and ex-HOD, Prof. R. Bhattacharjee, for permitting me to carryout this research work in the Department of Electronics and Electrical Engineering, IIT Guwahati.

To the faculty members of the department who helped me directly or indirectly during my research work. The kind support and valuable suggestions from them helped me a lot to improve myself academically and personally.

To all my dear colleagues of EMST laboratory, Dept. of EEE, IIT Guwahati. In particular, I want to thank Dr. Syed, Deepak K. T., Ramesh K., Anurag, Jiss, Nagaraj, Biswajit, Banriskhem Khonglah, Dr. Swati Banerjee, Bhanu Priya, Tilendra and Rohan for being the most fun labmates to share the final sprint with. My sincere gratitude to all the research scholars of EMST and Signal Informatics laboratory who work with me, and it is a great research support and help. I would like to express my sincere gratitude to Dr. L. N. Sharma and Mr. Sanjib Das, Senior Technical Officers, for their enormous help whenever required. Also, I would like to thank seniors Dr. Debadatta Pati, Dr. Gayadhar Pradhan, Dr. S.R. Nirmala, Dr. Govind D., Dr. Sumitra Shukla, Dr. Haris B. C., Dr. Sunil Y. and Malaya Kumar Nath for their help and valuable suggestions.

To my friends inside and outside the university – thanks for putting up with me and my thesis! Having your support along the way has made it so much easier. Time has passed quickly. It's difficult to recall and acknowledge each and every one. If unknowingly, I have missed you, kindly understand.

Last but not the least, I am grateful to my parents who in spite of their own difficulties, have stood

as a constant source of inspiration in every stage and shown moral support to carry out this research work successfully. My greatest debt of gratitude is owed to my parents. I am also thankful to my younger brother, Bhabani Sankar, for his constant encouragement. Finally, it is the love, affection, moral support and sacrifice of my wife “Anjali", which has made this research a success. I sincerely acknowledge the help and support provided by her, and I am extremely grateful. This dissertation is dedicated to my parents, my wife, my brother and to The Almighty.

Sibasankar Padhy

Abstract

Simultaneous recording of the electrocardiogram (ECG) from different body locations provides the spatial perception of cardiac events. Cardiologists use multilead ECG (MECG) comprising of the standard 12-leads to diagnose the cardiac diseases. This standard MECG system helps study the spatio-temporal orientation of heart's electrical vector. This data has three types of correlations: intra-beat, inter-beat and inter-lead. These correlations need to be exploited for different MECG applications. Several methods have been proposed for this purpose, either in time-domain or in transform-domain, where only one type of correlation out of the three has been exploited. Recent works attempted on exploitation of only spatial (inter-lead) correlation of MECG data in transform-domain using principal component analysis. However, joint analysis of multiple beats and multiple ECG leads that provides both spatial and temporal distribution of cardiac phenomena can be used to exploit combination of two or all types of correlations.

The objective of this thesis is to propose MECG data processing techniques for various ECG applications in transform-domain. Singular value decomposition (SVD) and higher-order SVD (HOSVD) are used for the transformation. In addition, multiscale decomposition and multiscale analysis-by-synthesis (MAS) have been added to handle the diagnostic features effectively. More specifically, the present thesis covers three separate but interconnected problems:

First problem deals with exploitation of both intra-beat and inter-lead correlations present in the MECG data using multiscale SVD. The work employs multiscale decomposition (MSD) on MECG data. It is found that wavelet coefficients of all leads at each scale are correlated. A new thresholding technique is proposed to select the singular values depending on *variation* of the diagnostic importance of the wavelet subbands. In addition, time and computational complexities are compared with existing techniques to validate fast processing nature of the proposed method.

Second problem deals with a novel third-order tensor representation of MECG data, followed by correlation exploitation and feature extraction for MI classification. MSD and HOSVD are employed to decompose the tensor data in wavelet domain. Different mode features from the reduced MECG tensor are extracted for detection and localization of MI. Support vector machine is used as the classifying technique. In addition, accuracy of the proposed method is evaluated without over-fitting training and testing datasets. The proposed method outperforms the existing algorithms in terms of dimensionality reduction and classification performance.

Third, a study on TWA analysis, a cardiac risk stratifier, is carried out to investigate the progression of acute MI in different leads over period of time. For this purpose, a new method for detection of TWA

is proposed, and TWA amplitude is estimated using a standard technique. The only-T-wave morphology is extracted using multiscale analysis-by-synthesis (MAS) technique. The HOSVD is applied on the subband reconstructed T-wave tensor to determine a tensor, containing alternans information that helps detect presence of TWA. Proposed algorithm is tested with publicly available TWA/CinC challenge database, containing synthetic and real datasets. Results suggest that MAS with HOSVD on tensors are more effective in detecting TWA. After validating TWA detection, study is further conducted with twenty datasets of six patients suffering from different types of MI. This study reveals that subjects with anterior or lateral MI have more sustained TWA, whereas subjects with infarction in inferior or septal wall show non-sustained TWA.

Keywords: *Multilead electrocardiogram, singular value decomposition (SVD), higher-order SVD, myocardial infarction, tensor decomposition, t-wave alternans, support vector machine, multiscale analysis-by-synthesis*.

Contents

List of Figures

List of Tables

List of Acronyms

ALMI	Antero-Lateral Myocardial Infarction
AMI	Anterior Myocardial Infarction
ASMI	Antero-Septal Myocardial Infarction
AWGN	Additive White Gaussian Noise
CANDECOMP	Canonical Decomposition
CCU	Central Control Unit
CR	Compression Ratio
CS	Compressive Sensing
DCT	Discrete Cosine Transform
DFT	Discrete Fourier Transform
DLT	Discrete Legendre Transform
DWT	Discrete Wavelet Transform
dB	Decibel
ECG	Electrocardiogram
ECE	Energy Contribution Efficiency
EMG	Electromyogram
FFT	Fast Fourier Transform
HC	Healthy Control
HOSVD	Higher-Order Singular Value Decomposition
ICA	Independent Component Analysis
IDWT	Inverse Discrete Wavelet Transform transform
ILMI	Infero-Lateral Myocardial Infarction
IMI	Inferior Myocardial Infarction
IPLMI	Infero-Postero-Lateral Myocardial Infarction
KLT	KarhunentLove Transform
LMI	Lateral Myocardial Infarction

LTMIL	Latent Topic Multiple Instance Learning
MAS	Multiscale Analysis-by-Synthesis
MBP	Mean Beat Period
MECG	Multichannel Electrocardiogram
MHOSVD	Multiscale Higher-Order Singular Value Decomposition
MI	Myocardial Infarction
MMAM	Modified Moving Average Method
MOS	Mean Opinion Score
MRA	Multiresolution Analysis
MRED	Multiscale Relative Energy Density
MRFEC	Multiscale Root Fractional Energy Contribution
MSA	Multiscale Analysis
MSD	Multiscale Decomposition
MSPCA	Multiscale Principal Component Analysis
MSV	Mode-n Singular Values
MSVD	Multiscale Singular Value Decomposition
mita	MIT-BIH Arrhythmia
mitsva	MIT-BIH Supraventricular Arrhythmia
MMECE	Multiscale Multivariate Energy Contribution Efficiency
NMWE	Normalized Multiscale Wavelet Energy
PAM	Pulse Amplitude Modulation
PCA	Principal Component Analysis
PNN	Probabilistic Neural Network
PRD	Percentage Root Mean Square Difference
QMF	Quadrature Mirror Filter
QLV	Quad Level Vector
RBFN	Radial Basis Function
SCD	Sudden Cardiac Death
SM	Spectral Method
SPIHT	Set Partition in Hierarchical Trees
SVD	Singular Value Decomposition
SVM	Support Vector Machines

SNR	Signal-to-Noise Ratio
TMFD	Template Matched-Filter Detector
TWA	T-wave Alternans
TWAR	TWA ratio
WBSN	Wireless Body Sensor Network
WDD	Weighted Diagnostic Distortion
WEDD	Wavelet Energy based Diagnostic Distortion Measure
WHO	World Health Organization
WP	Wavelet Packet
WT	Wavelet Transform

1

Introduction

Contents

This thesis work is based on analysis of multilead electrocardiogram (MECG) data processing in transform-domain. The electrocardiogram (ECG) reflects cardiac symptoms of a patient and is used extensively to identify cardiac problems in these patients. It records the electrical activity of the heart over a period of time, but it gives only one look at a time and misses vital information from other parts of the heart. Analysis of spatio-temporal dynamics during different cardiac ailments faces difficulties to obtain detailed information of the heart using a single lead ECG. Hence, in clinical practice, the standard 12 leads, which give minute inspection of the heart, are used [2]. For example, myocardial infarction (MI) is a cardiac ailment which is caused due to the blockage of blood flow, or consequently, poor oxygen amount to the muscular wall of heart. The precise measurement of combined 12-lead ECG signals helps indicate exactly where the infarct is located [3].

For proper diagnosis, patients are monitored for several hours, and data is recorded with high sampling frequencies. This generates a huge amount of data. In real-time scenario, it becomes difficult to process the high-volume data and makes hard to extract features from this. The long-term recording makes the MECG data temporally (intra-beat and inter-beat) and spatially (inter-lead) correlated. These need to be exploited for various purposes like dimensionality reduction, feature extraction, classification, cardiac risk identification, etc. Different transform-domain-based methods have received a great deal of attention over the past years because of their high decorrelation property. In these methods, mostly single type of correlation has been exploited. Simple and efficient algorithms that can exploit two or more types of correlations simultaneously can be employed to meet various purposes. Also, during data processing, it is highly essential to preserve the significant diagnostic parameters of the ECG signal.

The work presented in this thesis is broadly divided into three major contributions. First, the MECG data is decomposed using multiscale singular value decomposition (MSVD). The SVD exploits both intra-beat and inter-lead correlations present in wavelet transformed MECG data. Second, the MECG data is represented as a third-order tensor structure that helps exploit inter-beat correlation including the above two. This is accomplished by applying HOSVD on the wavelet transformed MECG tensor. Further, features are extracted (from the reduced MECG tensor) for detection and localization of MI. Third, a study on T-wave alternans (TWA), a cardiac risk stratifier, analysis is carried out to investigate the progression of acute MI in different leads over a period of time. Prior to this, TWA analysis is validated with semi-synthetic and real ECG signals.

The rest of this chapter is prepared as follows. The first two sections (Section 1.1 and 1.2) give a brief idea to ECG with different morphological features and MECG system, especially 12-lead ECG.

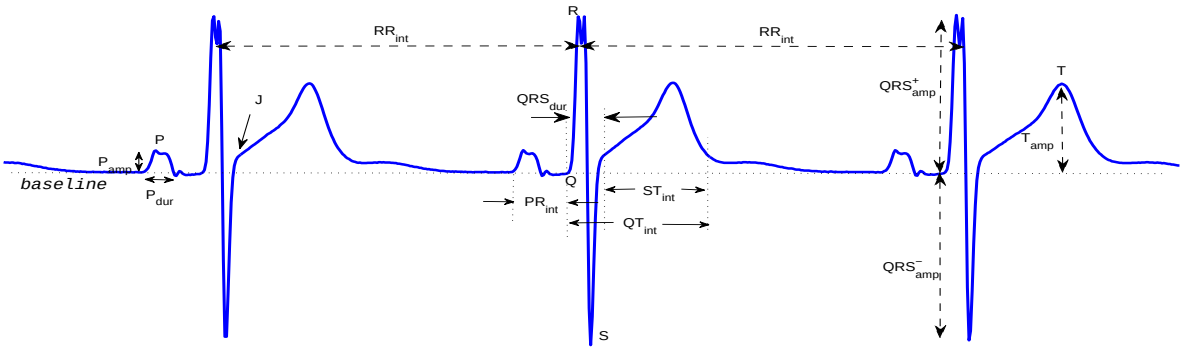

Figure 1.1: Amplitude and duration of some ECG diagnostic features

Section 1.3 presents different ECG applications in this field. In Section 1.4, different ECG/MECG correlation exploitations methods, starting from the early time-domain-based methods to recent hybrid transformation techniques, with regard to dimension reduction are discussed. Section 1.5 presents a literature survey on feature extraction techniques for MI classification. Literatures on TWA analysis are discussed in Section 1.6. Scope of the work is presented in Section 1.7. Finally, the organization of the thesis is presented in Section 1.8.

1.1 ECG and its Morphological Features

As this thesis deals with MECG data processing, it is necessary to discuss a brief review on ECG and its significant morphologic features. Our heart is a rhythmically beating muscle (myocardium) that pumps oxygen and nutrient rich blood throughout the body. An electrical current wave passes through the entire heart, which initiates myocardial contraction. The electrical current spreads over the heart muscle in a coordinated pattern. This results in a measurable change in potential difference on the body surface of the subject. The resultant amplified signal is known as the ECG [2, 4].

The ECG signal consists a number of heartbeats that comprises of different morphological features or characteristic waves: P-wave, QRS-complex, ST-segment and T-wave. Figure 1.1 shows a heartbeat segment of ECG with amplitude and duration label of PQRST complex parameters. The significance of these features are briefly presented here as:

- **P-wave:** It represents depolarization of the atria, which starts when an electrical impulse initiated at sinoatrial node. It constitutes composite electrical activation of left and right atria. Its duration is normally less than 80 ms and shape is typically upright in most leads except for aVR.

- **QRS-complex:** It represents rapid depolarization of right and left ventricles. The ventricles have a larger muscle mass compared to the atria, which results the QRS-complex visible as a sharp

and tall wave. Its duration normally ranges between 80 to 100 ms.

- **ST-segment:** It represents the period from the end of systole to the beginning of repolarization of the ventricles. Its duration is usually about 100 to 120 ms. It may be termed as a non-event as it appears as a flat line between the QRS complex and the T wave. However, myocardail infarction or ischemia could cause the ST-segment to be depressed or elevated. Hence, during the diagnosis of cardiac problems, the amplitude in deviation and shape of the ST-segment play an important role.

- **T-wave:** The T wave represents the repolarization of the ventricles. Its normal duration is approximately 160 ms and is generally upright in all leads except aVR and V1. Inverted T-waves can be a sign of myocardial ischemia and peaked T-waves can be a sign of hyperkalemia or very early myocardial infarction.

Besides these, there are other morphological features like PR-interval, QT-interval, RR-interval etc. of an ECG signal, which are studied during the diagnosis of a cardiac ailment.

1.2 Multilead Electrocardiogram

The electrical activity of the heart is recorded on the body surface by attaching a set of electrodes to the skin. In an ECG recording system, a lead is referred to the difference in the voltage between a pair of electrodes. The ECG is typically recorded with a multiple lead configuration which includes unipolar or bipolar leads, or both. A unipolar lead reflects the voltage variation of a single electrode, whereas a bipolar lead reflects the voltage difference between two electrodes. Each lead views the heart from a different angle. This helps the clinician determine pathologies through spatial correlation of events on specific leads [2].

A variety of lead configurations are used in clinical practice, from a simple single lead to 2- or 3-lead, or standard 12-lead system. The choice of a particular lead system is guided by the type of clinical information desired and by various clinical issues and practical considerations. The two lead systems that receive the most attention are the standard 12-lead ECG and the orthogonal lead system. Our whole work is based on analysis of the 12-lead ECG system.

12-lead ECG

The heart is a three-dimensional structure. Its electrical currents spread out in all directions across the body. The most widely used standard 12-lead ECG system comprises of three limb leads (I, II and

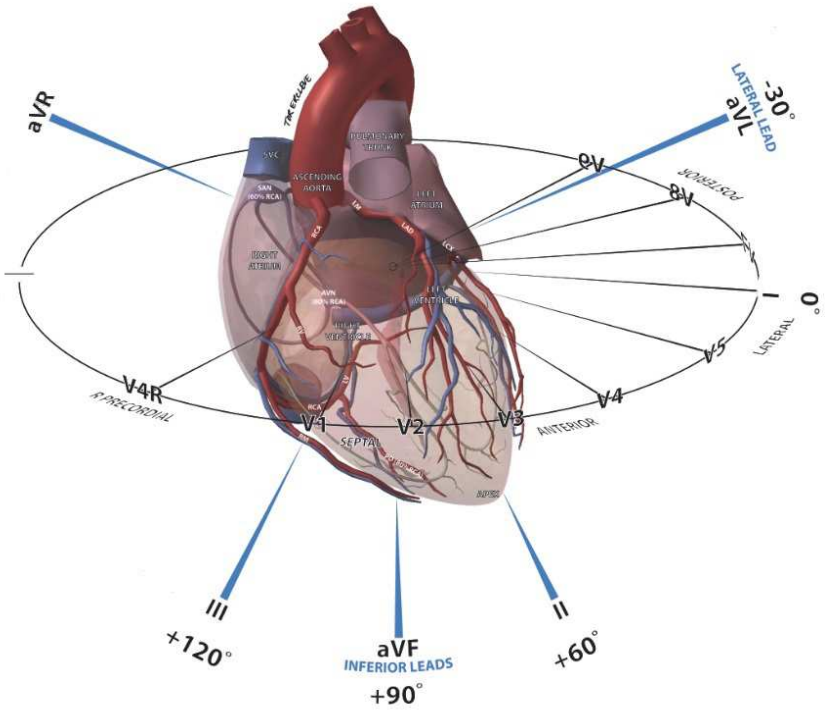

Figure 1.2: Spatial relationships of the six limb leads, which record electrical voltages transmitted onto the frontal and horizontal plane of the body [1].

III), three augmented leads (aVR, aVL and aVF), and six precordial leads (V1, V2, $\cdots$, V6) [2, 4].

The electrical voltages transmitted onto the frontal and horizontal plane of the body are recorded by the six limb leads and six precordial leads, respectively. Figure 1.2 shows the spatial view of different leads along frontal and horizontal planes. Together, these 12 leads provide a three-dimensional picture of atrial and ventricular depolarization and repolarization.

The importance of multiple leads can be illustrated in the diagnosis of a cardiac disease, say, myocardial infarction (MI). An MI typically affects one localized portion of either anterior or inferior or lateral portion of the ventricle. The changes in ECG produced due to anterior MI are usually seen in the chest leads (V1-V4). The changes seen with an inferior MI usually appear only in leads such as II, III, and aVF. Similarly, changes due to lateral MI appear only in leads such as I, aVL, V5, and V6.

1.3 ECG/MECG Data Processing

Cardiologists get information about heart by observing morphological features from the time-domain ECG signal and can state the pathological condition of a cardiac patient. It is cumbersome for a cardiologist to observe the large amount of MECG data. Manual identification of any change occurring in the 12-leads and diagnosis from huge dataset is difficult, time consuming and may sometimes result in incorrect diagnosis. This hurdle can be overcome by processing the ECG/MECG data automatically

using computer-aided systems. In the broad sense, ECG/MECG processing refers to the study of ECG signals and the ensuing processing methods. Some of the main applications of ECG/MECG processing can be categorized as follows:

Noise elimination: One of the applications in almost every research on ECG signal is to get noise free ECG with distinct morphological features. During recording, ECG is contaminated with different types of noise due to power-line interference, muscle contraction, and motion artifacts, etc [5–9]. Challenges are there to remove these noise components without affecting the diagnostic features of ECG signals.

Data dimension reduction: The ECG/MECG data recorded for longer duration produces a large amount of redundant data. Dimensionality reduction refers to the process of reducing data dimension by removing the redundant information present in the original data [10]. The goal of the dimensionality reduction for physiological signals like ECG is not only to achieve higher compression ratio (CR) but also to preserve the diagnostic information in the signal. Another challenge in today's computationally-intensive applications is fast processing with less computations.

Feature extraction and classification: Feature extraction refers to the task of extracting informative, relevant and non-redundant features from ECG signals which can facilitate in attaining good classification performance. Feature extraction is related to dimensionality reduction. A reduced feature set is expected to perform faster. Main challenges are to extract discriminant features from the ECG signals in the presence of noise.

In the classification task, two or more classes are discriminated from each other by creating a boundary between them. ECG classification is an important task in diagnosing cardiac patients by classifying normal and abnormal classes. In this thesis, MI classification has been considered. Detection of MI is a binary-class problem whereas localization of MI is a multi-class case. Generally, the classification problem is followed after extraction of features. Challenges are expressed in terms of accuracy of the classifier.

Signal separation: ECG signal separation is an another problem where the signal of interest is separated from a composite signal. One of the common problems in this case is separation of fetal ECG from maternal ECG [11]. If ECG sensors are placed on the mother's abdomen, it is possible to record multiple differential signals between each pair of electrodes. Also, the amplitude of the fetal

ECG is so small that it makes difficult to distinguish or analyze this signal. Sometimes it happens that diagnostic features of fetal ECG overlaps with that of maternal ECG because of their overlapping frequency ranges. The spectrum of maternal ECG may be up to 100 Hz, while the abdominal fetal ECG frequencies are beyond 100 Hz. The frequency band of the QRS-complex overlaps largely between the maternal and fetal ECGs [12].

Cardiac risk identification: Cardiac risk identification refers to the task for a machine to state the risk level of a cardiac patient from the measured indices, which include T-wave alternans (TWA), QT-interval, ST-segment elevation, etc. In this thesis, TWA indices are considered. The challenge is there in findings the clinical significance of TWA.

■

A general block diagram for ECG/MECG data processing is shown in Figure 1.3. Preprocessing stage includes different tasks like beat detection, amplitude and period normalization, artifact and noise removal, etc. Now-a-days, beat detection has become a part of preprocessing stage in most of the ECG applications. This is accomplished by following the Pan-Tompkin's algorithm [13] or wavelet-based ECG delineator [14]. The common types of noise that affect the ECG signal are baseline-wander, electrode motion artifact, muscle artifact, and power-line interference. Different filtering techniques are used to get rid of these effects. Baseline wander is a low-frequency artifact whose spectral content is below 0.5 Hz [15]. Different methods such as high-pass filtering [16], empirical mode decomposition [17], have been proposed to suppress the baseline. Powerline interference [5] is caused due to te improper grounding of ECG equipment and interference from nearby equipment. These interferences can be removed by linear and nonlinear filtering. A widely accepted wavelet-based signal denoising using wavelet shrinkage and soft thresholding is presented by Donoho [7]. Thakor and Zhu [6] applied various adaptive filtering techniques to remove the baseline-wander, power-line interference and noises due to muscles and motion. Apart from these, amplitude normalization is another preprocessing task that is being performed prior to further processing [18].

In data arrangement stage, single lead or MECG data is processed accordingly to get maximum correlation. In [19–22], the single lead ECG is arranged as 2-D matrix after peak detection and period normalization, which generally helps exploit inter-beat correlation. A complex lead piling process is followed with an assumption to exploit inter-beat and inter-lead correlations in case of MECG data [22]. In a recent method [16], MECG data is processed directly, which makes use of inter-lead correlation.

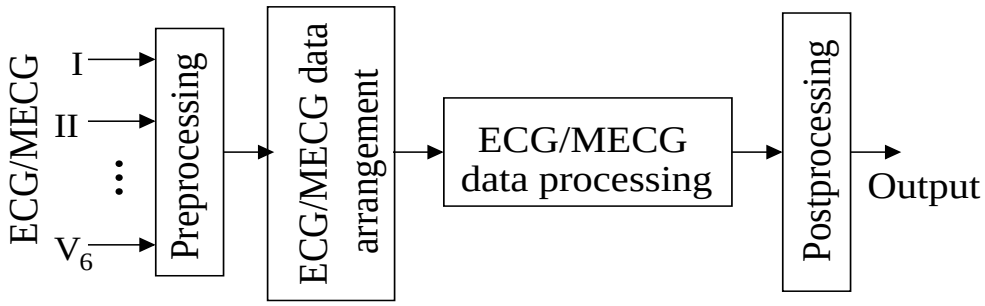

Figure 1.3: A general block diagram for MECG data processing

In data processing stage, ECG signal is processed for various purposes stated earlier in this chapter either in time-domain or in some other transform-domain. In the next three sections, we discuss about different ECG applications in time-domain and transform-domain. During postprocessing, the transformed coefficients are used either for signal reconstruction or for feature extraction or for other purposes.

1.4 Correlations Exploitation for Dimensionality Reduction

In literature, many ECG/MECG correlation exploiting methods have been reported since the late 1960s mainly for data dimensionality reduction. As discussed earlier, the MECG data has three types of correlations, viz. *intra*- and *inter-beat*, and *inter-lead* correlations. These correlations are exploited to reduce the data dimension for noise reduction or data compression purposes. A survey on main techniques for exploiting different types of correlations which are intended for data compression in most of the articles is presented in this section. These can be classified as time-domain- and transform-domain-based methods, depending on the domain in which these techniques are applied.

1.4.1 Time-domain-based methods

Time-domain-based ECG/MECG data processing methods find information present in ECG signal(s) directly from actual signal samples or morphological features. The very early time-domain-based ECG compression algorithms are amplitude zone time epoch coding (AZTEC) [23, 24], Fan/SAPA (scan-along polygonal approximation), turning point (TP) [25], coordinate reduction time encoding system (CORTES) [26].

The AZTEC algorithm, developed in late 1960's for preprocessing real-time ECG's for rhythm analysis, was used as a data reduction scheme by the same authors [24]. Even though it achieved a sample reduction ratio (SRR) up to 5:1, the reconstructed signal, P- and T-waves in particular, suffer from high distortions (percentage root mean square difference (PRD) = 28%) which makes it unacceptable to

the cardiologists. Mueller developed the TP algorithm for the purpose of reducing sampling frequency. Limitations with this method are fixed and poor SRR (2:1) and distortions in the reconstructed signal. In early 1980's, Abenstein and Tompkins proposed the CORTES scheme by combining the advantages of both AZTEC and TP techniques. Among these three, CORTES scheme was found to perform better in terms of PRD (7%) while keeping same SRR as that of AZTEC algorithm. To improve distortions in the reconstructed signal of AZTEC algorithm, Ishijima et al. [27] proposed the SAPA algorithm, where the signal is represented by consecutive straight lines. A modified AZTEC algorithm was proposed in [28] to improve reconstructed signal fidelity. Further, the improved AZTEC proposed by Kumar et al. [29] incorporated two steps to the previously reported adaptive AZTEC algorithm. This method achieved a CR up to 9.91 with PRD ranges from 4.5 to 7.9%.

It is assumed till 1990's that time-domain-based methods perform better compared to the transformation methods in regard particularly to processing speed or data reduction ratio [10]. However, these methods do not treat diagnostic features of the ECG signal well, and hence, the reconstructed signal fidelity is not acceptable to the cardiologists. Also these methods do not make use of different correlations of ECG signal(s). Hence, transform-domain-based methods have attracted the attention of the researchers.

1.4.2 Transform-domain-based methods

In signal processing applications, the reason behind the transformation of the signal from one domain to other is due to the difficulty in extraction of desired information from the original signal. It helps represent the original signal in a few number of transformed coefficients by retaining the signal energy in them. Typically, adjacent samples of an ECG signal are highly-correlated, and the transformation tries to decorrelate the signal samples. Various methods have been proposed to make good use of different types of correlations of ECG/MECG data. Transform-domain-based methods can be categorized as *data independent* or *data dependent* techniques based on the basis functions chosen. The works presented in this thesis are based on the combination of both data dependent and data independent transforms.

1.4.2.1 Data independent transforms

Data independent transforms, as the name suggests, are those transforms which do not depend on the data to generate the basis functions or transform vectors. Set of basis functions are generated based on a predefined function. Different data independent techniques that include the Fourier transform (FT) [30], the Walsh transform [31, 32], the discrete cosine transform (DCT) [15, 33–35], the wavelet

transform (WT) were proposed for different ECG applications. Among these, WT has been used widely because of its both time-frequency localization properties, high energy compaction capability and easy implementation [36–38]. The wavelet-based methods outperform the traditional time-domain and frequency-domain methods.

Wavelet-based techniques

There are numerous articles on wavelet-based analysis those treat ECG signals for different applications. The advantage with WT is that, many coefficients in the wavelet domain are so small, which can be set to zero without losing any significant information [39]. Many 1-D and 2-D wavelet-based dimensionality reduction methods were reported. The 1-D methods are widely attempted because of their simple structure and include the following stages: preprocessing, wavelet decomposition, and quantization and encoding of wavelet coefficients.

Ramakrishnan and Saha [40] proposed a wavelet-based linear prediction for ECG coding. The DWT is applied on period and amplitude normalized (PAN) beats. The selected wavelet coefficients are linearly predicted and the prediction error sequence is transmitted. This method achieved an average compression ratio (CR) of 18:1 (approx) with the average PRD value of 11:1% (approx). This technique exploited both *intra-* and *inter-beat* correlations by reducing PAN wavelet coefficients. Ahmeda and Abo-zahhad proposed a hybrid technique based on the combination of WT and linear prediction [41]. It achieved an average CR of 20:1 with PRD less than 4%. However, computational efficiency of this method has been degraded because of different stages such as beat detection, period and amplitude normalization, and interpolation filter, included in this method. Furthermore, improper designing of interpolation filter arises the aliasing effect. Alesanco et al. [42] proposed another ECG compression method for telemonitoring applications. It has different intermediate stages including preprocessing (baseline removal, beat delineation), template matching, WT, coefficient thresholding, adaptive pulse code modulation and Huffman coding. The compression performance depends on the accurate segmentation of the beats of real time ECG signals. Another limitation in this method is its complexity due to a number of steps involved. To reduce the complexity of these methods, later, low complex wavelet-based thresholding methods were proposed. These methods utilize preprocessing, WT, thresholding and quantization of the wavelet coefficients, etc. Rajoub [18] proposed a wavelet-based ECG data compression technique. After applying DWT, wavelet coefficients were thresholded based on energy packing efficiency and encoded by coding significance map and significant coefficients. This method achieved a CR value of 22.19:1 with a low PRD value of 1.06%. To enhance the reconstruction quality, both the thresholding and the entropy coding schemes were carried out in [43],

utilizing the PRD as the target to terminate compression. However, PRD cannot not be considered as a good measure of quality of compressed signals, and a low PRD value does not always guarantee the clinical acceptance. To improve the reconstruction performance, Blanco-Velasco et al. [44] presented a thresholding-based method for ECG compression using wavelet packet (WP). The 4th level WP decomposition using the biorthogonal wavelet filter as mother wavelet was applied to the ECG signal. By using WP, the signal energy is suitably packed in fewer wavelet coefficients. This method achieved CR around 10:1 with PRD value under 3%. Tai et al. [45] proposed a 2-D wavelet-based ECG data compression method. It employed modified set partitioning in hierarchical trees (SPIHT) algorithm. An ECG signal was cut and aligned to form a 2-D data matrix, and then 2-D WT and the modified SPIHT were applied. The modified SPIHT algorithm used the redundancy present among medium- and high-frequency subbands of the wavelet coefficients. This approach exploits *intra-beat* and *inter-beat* correlations that helped achieve CR of 10:1 and 20:1 with the corresponding PRD values of 1.57 and 3.81%, respectively.

The 2-D ECG compression methods performs better than the 1-D methods in terms of CR, but at the cost of computational time and space complexity. This is due to additional steps needed during the preprocessing. These methods are suitable for off-line processing of long duration ECG signals. Earlier discussed 1-D methods are able to exploit only one type of correlation, especially, *intra-beat* correlation, whereas the 2-D methods are able to exploit both *intra-* and *inter-beat* correlations, but with increased number of computations.

1.4.2.2 Data dependent transforms

In contrast to the data independent transformation techniques, here the basis sets, which are generally orthonormal, are obtained from the data using an orthogonal transformation. These transforms generate their transform vectors (basis sets) based on either a priori knowledge of the data or by analysis of the data. Different data dependent transformation techniques, Karhunen-Loève transform (KLT) or principal component analysis (PCA), singular value decomposition (SVD), etc. are applied on ECG/MECG data for various purposes. PCA decomposes the covariant structure of the dependent variables into orthogonal components by calculating the eigenvalues and eigenvectors of the data covariance matrix. SVD decomposes directly the data dependent variables into orthogonal components by calculating the singular values and singular vectors of the data matrix. The main objective of these methods is to decorrelate the original signal and repack the signal energy with fewer coefficients. The advantage of such techniques is that they can adjust themselves to the characteristics of the data, while the main disadvantage is that they tend to be more computationally intensive. There is also the

problem of storage of the transform vectors as these are unique for the data set under analysis. This overhead can become relatively large if the number of signals in the set is small, or if the length of each signal is large.

For ECG/MECG dimensionality reduction, KLT-based methods have been proposed [8, 46–49]. Young and Huggins [46] studied the temporal characteristics of the ECG signal and named the theory as *intrinsic component theory*, which is also known as the eigenvalue problem . Later, Ahmed et al. [47] proposed KLT-based ECG compression. It is shown that almost all of the 128 ECG samples energy is packed into nearly 45 KLT components. In 1998, Blanchett et al. [49] proposed a KLT-based quality controlled single-lead ECG compression. In order to reduce the computation of KLT, they adopted a multirate sampling strategy where ECG samples are down sampled. Further for computational and storage efficiency, Olmos et al. [8] applied KLT to the entire beat signal and to independent windows (P-wave, QRS-complex and ST-T complex). They concluded that KLT to the independent windows performs better (CR = 17.12:1) at the cost of MSE (0.44%) compared to the entire beat signal (CR = 12:1, MSE = 0.3%). Another robust extension of classical PCA by analyzing shorter signal segments was suggested in [50]. The main disadvantage with KLT- or PCA-based methods is that they tend to be more computationally intensive as these are based on determining the eigenvalues and corresponding eigenvectors of the covariance matrix of the original data. Also in these methods, MSE was evaluated which is not a meaningful error measure from the preservation of diagnostic information. Wei et al. [21] proposed the SVD-based compression method for single lead ECG data, which does not require evaluation of covariance matrix. The proposed method was able to exploit *intra-* and *inter-beat* correlations of the ECG signal. It achieved a CR value of 10:1 with a low PRD value of 1.18%.

Keeping in view of the importance of the MECG data, efforts on exploiting the *inter-lead* correlation among the leads have been carried out. Cetin et al. [48] proposed a MECG compression technique using KLT and DCT to remove the *inter-lead* correlation among leads. This method achieved a CR value of 6.17:1 with a PRD value of 6.19%. This low CR is due to the high morphologic variability among the leads compared to lower variability in ECG samples. However, to exploit both *intra-beat* and *inter-lead* correlations in MECG data, authors followed a complex lead piling process prior to applying SVD [22].

Besides dimensionality reduction, these data dependent transforms have been used for other ECG applications. The KLT-based transform has been used for different ECG/MECG applications, including QRS representation and noise estimation [51], ST-T complex analysis for alternans detection [52]. PCA has been used widely on ECG/MECG data for beat detection and classification [53–55], ECG

feature extraction for studying the effect of diabetes [56], and cardiac risk identification using TWA [57–59]. PCA was also used as a tool for separating respiratory and non-respiratory segments in an ECG signal [60]. Similarly, SVD also has been used on ECG/MECG data for noise filtering [15], dimensionality reduction [21, 61–63], and fetal ECG extraction [11].

1.4.2.3 Hybrid transforms

The most attractive feature of WT which has drawn attention of many researchers is its simultaneous interpretation of the ECG signal in both time- and frequency-domains. Similarly, data dependent transforms linearly project the high-dimensional original data to a set of uncorrelated components in a low-dimensional feature space. Therefore, WT combined with PCA has been one of the most powerful approaches in recent years. A multiscale PCA-based MECG data dimensionality reduction technique was proposed [16], with a hypothesis to enhance the performance in terms of preservation of diagnostic information. Although the MECG data was considered, the MSPCA algorithm exploited only spatial or *inter-lead* correlation of the MECG data.

1.5 Feature Extraction for MI Classification

Myocardial infarction (MI) is a cardiac disorder that occurs due to the blockage of oxygen rich blood flow to the heart muscle. It can be detected by evaluating the clinical features, or by elevated values of biochemical markers of myocardial necrosis, or by imaging technique [64]. Following the last two procedures, it takes a long time to notice the probability of positive MI. More details about MI and its symptoms in ECG leads can be studied in [64]. However, MI produces certain changes in the ECG signal (Q wave, ST deviation, and T wave inversion). Hence, analysis of clinical features from the MECG is essential for detection and accurate localization of MI.

In this task, the objective is to extract discriminative features, decide whether MI is present or not, and then localize the infarction in the heart wall where it is. Detection compared to localization is an easier process. For localization, it is essential to study the MECG (12-lead ECG), which provides the spatio-temporal views of the heart (Section 1.2): (i) from anterior using V1 to V4, (ii) from lateral using I, aVL, V5 and V6, and (iii) from inferior using II, III and aVF. Based on this, MI has been classified as anterior (AMI), antero-lateral (ALMI), antero-septal (ASMI), inferior (IMI), infero-lateral (ILMI), infero-posterior (IPMI), infero-postero lateral (IPLMI), lateral (LMI), posterior (PMI), and postero-lateral (PLMI). Depending on the location of the infarction, cardiologists mark alterations in the MECG, and thereto in localized ECG. However, manual identification of these changes in MECG from a huge

database is difficult and may lead to incorrect diagnosis in the presence of noise. Accurate diagnosis of MI depends on how effectively different types of MI's are classified. The computerized methods can determine these minute variations in MECG and can enhance the classification accuracy. For this to happen, it is essential to evaluate the characteristics of the MECG by extracting discriminate features.

Many feature extraction techniques for MI detection have been proposed [65–69]. Methods based on processing of ECG signal in time-domain have included use of QRS measurement and neural networks [70], ST elevation parameters using neural-fuzzy approaches [71], Q- and T-wave amplitude and ST-deviation features [66], ST-segment analysis using multiple instance learning [67]. Among these methods, Arif's method [66] achieved the best performance with MI classification accuracy over 98%. Although time-domain features are direct measures for MI, in the presence of noise, these feature or parameter values alter. This may affect the final performance. To extract information which may not be readily available from the original time-domain signal, transform-domain tools are applied to single or multilead ECG signals to capture more discriminating features. Jayachandran et al. [72] used energy-entropy characteristics using DWT to achieve MI detection accuracy of 95%. Banerjee et al. [73] employed the cross wavelet transform and wavelet coherence techniques for analysis and classification of ECG signals. Their study showed distinguishing characteristics over the QRS complex area and T-wave region. This method classified normal and inferior MI data with accuracy, sensitivity, and specificity of 97.6%, 97.3%, and 98.8%, respectively. Sharma et al. proposed a multiscale energy and eigenspace approach for classification of MI. This approach achieved a detection and localization accuracies of 96% and 99.58%, respectively. Instead of classifying one or two types of MI from normal subjects, this method classifies six types of MI. A detail review on different feature extraction techniques from the perspective of feature dimension size and performance measures will be discussed in Chapter 2.

1.6 TWA Analysis

T-wave alternans (TWA) is a cardiac phenomenon in which repolarization morphology (amplitude, wave shape or polarity) consistently fluctuate on an every-other-beat basis [59, 74–77]. TWA has been recognized and linked to arrhythmogenesis for more than a century [78] and was considered to be a rare finding until the early 1980s. Adam et al. [79] in 1981 first measured non-visible microvolt-level TWA (μ-TWA). From here onwards, TWA refers to μ-TWA.

TWA has been associated with the risk of suffering life-threatening arrhythmias, including acute myocardial ischemia and infarction, heart failure, and congenital diseases, including Brugada syndrome

and long QT syndrome [80]. It is studied extensively as an index of sudden cardiac death (SCD) risk identification [81], including patients with dilated cardiomyopathy [82], long QT syndrome [83], ischemic cardiopathy [84], previous myocardium infarction [85–87], etc. In this thesis, we will study the TWA analysis for risk analysis in **post-MI** cases.

TWA usually is non-visible to the naked eye as its amplitude can be below than the noise level. Prior to clinical validation using TWA as a risk stratifier, accurate methodological evaluation, including TWA detection and estimation is necessary. A number of signal processing techniques have been proposed to detect and quantify TWA. Martinez and Olmos [74] discussed methodological approaches of most of the methods till the year 2005. Earlier to this study, criteria for the TWA analysis were diverse. In [74], existing methods were discussed in the light of three-stage unified framework involving preprocessing, data reduction and TWA analysis. The TWA analysis in most methods are based on the short-time Fourier transform of time-domain beat-to-beat series. The most widely used among these are the spectral method (SM) by Smith et al. [88], modified moving average (MMA) method by Nearing and Verrier [89]. Another method based on linear and nonlinear filtering of beat-to-beat series is the Laplacian likelihood ratio method [90, 91]. Drawbacks in earlier methods are their sensitivity to the presence of nonalternant components with high amplitude or their poor sensitivity to low-level TWA [59]. Some of the methods only detect TWA, but do not estimate the TWA waveform. Hence, these methods cannot be relied for arrhythmic risk identification [92]. Till 2008, the TWA analysis methods were developed for single lead ECG and are applied to each lead of MECG independently. In Physionet/CinC challenge 2008[1], with a theme for 'Detecting and Quantifying T-Wave Alternans', few methods [57, 93, 94] were proposed for multilead ECG. Monasterio et al. [59, 95] proposed a PCA- and periodic component analysis-based TWA analysis schemes for MECG data. The hypothesis behind these methods is to exploit spatial redundancy of MECG data. Later different methods [76, 77] have been proposed to improve TWA analysis performance.

1.7 Scope of the Present Work

The MECG data provides the electrical activity of the heart from different locations. For proper diagnosis, clean signals with all morphological waves are required. Preprocessing of these signals is performed to improve their quality. Then, the signal processing is carried out for different purposes, which are mentioned in Section 1.3, either in time-domain or in transform-domain. However, the long duration MECG data, which is spatially and temporally correlated, is cumbersome to analyze in time-

[1] http://physionet.org/challenge/2008/

domain. Correlations present in the MECG data can be exploited for various MECG data processing applications.

This research will address analysis on the spatio-temporal dynamics of the heart by exploiting different types of correlations. Though several works are reported in the literature for this purpose, simultaneous analysis of multiple leads and ECG cycles information is a limitation in this field. It is expected that simultaneous analysis may reveal some extra information which will help enhance the performance of various ECG processing applications. The available methods consider either of the information but not both. Considering applications like dimensionality reduction, data dependent transform methods are found to perform better over others because of their high decorrelation property. Meantime, multiscale analysis of WT using dyadic structure is being used to preserve the diagnostic information of ECG signal effectively. This is because of its grossly segmentation capability of ECG signal into components that appear at different scales. Combining data dependent transforms with WT can be a better approach for simultaneously reducing the dimension and extracting discriminative features for different tasks. The recently proposed PCA algorithm exploited inter-lead correlations in multiscale domain for data dimensionality reduction and feature extraction [16, 68]. There are still possible ways to exploit other types of correlations using effective data dependent transformation techniques. Meantime, the correlations have been exploited for data dimensionality reduction in most of the articles. There is a scope to study the effects of correlation exploitation for other ECG/MECG applications.

In another perspective, it is a well established fact that the reconstructed subband signals are correlated [16, 96, 97]. The other aspect of multilead correlations in wavelet domain is not studied extensively. Authors in [16, 68] have applied PCA on the wavelet coefficients. A fundamental question raises here: whether the subband wavelet coefficients of all leads in a particular scale are spatially and temporally correlated or not? And the answer is yes. It is expected that exploitation of correlations present in wavelet coefficients not only will improve the storage efficiency and the computational time but will help for other purposes, also.

1.8 Organization of the Thesis

The rest of the thesis is organized as follows:

In **Chapter 2**, related reviews on ECG (single and multilead) signal processing methods such as ECG correlation exploitation techniques, classification of MI, TWA detection and estimation techniques are portrayed.

Chapter 3 presents a fast and computationally efficient MECG data processing algorithm. Application of SVD directly on wavelet transformed MECG data exploits both intra-beat and inter-lead correlations, and simultaneously retains diagnostic features of the ECG signal. Based on drawbacks of existing thresholding techniques, a multiscale energy based new thresholding method is proposed. Finally, a simulation study of the proposed method for wireless body sensor network is presented. The effectiveness of the proposed method for this type of applications is demonstrated by evaluating computational and time complexity of the proposed method and comparing these with the state-of-the-art methods.

Chapter 4 proposes a novel third-order tensor representation of MECG data that helps exploit all three types of correlations. This chapter illustrates the proposed new structure in two applications, namely data dimensionality reduction scheme and classification of MI. An energy-based thresholding technique is proposed to reduce the dimension of the MECG tensor. Mode singular values and normalized multiscale wavelet energy features are extracted from the reduced tensor MECG for classification of MI. Classification performances are evaluated by without over-fitting training and testing data. Then these performances are compared with the state-of-the-art methods.

Chapter 5 discusses a novel TWA detection and estimation approach for MECG data. Experiments are conducted in semi-synthetic and real ECG databases. TWA detection and estimation results are validated by evaluating some statistical techniques. Later, an informative study on MI progression over a period of time is presented by analyzing the TWA amplitude variation in different leads.

A summary of the present work with major contributions is discussed in **Chapter 6**. Further research on higher-order representation of MECG data volume are also presented.

2

Transform Methods for ECG/MECG Analysis: A Review

Contents

Research on MECG data processing has experienced noticeable advances in the last few years, and several techniques have been published. As discussed in the last chapter, the objective of this thesis is to develop MECG data processing methods for three separate but interconnected topics, viz. dimensionality reduction, feature extraction for MI classification, and TWA analysis to study MI progression in post-MI cases. These tasks are based on simultaneous exploitation of spatio-temporal correlations using data dependent transformation techniques. These transformations are carried out on wavelet transformed data.

This chapter reviews the related works on above mentioned three topics, and distortion measures those are carried out or used in this thesis. It is difficult to present a review on these topics altogether, hence, these have been reviewed separately. Accordingly, this chapter is divided into a number of sections. As the data dependent transformation techniques are applied on the wavelet transformed MECG data, it is necessary to review the wavelet applications to ECG signals. In Section 2.1, we discuss a brief review on DWT, multiresolution analysis and synthesis, multiscale decomposition of MECG data. In Section 2.2, a review on data dependent transformation techniques for ECG correlation exploitation is presented. This section also presents a comparative analysis among these techniques. This is followed by reviews on feature extraction methods for MI classification in Section 2.3. This section also summarizes the most popular SVM classifier with performance evaluation measures. In Section 2.4, TWA analysis methods starting from the classical to very recent ones with their limitations are reviewed. Towards the end of this chapter, ECG databases and distortion measures used in this thesis are discussed in Sections 2.5 and 2.6.1. Finally, motivation of the work is drawn in the last section.

2.1 Wavelet Transform Application to ECG Signal

Wavelet transform (WT) is a mathematical tool, used for simultaneous signal analysis in the time- and frequency-domains, and classifies local and transient components at various scales. A detail description on WT is presented in [38]. It has attracted researcher's attention for nonstationary signals like ECG because of its better time-frequency localization property [14, 16, 18, 39, 40, 96, 98–101]. It localizes ECG diagnostic parameters simultaneously in both time- and frequency-domains and grossly segments these in different subbands. An excellent review on wavelet transform and its application on ECG signal can be found in [102]. In this section, we discuss briefly on DWT (a data independent transform technique) and MRA property. Multiscale decomposition of MECG data is also discussed to build the motivation of this thesis.

A wavelet family $\psi_{a,b}(t)$ contains the set of elementary basis functions which is generated by dilations and translations of a unique admissible mother wavelet $\psi(t)$ [36–38] and is represented as

$$\psi_{a,b}(t) = \Big(\frac{1}{\sqrt{|a|}}\Big)\psi\Big(\frac{t-b}{a}\Big) \tag{2.1}$$

where a, $b \in \mathbb{R}$ and $a \neq 0$. Dilation and translation of the mother wavelet continuously generates redundant information, and hence it is dilated and translated discretely. For this, parameters are set as $a = a_0^j$ and $b = kb_0a_0^j$, where j, $k \in \mathbb{Z}$ are dilation (scale) and translation parameters [103], respectively, and $a_0 > 1$, $b_0 > 0$. The discretized wavelet is represented as

$$\psi_{j,k}(t) = \Big(\frac{1}{\sqrt{|a_0^j|}}\Big)\psi\Big(\frac{t-kb_0a_0^j}{a_0^j}\Big) = a_0^{-j/2}\psi(a_0^{-j}t - kb_0) \tag{2.2}$$

The corresponding discrete wavelet transform (DWT) coefficients are given as

$$w_{j,k} =< x(t), \psi^*_{j,k}(t) >= \frac{1}{\sqrt{2^j}}\int x(t)\psi^*(2^{-j}t - k)dt \tag{2.3}$$

The parameters a_0 and b_0 are selected in such a manner, the family of dilated mother wavelet forms an orthonormal basis. The usual choice for a dyadic DWT is $a_0 = 2$ and $b_0 = 1$, and the discrete wavelet family is given by $\psi_{j,k}(t) = 2^{-j/2}\psi(2^{-j}t - k)$, constitutes an orthonormal basis. The signal $x(t)$ can be represented as a linear combination of these basis functions as

$$x(t) = \sum_{j=-\infty}^{\infty}\sum_{k=-\infty}^{\infty} w_{j,k}\psi_{j,k}(t) \tag{2.4}$$

The above choice of a_0 and b_0 leads to multiscale decomposition technique where it decomposes a signal into a number of scales with different time and frequency resolutions.

2.1.1 Multiresolution/multiscale analysis and synthesis

In this subsection, a brief discussion on multiresolution analysis (MRA) is presented. Sometimes authors have used multiscale decomposition (MSD) in place of MRA. A complete discussion on MRA theory can be found in [36,37]. Wavelet analysis is described using two basic functions, the scaling $\phi(t)$ and the wavelet $\psi(t)$ functions. The wavelet function is formed by dilation and translation of a single function $\psi(t)$ and is given as $\psi_{j,k}(t) = 2^{-j/2}\psi(2^{-j}t - k)$. The scaling and the wavelet functions together resolve the signal into coarse (low resolution) and detail (high resolution) components, respectively, as

$$x(t) = A_j(t) + D_j(t) + D_{j-1}(t) + \cdots + D_1(t) \tag{2.5}$$

where $A_j(t)$ and $D_j(t)$ are the approximation and the details components at level j.

The dyadic WT is implemented using a multiresolution pyramidal decomposition technique. The approximation $A_j(k)$ and details $D_j(k)$ coefficients can be defined using the scaling function $\phi(t)$ and the wavelet function $\psi(t)$ as $A_j(k) =< x(t), \phi_{j,k}(t) >$, $D_j(k) =< x(t), \psi_{j,k}(t) >$, and $A_j(k) = A_{j+1}(k) + D_{j+1}(k)$. The next coarser, $j+1$ scaling (A_{j+1}) and wavelet (D_{j+1}) coefficients are obtained as follows. The jth scale coefficients (A_j) are filtered using two finite impulse responses of low-pass and high-pass digital filters, followed by the down-sampling process which results A_{j+1} and D_{j+1} coefficients, respectively. In general, at jth decomposition level, the details subbands are denoted as D_j, $j = 1, 2, \cdots, L$ and the approximation subband is denoted as A_L, where L is the wavelet decomposition level.

The bandwidth (ΔF_j) of jth wavelet subband is given as [96]

$$2^{-j-1} F_s \;\leq\; \Delta F_j \;\leq\; 2^{-j} F_s \tag{2.6}$$

where F_s is the sampling frequency of the signal. Based on different sampling frequencies, Al-Fahoum heuristically derived the value of L that satisfies the frequency span of ECG morphological features [104] and is given as

$$L = \lfloor \log_2 F_s - 2.96 \rfloor \tag{2.7}$$

where $\lfloor . \rfloor$ is the floor value of a number.

The recombination of the wavelet coefficients to reconstruct the original signal is basically a *synthesis* problem. Unlike the analysis process, here, the algorithm simply inverts the process, by combining and upsampling technique with linear filtering operations.

2.1.2 Multiscale decomposition of MECG data

In [96], authors had shown that, ECG diagnostic or morphological features are grossly segmented into different subbands. In the follow-up articles [16, 105, 106], the same concept was extended for MECG data. It is a well-known fact that, the synthesized or reconstructed subband signals of all leads at a particular scale are correlated, which have been shown in [107, cf. Ch. 2, pp. 41]. Analyzing further, an MECG data ($F_s = 500$ Hz) is wavelet decomposed with six levels. The original leads and their subband wavelet coefficients (not the reconstructed subband signals) are shown in Figure 2.1. In this figure, only five ECG signals (I, II, V1, V2 and V5) have been plotted. Depending on the frequency content of the morphological features of the ECG signal, these are segmented into different subbands. In this figure, we can observe that, *the wavelet coefficients of all leads at each scale are spatially and temporally correlated*. Hence, there is a need of exploiting the correlations present in subband wavelet

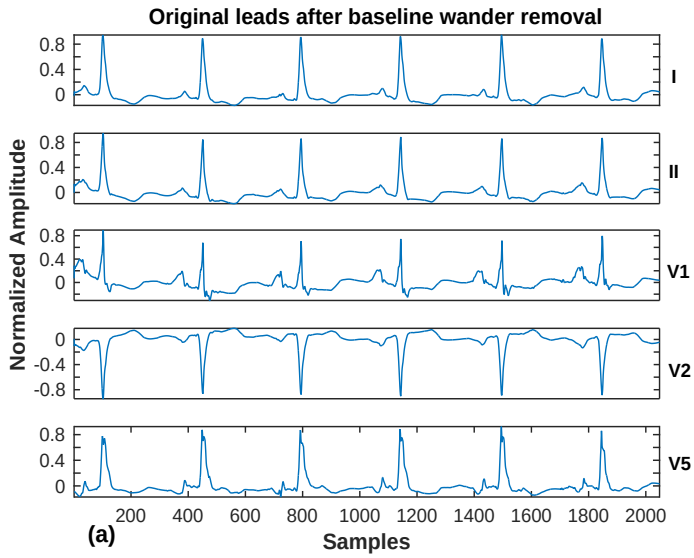

Figure 2.1: Original ECG leads after baseline-wander removal and their subband coefficients with six level decomposition. In panels (a) subplots showing time-domain I, II, V1, V2, V5 leads

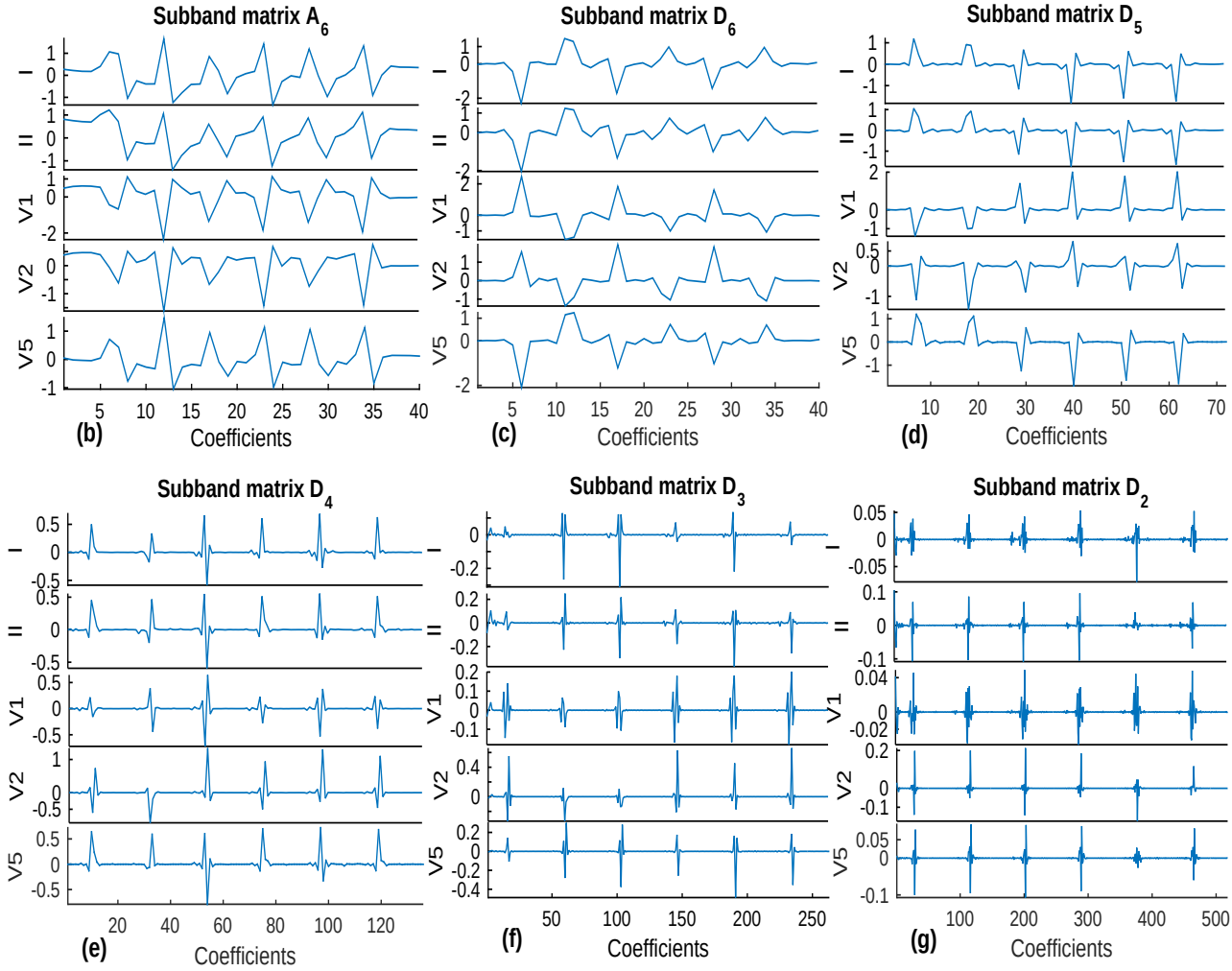

Figure 2.1: (Contd...) Plots showing subband wavelet coefficients of (b) A_6, (c) D_6, (d) D_5, (e) D_4 (f) D_3 (g) D_2 subbands. These wavelet coefficients at a particular subband are spatio-temporally highly correlated.

coefficients using a data dependent transform technique. In this thesis, correlations present in both subband wavelet coefficients (Chapters 3 and 4) and reconstructed subband signals (Chapter 5) have been exploited.

In the present times, wavelet transform-based methods are being popularly used in ECG processing. However, it is evident from the literature that, WT methods have been applied to a single lead ECG where sample or beat dependencies have been exploited. It is difficult to analyze spatial resolutions/correlations using WT. Applying data dependent transforms like PCA or SVD on these wavelet coefficients may exploit spatial or spatio-temporal correlations.

2.2 PCA- and SVD-based ECG Analysis: A Methodological Review

In this section, the existing PCA- and SVD-based ECG analysis methods those exploit different correlations are reviewed, compared and discussed in the light of the three-step common framework, viz., preprocessing, transformation and thresholding with performance measure. Prior to this, a basic review on PCA and SVD is presented as these are common in the methods to be discussed.

2.2.1 PCA/KLT and SVD

The major concern with high dimensional ECG datasets is that, all the recorded signals or the constituent features are not important for interpretation. PCA and SVD are the most established techniques in multivariate statistical analysis and have been applied to various ECG applications (Chapter 1). The reason being PCA and SVD are used for most of the ECG applications that there is a large amount of redundant information along with noise and artifacts which are unnecessary for diagnostic applications.

PCA/KLT: Principal component analysis is the common data dependent transformation technique that is being used in different fields [108]. In signal processing field, it is also interchangeably named as Karhunen-Loève transform (KLT). It converts a set of observations of possibly correlated variables into a set of values of linearly uncorrelated variables called principal components (PCs) [109–111]. The PCs retain most of the information, both in the sense of maximum variance of the features and minimum reconstruction error. Let the data matrix $\mathbf{X}_{m\times n}$ with $m < n$. First, the sample covariance matrix is calculated as $\mathbf{R_X} = \mathbf{E}[(\mathbf{X}-\mu)(\mathbf{X}-\mu)^{\mathbf{T}}]$ or $\mathbf{R_X} = \mathbf{E}[(\mathbf{X}-\mu)^{\mathbf{T}}(\mathbf{X}-\mu)]$, where μ is the mean of the data matrix $\mathbf{X}$. The transformation matrix $\mathbf{V}$ is obtained by solving the eigenvector equation

$$\mathbf{R_X V} = \mathbf{V\Lambda} \tag{2.8}$$

where $\mathbf{V}$ and $\mathbf{\Lambda}$ are eigenvector and eigenvalue matrices. Finally, the KLT $\mathbf{Y}$ of $\mathbf{X}$ is given as

$$\mathbf{Y} = \mathbf{V}\mathbf{X}. \tag{2.9}$$

The eigenvectors in $\mathbf{V}$ are ranked from the highest to the lowest corresponding eigenvalues. The first PC (highest eigenvalue) has the largest possible variance in the data, while each successive component also has the highest possible variance, under the condition that all components are mutually uncorrelated. Although KLT and PCA are interchangeably described in literature and are quite equivalent, the only difference is that, KLT analyzes the spectrum of the covariance matrix ($\mathbf{R_X}$), whereas PCA analyzes the spectrum of the sample covariance matrix ($\hat{\mathbf{R}}_\mathbf{X}$) where sample means have been removed. As the transformation matrix $\mathbf{V}$ is formed from the covariance matrix, one thing we can observe from the computation of PCA is that, it models only single-factor (either row-space or column-space) variation, but not both.

SVD: The key idea of the SVD is also to capture the significant information of the data matrix. It decomposes the data matrix $\mathbf{X}$ as

$$\mathbf{X} = \mathbf{U}\mathbf{\Sigma}\mathbf{V}^\mathbf{T} \tag{2.10}$$

where $\mathbf{U}$ and $\mathbf{V}$ are left and right orthonormal matrices, respectively, and $\mathbf{\Sigma}$= $[diag\{\sigma_1, \sigma_2, \cdots, \sigma_m\} : \mathbf{0}] = [\hat{\mathbf{\Sigma}} : \mathbf{0}]$, $\sigma_1 \geq \sigma_2 \geq \cdots \geq \sigma_m > 0$, is the singular value matrix and $\sigma_i's$ are singular values (SVs). The matrix $\mathbf{U}$ contains eigenvectors of the covariance matrix $\mathbf{R_1} = \mathbf{X}\mathbf{X}^\mathbf{T}$ whereas $\mathbf{V}$ contains that of the covariance matrix $\mathbf{R_2} = \mathbf{X}^\mathbf{T}\mathbf{X}$. Hence, SVD can model both row- and column-space variations [112]. Details on SVD and how SVD models both spaces will be discussed in Chapter 3.

Unlike PCA/KLT, the data matrix can be approximated directly using few SV coefficients (say $K =$ min(m, n)) and is represented as following

$$\hat{\mathbf{X}} = \sum_{i=1}^{K} \mathbf{u}_i \sigma_i \mathbf{v}_i^T \tag{2.11}$$

where $\hat{\mathbf{X}}$ is the reconstructed data matrix.

While formally both PCA/KLT or SVD solutions can be used to calculate the corresponding PCs or SVs in a similar manner, the extra step of calculating the covariance matrix $\mathbf{R} = \mathbf{X}\mathbf{X}^\mathbf{T}$ or $\mathbf{R} = \mathbf{X}^\mathbf{T}\mathbf{X}$ leads to numerical rounding errors and requires more computations when calculating the eigenvalues/vectors [113]. Hence, it is better to use SVD over PCA.

2.2.2 Steps for implementation of PCA- or SVD-based methods

As mentioned earlier, a three-step common framework for PCA- or SVD-based ECG/MECG dimensionality reduction methods is discussed here. Table 2.1 summarizes a quick review on the most relevant similarities and differences of these methods.

2.2.2.1 Preprocessing stage

The basic and foremost step in any ECG application is preprocessing where a signal is conditioned for further processing. The preprocessing stage includes baseline cancellation, beat detection, period normalization, and noise filtering to accelerate further processing. In correlation exploitation transform techniques, basically baseline wander cancellation is performed using spline interpolation or filtering technique (Chapter 1). To apply these data dependent transforms, ECG or MECG data need to be represented in 2-D matrix form. Methods dealing with the single lead ECG [21, 22] follow R-peak detection and period normalization. Period normalization is performed using interpolation technique or zero-padding scheme [19]. However, authors in [21] followed a different technique for period normalization. An ECG segment $\mathbf{y}_i = [y_i(1), y_i(2), \cdots y_i(n')]$ can be converted into a segment $\mathbf{x}_i = [x_i(1), x_i(2), \cdots x_i(n)]$ that holds the same signal morphology with a different length ($n' \neq n$) using the following expression

$$x_i(j) = y_i(j') + (y_i(j'+1) - y_i(j'))(r_j - j') \tag{2.12}$$

where $r_j = \dfrac{(j-1)(n'-1)}{n-1} + 1$ and j' is the integral part of r_j. The mean beat period (MBP) is chosen as normalized length n and is also retained as the beat information.

After detection and normalization, *m* number of beats are arranged in rows whereas their corresponding *n* samples in columns of a matrix $\mathbf{X}$ which is given as

$$\mathbf{X} = [\mathbf{x}_1;\ \mathbf{x}_2;\ \cdots\ \mathbf{x}_m] \tag{2.13}$$

where $\mathbf{x}_i = [x(1)\ x(2) \cdots\ x(n)]$ is a row vector containing beat samples.

In case of MECG, Castells et al. [22] proposed a new lead piling approach to apply the data dependent transforms. The vector $\mathbf{x}_i$ is modified as $\mathbf{x}_{i,l}$ where the indices *i* and *l* denote beat and lead numbers, respectively. The leads $\mathbf{x}_{i,1},\ \mathbf{x}_{i,2}, \cdots\ \mathbf{x}_{i,l}$ of the *i*th beat are piled into an $ln \times 1$ vector $\mathbf{x}'_i$, and it is given as $\mathbf{x}'_i = [\mathbf{x}_{i,1};\ \mathbf{x}_{i,2};\ \cdots\ \mathbf{x}_{i,l}]$. Then the $ln \times m$ multilead data matrix $\mathbf{X}'$ is given as

$$\mathbf{X}' = [\mathbf{x}'_1;\ \mathbf{x}'_2;\ \cdots\ \mathbf{x}'_m]. \tag{2.14}$$

This lead piling procedure requires more time and computations. To simplify the computational

complexity, multilead ECGs were processed without using the lead piling process. The multilead ECGs were replaced with a number of beats in (2.13) to form the data matrix [16, 48]. Here, a fixed number of ECG samples were considered. Additionally, in [48], the redundant leads (III, aVR, aVL, aVF) from standard 12-lead ECG data were discarded. Then the order of the ECG leads were rearranged to bring correlated leads close to each other. It is expected high correlation among the precordial leads (V1$-$V6) as these represent heart vector amplitude variations with respect to time from six different narrow angles. The limb leads (I and II) have relatively less energy contents with respect to the precordial leads. Hence, the precordial leads followed by the limb leads were arranged in the data matrix.

2.2.2.2 Transform stage

Transform techniques convert ECG samples into coefficients reflecting characteristics of the morphological waves. In this stage, the data matrix is transformed using (2.9) or (2.10), depending on the transform is being used. In most of the methods [47–49], KLT/PCA was applied directly on the data matrix $\mathbf{X}$. As PCA can model only single-factor variation, methods for single lead ECG exploit *intra-beat* correlation [47,49], whereas in case of MECG data, *inter-lead* correlation has been exploited [48]. Wei et al. [21] applied SVD on single lead ECG to exploit both, *intra-* and *inter-beat* correlations.

To preserve the diagnostic information of the MECG data, multiscale PCA (MSPCA) algorithm was proposed [16]. After arranging fixed ECG samples (4096) of 12-lead ECG in a matrix form of size 12$\times$4096, MRA using DWT was applied to each lead samples. The L-level decomposition resulted $L+1$ subband matrices; one approximation subband matrix ($\mathbf{A}_{\mathrm{L}}$) and L number of detail subband matrices ($\mathbf{D}_{\mathrm{L}}$, $\mathbf{D}_{\mathrm{L\text{-}1}}, \cdots, \mathbf{D}_{1}$). Then PCA was applied on these matrices. This method as expected exploits only *spatial* or *inter-lead* correlation of MECG data. Hence, there is a need of algorithm(s) for MECG data which can exploit spatio-temporal (intra-beat, inter-beat, and inter-lead) correlations simultaneously.

2.2.2.3 Thresholding stage with performance measure

Thresholding stage

The information preserved in this stage will be accessible for further analysis like reconstruction, feature extraction, etc. It is, therefore, important that ECG morphological features are well preserved in the reduced coefficients. Transform-based methods pack the energy of the signal into a few coefficients $K < \min(m, n)$. This requires thresholding of PCs or SVs. The criteria to select these PCs and SVs is diverse. In most methods [47–49], a straightforward way to choose the value of K is by select-

ing a fixed number of PCs, and this value is chosen based on a minimum mean square error. In [47], the value of K was selected in between 32 and 64 out of 128. It is not always possible to preserve the diagnostic features using a fixed number of PCs. Since the information energy of the matrix $\mathbf{X}$ can be expressed as the sum of squared SVs, an energy-based thresholding was used in [21] to retain most of the signal energy. The percentage of information energy within a certain SVs was defined as the energy ratio (ER), which was given as

$$ER(\%) = \frac{\sum_{i=1}^{K} \sigma_i^2}{\sum_{i=1}^{\text{rank}(\mathbf{X})} \sigma_i^2} \times 100 \tag{2.15}$$

In this method, basically a fixed percentage of the information energy of the data matrix is retained. In abnormal conditions, the reconstruction signal fidelity using a fixed value selection of PCs or energy-based thresholding of SVs is not always acceptable. These types of thresholding introduce distortions in abnormal ECG signals (for example in [21, cf. Figures 8 and 12]).

To reduce distortions, another thresholding technique based on average fractional energy contribution (AFEC) of the eigenvalues in different subbands was proposed. The AFEC for a particular subband was defined as the ratio between the sum of eigenvalues of that particular subband to the sum of eigenvalues of all subbands. Mathematically, the AFEC for a details subband (say, $D_j,\ j = 1, \cdots L$) was expressed as

$$\eta_{D_j} = \frac{1}{m}\left(\frac{\sum_{i=1}^{m} \lambda_{D_{j_i}}}{\sum_{i=1}^{m} \lambda_{A_{L_i}} + \sum_{j=1}^{L}\sum_{i=1}^{m} \lambda_{D_{j_i}}}\right) \tag{2.16}$$

where m denotes number of leads, $\lambda_{A_{L_i}}$ is the *i*th eigenvalue of the subband A_L, and $\lambda_{D_{j_i}}$ is the *i*th eigenvalue of the subband D_j. AFEC for the approximation subband was defined in a similar manner, by replacing the sum of eigenvalues corresponding to the approximation subband matrix in the numerator (2.16). The AFEC-based thresholding technique selects different number of eigenvalues from different subbands based on their diagnostic importance. However, this thresholding technique does not take any account on the *variation of relative energy* across subbands.

Performance measure

Transform-based correlation exploitation techniques for ECG compression are usually lossy, i.e. reconstructed signal differs from the original signal. Although a certain amount of distortion is accepted, but it should not be at the cost of diagnostic features of the ECG. Several error measures have been proposed to measure the distortion level. The KLT is the optimum transform for random signal repre-

sentation with respect to the mean-square error (MSE) criterion [47, 49, 114]. The algorithm [47] which exploits *intra-beat* correlation achieved SRR of 3:1 for the MSE value of 0.34 %. Here, 128 ECG samples energy was packed into about 45 KLT coefficients. Similarly, another KLT-based algorithm by Olmos et al. [114] resulted a CR of 12:1 for the MSE value of 0.3 %. Although KLT approach is shown to provide a high compression ratio, the computational time needed to calculate the KLT basis functions is very intensive [10, 49]. Authors in [49] claimed that the KLT-based quality controlled algorithm achieved an SRR of approximately 23:1, but they did not evaluate any distortion measures. However, the only error measured in these methods is MSE which distributes the error equally over all portions of the ECG signal, and hence, it is not subjectively meaningful in many cases. It is difficult to define the clinically acceptable MSE value for a given compression method due to different dynamic ranges of ECG signals. In the last two decades, PRD (Section 2.6.1), a non-diagnostic objective distortion measure, has been used extensively. The truncated SVD algorithm [21] that exploits intra- and inter-beat correlations, resulted a CR value of 10:1 with a low PRD value of 1.18 %. The low morphologic variability among samples and beats helps result high CR in case of single lead ECG signals. The KLT-based MECG compression algorithm achieved CR of 6.19:1 with a PRD value of 3.7 %. As the MSPCA-based method [16] is able to exploit only inter-lead correlation of MECG data, it turns out to result a poor CR compared to single-lead ECGs. This is due to high morphologic variability among the leads. An SRR of 1.45:1 and an acceptable CR of 5.98:1 with PRD of 2.09 % were achieved. PRD may not be a good measure of quality of the compressed signal, and also a low PRD value does not necessarily mean clinical acceptance of morphological features of ECG signal.

2.3 Feature Extraction Methods for MI Classification

Over the last decades, evaluation of MI, the most common complications of coronary artery disease, has evolved from visual inspection of the ECG to the use of computerized methods for classification of different types of MI. Detection is the process of classifying an abnormal MI case from a normal case, where as localization is the process of specifying the region of the coronary artery or the heart muscle which have been affected. In this thesis, classification refers to both detection and localization as a whole unless it is specified. This section reviews various feature extraction methods those have been reported in the literature for MI classification.

Arif et al. [66] used time-domain ECG features of 12 leads for classification of MI. For each beat, Q-wave amplitude, T-wave amplitude and ST-deviation parameters are extracted and combined for 12-leads. This results a 36-dimensional feature vector for each beat. Features are extracted from 20,160

Table 2.1: Reviews on data dependent transform techniques for correlation exploitations

Methods	#Leads	Preprocessing	Description	Type of correlation	Results	Remarks
Ahmed et al. 1975	3		KLT and DCT	intrabeat	SRR: 3:1 MSE: <0.0034	MSE-based distortion measure
Cetin et al. 1993	12	Rearrangement of leads to get max. correlation [V1, V2, ... V6, I, II]	KLT and DCT	intrabeat	CR: 6.19:1 PRD: 3.70%	
Blanchett et al. 1998	1		KLT	intrabeat		
Wei et al. 2001	1	QRS detection, Period normalization based on MBP	Truncated SVD	intrabeat & interbeat	CR: 10:1 PRD: 1.18%	Reconstruction signal fidelity is poor in abnormal conditions
Castells et al. 2007	1, 12	N. S.	PCA, SVD	intrabeat or interbeat intrabeat & interlead	Not reported	
Sharma et al. 2012	12	ECG segmentation of fixed 4096 samples Baseline cancellation using Butterworth HPF Amplitude normalization	MSPCA Threshold: subband energy-based eigen values thresholding	interlead	Database: CSE CR: 5.98 PRD: 2.09%	Does not based on variation of relative energy across subbands

ECG beats for their study. KNN classifier is used. It achieves sensitivity and specificity of 99.9% for detection of MI, accuracy of 98.8% for localization of MI. Meanwhile, it has to perform various steps including extraction of beat-wise time-domain features.

Sun et al. [67] proposed a technique based on latent topic multiple instance learning (LTMIL) for automatic detection of MI without labeling any heartbeats. After detecting fiducial points using [13], ST-segments of each one-lead heartbeat is sampled to 200 points. Features are extracted using a five-order polynomial fitting technique. This requires six polynomial coefficients to represent ST-segment information of one-lead heartbeat. Two other ECG morphological features considered are the ratio of the average ST-segment length to the average RR-interval length, and the height-to-length ratio of the ST-segment for each heartbeat. The feature vector dimension becomes $74\ (=12\times 6+2)$ for each beat. This method achieved sensitivity and specificity values of 92.3 ± 0.84 and 88.1 ± 2.3, respectively, by using support vector machine (SVM) classifier. In this method, MI abnormality due to the Q-wave has not been considered. Performance of this method also depends on the accurate detection of ST-segment characteristics.

In a recent work, Liu et al. [69] proposed a polynomial fitting based feature extraction technique for detection of MI. A given ECG signal is fitted with a 20th order polynomial function defined as *Poly*ECG-S. This method shows an accuracy level of 94.4% with the test dataset.

The above discussed time-domain-based feature extraction algorithms result better detection accuracy but these do not perform well during localization of MI, for instance, localization accuracy in [67] is 76.6 %. This is due to the non-stationary behavior of ECG is not depicted properly by time-domain features. Hence, the original MECG data is transformed from time-domain to other domain where concealed and discriminant features are extracted.

In a recent work [68], authors proposed a multiscale energy and eigenspace analysis technique for classification of MI. After preprocessing and multiscale analysis, energy and eigenspace features are extracted. The multiscale energy of a particular subband is given by

$$E_D^m = \frac{\sum_{k=1}^{q}[w_{j,k}^m]^2}{q} \tag{2.17}$$

where $w_{j,k}^m$ is the kth wavelet coefficient at jth level of mth lead, and q is the number of coefficients in a particular subband. The multiscale eigenvalue features are extracted by applying PCA, which follows covariance matrix formation and eigenvalue decomposition, on the multiscale matrices. Then six dominant eigenvalues from $\mathbf{A}_6$, $\mathbf{D}_6$, $\mathbf{D}_5$ and $\mathbf{D}_4$ are considered. This results $24\ (=6\times 4)$ eigenvalues and $48\ (=12\times 4)$ multiscale energy elements. Hence, a 72-dimensional feature set is extracted from

each MECG frame. Each frame contains 4 beat information. After performing a correlation-based feature selection, feature set dimension is reduced to 60. Then localization is performed on the MI detected MECG frame where again multiscale energy and eigenvalues are extracted from single-beat data matrix. During localization, 72-dimensional feature vector is considered. A limitation in [68] is that the extraction of features in two stages (for detection and then for localization) may require more computations. Another limitation of this method is that, heartbeats from the same subjects are used in both training and testing datasets. Authors claimed that frame-specific (comprising of four beat periods from MECG data) analysis is better than earlier beat-specific techniques.

Selection of large feature dimension may have an adverse effect on computations and storage. This motivates to reduce the dimension of the feature vector. Another limitation in [68] is that the extraction of features in two stages (for detection and then for localization) requires more computations. These restrictions inspire us to develop a new feature extraction algorithm for MI classification from a third-order MECG tensor.

2.3.1 Support vector machine classifier

In the previous section, we reviewed some feature extraction methods for MI detection (and localization) and their classification performances. To classify a MI case from a HC case, there is a need of classifier which performs this task. For this purpose, the popular and high-performance SVM classifier is being used in most of the methods [115]. In a classification task, the data is separated into training and testing sets. Each instance in the training set contains one “target value" (i.e. class labels) and several “attributes" (i.e. the feature variables). Given only the test data features, SVM develops a model, based on the training data, which predicts class labels of the test data. Let us consider a two class classification task: Given a training set of feature-label pairs (x_i, y_i) for N samples, $i = 1, 2, \cdots, N$ where $x_i \in R^N$ and $y_i \in [-1, 1]$. As the data is not always linearly separable, some of training set data points are mislabeled. The goal is to maximize the margin while softly penalizing points that lie on the wrong side of the margin boundary. It requires the solution of the following primal optimization problem:

$$\begin{aligned} \underset{w,b,\xi}{min} \quad & \frac{1}{2}w^T w + C\sum_{i=1}^{N}\xi_i \\ \text{subject to} \quad & y_i(w^T\phi(x_i) + b) \geq 1 - \xi_i, \\ & \xi_i \geq 0, \quad i = 1, \cdots, N \end{aligned} \tag{2.18}$$

where the parameter $C > 0$ controls the trade-off between the slack variable penalty and the margin. Details about the solution to the above primal can be found in [116]. The corresponding Lagrangian is

Table 2.2: Reviews on feature extraction for MI classification methods

Methods	Description	Datasets	#feature & Classifier	Results	Remarks
Reddy et al 1992					
Lu et al 2000	Time-domain fatures ST-deviation and T-wave amplitude	12-lead ECG 104 MI subjects 20 HC subects	Fuzzy logic & neural network	Detection Sen: 84.6 Spe: 90	Regarding data selection is not clear.
Jayachandran et al 2009	Energy entropy characteristics using DWT		Threshold based classifier	Detection Acc: 96.9	Overfitting of the training and testing datasets.
Arif et al 2012	Time-domain fatures Q- & T-wave amplitudes ST-level deviation	PTB: 12 lead 16960 MI beats from 10 types of MI 3200 HC beats	Det: 36 Loc: 36 Prunned & simple KNN	Detection Sen:97.2 Spe: 99.6 Localization Acc: 98.8	Overfitting of the training and testing datasets.
Sun et al 2012	LTMIL Polynomial fitting: Six polynomial coefficients for each beat	PTB: 12 lead 4 types of MI & HC classes	Det: 74 SVM & KNN	Detection Sen: 92.6 Spe: 82.4 Localization Acc:76.6	Non-overfitting of training and testing datasets.
Liu et al 2014	Polynomial fitting ECG signal is fitted with a 20th order polynomial function	PTB: 2 leads (I & V6)		Detection Acc: 94.4	
Sharma et al 2015	Transform-domain Multiscale energy and eigenspace features	PTB: 12 lead 148 MI subjects from 10 types of MI 52 healthy subjects	Det: 60 Loc: 72 KNN & SVM	Detection Sen: 93.0 Spe: 99.0 Acc: 96.0 Localization Acc: 99.6	Overfitting of the training and testing datasets
Acharya et al 2016	Transform-domain Entropy based features	PTB: 12 lead 148 MI subjects from 10 types of MI 52 healthy subjects	Det: 96 Loc: 96	Detection Sen: 99.45 Spe: 96.27 Acc: 98.80 Localization Sen: 9935 Spe: 99.16 Acc: 98.74	Overfitting of the training and testing datasets

given as

$$L(w,b,a) = \frac{1}{2}w^T w + C\sum_{i=1}^{N}\xi_i - \sum_{i=1}^{N} a_i\{t_i y(x_i) - 1 + \xi_i\} - \sum_{i=1}^{N}\mu_i\xi_i \tag{2.19}$$

where $\{a_i \geq 0\}$ and $\{\mu_i \geq 0\}$ are the Lagrange multipliers. Its dual form is represented as

$$\tilde{L}(a) = \sum_{i=1}^{N} a_i - \frac{1}{2}\sum_{i=1}^{N}\sum_{i=1}^{N} a_i a_j y_i y_j k(x_i, x_j) \tag{2.20}$$

with constraints $0 \leq a_i \leq C$ and $\sum_{i=1}^{N} a_i y_i = 0$. After solving a_i using the dual form (2.20), w and b can be solved as $w = \sum_{i=1}^{N} a_i y_i x_i$ and $b = y_i - w^T\phi(x_i)$. SVM finds a decision boundary that gives the smallest generalization error by maximizing the margin. More information about the classification using the SVM can be found in [117].

The nonlinear classification problems are separated using kernel tricks. Different types of kernels which are used in SVM models, include linear, polynomial, radial basis function (RBF), sigmoid and chi-square (χ^2):

- Linear: $k(x,y) = \mathbf{x}^T\mathbf{y}$
- Polynomial: $k(x,y) = (1+\gamma\mathbf{x}^T\mathbf{y})^d, \ \ \gamma > 0$
- RBF: $k(x,y) = e^{-\gamma||\mathbf{x}-\mathbf{y}||^2}, \ \ \gamma > 0$
- Sigmoid: $k(x,y) = \tanh(1+\gamma\mathbf{x}^T\mathbf{y}), \ \ \gamma > 0$
- Chi-square: $k(x,y) = e^{-\gamma\sum\frac{(\mathbf{x}-\mathbf{y})^2}{2(\mathbf{x}+\mathbf{y})}}, \ \ \gamma > 0$

2.4 TWA Analysis Methods

Since Adam's rediscovery on μ-TWA [79], there are a number of methods that have been proposed for automatic TWA analysis. These methods range from the widely-used spectral method [88] to the recent non-parametric signal processing technique [76] and template matched-filter based scheme [77]. Earlier to the year 2005, criteria for the TWA analysis are diverse. In 2005, Martínez and Olmos delivered an excellent classification with a broad review on TWA analysis in [74], where a common framework to describe the methodological principles of TWA analysis was proposed. Instead of reviewing those methods again, in this section, we will review and discuss the recent approaches in the last decade with two classical methods, the spectral method [88] and the modified moving average method [89]. Although the later method is performed in temporal domain, it has been reviewed and

put in this chapter because of its use (TWA estimation step) in Chapter 5. Table 2.3 presents a quick summary of these methods.

2.4.1 Spectral method

Smith et al. [88] first proposed the spectral method (SM) in 1988. The aligned ECG beats are used to generate beat-to-beat series ($\mathbf{X}$) with the amplitudes of corresponding points in consecutive ST-T complexes. Then, this series of amplitude fluctuations are subjected to Fourier analysis. As the spectrum is based on measurements taken once per beat, its frequencies are in units of cycles per beat (cpb). The frequency that corresponds to an oscillation occurring on every other beat is 0.5 cpb, and is referred to as the alternans frequency. Mathematically, The global detection statistic of the TWA component is given as

$$\begin{aligned} Z_l &= \frac{1}{N}\sum_{n=0}^{N-1} z_l(n) \\ &= \frac{1}{N}\sum_{n=0}^{N-1}\Big(\frac{1}{K}|STFT\{x_{k,l}(n)\}|^2_{f=0.5}\Big) \end{aligned} \tag{2.21}$$

where $z_l(n)$ is the individual statistics, K is the number of beats under analysis, N is the number of samples in ST-T complex. Detection is performed by means of a significance measure called the TWA Ratio (TWAR), which is calculated as the ratio of alternans power divided by the standard deviation of the noise. TWAR, mathematically, is given as

$$TWAR = \frac{Z_l - \mu}{\sigma} \tag{2.22}$$

where μ and σ are the mean and the standard deviation of the spectral noise measured in the band, typically around 0.4 cpb. TWA is considered to be present if TWAR ≥ 3.

The global TWA amplitude is estimated as the squared root of the alternant power and is given as

$$V_l = \sqrt{Z_l - \mu} \quad (\text{in } \mu\text{V}). \tag{2.23}$$

2.4.2 Modified moving average method

Nearing and Verrier [89] proposed the Modified Moving Average (MMA) method in 2002. The analysis is performed in the temporal domain. First, the alternate ECG beats are classified into two streams, A for even and B for odd ECG beats. The modified moving average complexes for both even and odd

beats are computed as [74]

$$\bar{A}_l(n) = \bar{A}_{l-1}(n) + g\Big(\frac{(A_{l-1}(n) - \bar{A}_{l-1}(n))}{8}\Big)$$
$$\bar{B}_l(n) = \bar{B}_{l-1}(n) + g\Big(\frac{(B_{l-1}(n) - \bar{B}_{l-1}(n))}{8}\Big) \tag{2.24}$$

where $l = 1, 2, \cdots K/2$ and n represents number of samples in a beat. The complexes are initialized with first even and odd beats as $\bar{A}_1(n) = A_1(n)$ and $\bar{B}_1(n) = B_1(n)$, respectively. The nonlinear limiting function $g(x)$ is given as

$$g(x) = \begin{cases} -K, & \text{if } x < -K \\ x, & \text{if } |x| \leq K \\ K, & \text{if } x > K \end{cases} . \tag{2.25}$$

The global detection statistic of the TWA component is defined as

$$Z_l = \max_n z_l(n) = |\bar{A}_l(i) - \bar{B}_l(i)| \tag{2.26}$$

where $z_l(n)$ represents the TWA amount at the lth beat and is calculated as the absolute difference between even and odd computed complexes. The MMAM does not include a detection stage, but analyzes TWA as a continuous variable along the complete ECG.

2.4.3 Recent methods for TWA analysis

This section describes the most relevant recent techniques for TWA analysis methods. Among the recent TWA analysis methods, we can find different approaches that include TWA analysis in multilead ECG using PCA [59] and πCA [95], nonparametric signal processing [76], tensor-based TWA detection [93], template matched-filter detector [77].

Monasterio et al. [59] proposed a multilead TWA analysis scheme using the principal component analysis (PCA). The basic motive of this article was to improve the TWA analysis performance by exploiting the spatial redundancy of MECG using PCA. In this method, the ECG signals are preprocessed, and then a fixed interval of 350 ms from ST-T complexes are selected for TWA analysis. The matrices containing ST-T samples of K number of beats are concatenated to form the data matrix

$$\mathbb{X} = [\mathbf{X}_0 \;\; \mathbf{X}_1 \;\; \cdots \;\; \mathbf{X}_{K-1}] \tag{2.27}$$

where $\mathbf{X}_k$ contains kth beat ST-T samples of all leads, $\mathbf{X}_k = [x_{k,1} \;\; x_{k,2} \;\; \cdots \;\; x_{k,L}]$, and L is the number of leads. Then the matrix $\mathbb{X}$ is detrended to cancel the background ST-T complexes. Detrending filter computes the difference between consecutive complexes. The resulted matrix ($\mathbb{X}'$) after detrending

Table 2.3: Summary of reviews on TWA analysis methods, N.S.: Not Specified

Methods	Preprocesing				TWA analysis		Remarks
	Linear Filtering	Baseline wander	QRS detection	Segmentation & alignment	Detection Technique	Estimation Technique	
SM [88] 1988	DC-360 Hz	block interpolation	matched filter	QRS (150 ms) and ST-T (225 ms). ST-T alignment	periodogram		
CM 1991	DC-60 Hz	cubic splines	interpolated derivative	ST-T segmentation ST-T alignment	zero-crossing counting		
MMAM [89] 2002	DC-50 Hz	cubic splines	N. S.	ST-T segmentation N. S.	non-linear moving average		
Burattini 2009	LPF, $F_c = 35Hz$			T-wave (160 ms)	Above three classical techniques		A comparative analysis was presented
multi-PCA [59] 2009	LPF, $F_c = 125Hz$	cubic splines	wavelet-based ECG delineator	ST-T (350 ms) N. S.	PCA-based transform	MLE	Able to analyze TWA in multilead ECG data. No lead-wise TWA analysis.
muti-πCA [95] 2010	LPF, $F_c = 15Hz$	cubic splines	wavelet-based ECG delineator	ST-T (350 ms) N. S.	periodic component analysis based transform	MLE	Overcome multi-PCA by separating TWA from non-alternant components. Presence of TWA in multilead ECG was projected into the first transformed lead, hence no lead-wise analysis
Non-parametric [76] 2014	LPF, $F_c = 50Hz$	LPF with spline interpolation	BPF with adaptive threshold	RR-fixed & RR-adjusted T-wave	subtraction of odd & even beats, followed by periodogram	MLE	Uses number of stages for TWA analysis. Inclusion or exclusion of certain stages may alter TWA analysis for a certain database.
Tensor-based [93] 2014	N. S.	cubic splines	wavelet-based ECG delineator	T-wave (250 ms)	Tensor decomposition, followed by periodogram	Not estimated	Limited TWA analysis No TWA estimation.
TMFD [77] 2014	N. S.	N. S.	wavelet-based ECG delineator	ST-T (300 ms) N. S.	Template matched filter detector	MLE	

is transformed using PCA. The transformation matrix is obtained by solving (2.8) where the sample covariance matrix is replaced with the sample correlation matrix $\hat{\mathbf{R}}_{\mathbb{X}'} = \frac{1}{(K-1)N}\mathbb{X}'\mathbb{X}'^{T}$. Then TWA detection is confirmed from the transformed data $\mathbb{Y}(= \mathbf{V}^{\mathbf{T}}\mathbb{X})$ using generalized likelihood ratio test (GLRT) statistic [74, 91]. A lead-wise TWA analysis (estimation) has not been studied in this method.

A multilead TWA analysis scheme using periodic component analysis (πCA) was also proposed by the same authors in [95]. To separate TWA from non-alternant components, the variance criterion of PCA is replaced by the periodical structure criterion to enhance the TWA analysis. Like to PCA method, steps from preprocessing to detrending of ST-T complexes remain same, except in evaluating the transformation matrix. The transformation matrix $\mathbf{V}$ is chosen as the eigenvector matrix of $(\mathbf{A}_{\mathbb{X}'}(m), \mathbf{R}_{\mathbb{X}'})$. The sample correlation matrix $(\mathbf{R}_{\mathbb{X}'})$ is defined earlier, and the spatial correlation of $(\mathbb{X}^{(m)'} - \mathbb{X}')$ is given as $\mathbf{A}_{\mathbb{X}'}(m) = \frac{1}{(K-1)N}(\mathbb{X}^{(m)'} - \mathbb{X}')(\mathbb{X}^{(m)'} - \mathbb{X}')^{T}$. Here, the matrix $\mathbb{X}^{(m)'}$, an equivalent of $\mathbb{X}'$, is generated by sliding the analysis window *m* beats forward. In this method, the transformation $\mathbb{Y}\ (= \mathbf{V}^{\mathbf{T}}\mathbb{X})$ projects the most periodic component into the first row of $\mathbb{Y}$. The limitation with this method is that it cannot be used to determine lead-wise TWA analysis. This is because the TWA, if present, is projected into the first transformed lead.

A tensor based detection of TWA in MECG data was proposed in [93] where MECG tensor was decomposed using Canonical decomposition. This method is based on extracting information from the time-domain T-wave signal and has been tested with few datasets where either macroscopic TWA or no sign of TWA are considered. It requires to find exact locations of fiducial points (off-set and on-set of ST-segment and T-wave) while dealing with time-domain methods. Also a benchmark evaluation on study for TWA detection has not been presented in this work.

In 2014, Goya-Esteban et al. [76] proposed nonparametric signal processing method for validating TWA analysis. This method proposed a systematic methodology for optimizing global performance of TWA analysis systems. For this purpose, a set of decision statistics were proposed to evaluate the performance, and a nonparametric hypothesis test was used to make system decisions. Both temporal and spectral methods were analyzed.

The template matched-filter detector (TMFD) was proposed by Bashir et al. [77] recently in 2014. This method is based on alternant energy within the repolarization complexes. After QRS-complex and T peak detection, beats are aligned over the fiducial points. Then ST-T segmentation is carried out. After that, these ST-T complexes are modeled as sum of signal and noise.

2.5 ECG Databases

In this thesis, two databases, namely the PTB diagnostic ECG database and the TWA/CinC challenge database are used for the evaluation of the methods which will be discussed in subsequent chapters.

2.5.1 PTB database

The PTB diagnostic ECG database was compiled by the National Metrology Institute of Germany. It contains 549 records of 290 subjects of different diagnostic classes. There is no clinical summary for 22 subjects. Rest 268 subjects are classed as follows: myocardial infarction (148), cardiomyopathy (18), bundle branch block (15), dysrhythmia (14), myocardial hypertrophy (7), valvular heart disease (6), myocarditis (4), healthy control (52), and others (4). Each record includes 15 continuous-recorded signals: the conventional 12 leads and 3 Frank leads. Each signal is digitized at 1000 samples per second, with 16 bit resolution. This database contains 52 healthy subjects' data with each having one to three records. Each signal is digitized at 1000 samples per second, resolution of 16 bit with 0.5 μV/LSB. But, to keep a constant sampling frequency over other databases considered in this work, we resampled each ECG signal to 500 Hz. Only eight independent leads (V1, V2, $\cdots$, V6, I, II) were processed.

In this thesis, the analysis of this database (selected records depending on the requirement) using MSVD, MHOSVD, and MAS-MHOSVD is reported in Sections 3.3, 4.4, 4.5, 5.3, and 5.5 as an example of application to a publicly available dataset.

2.5.2 TWA/CinC challenge database

This database is equipped with 100 multilead ECG records. Since records are collected from various databases of physionet, these have been resampled and scaled at 500 Hz with 16 bit resolution over a $\pm$32 mV range, to present them in a uniform format. The approximate duration of these records are 2 minutes. The subjects include patients with myocardial infarctions, transient ischemia, ventricular tachyarrhythmias, and other risk factors for sudden cardiac death, as well as healthy controls and synthetic cases with calibrated amounts of TWA. These 100 records include 2-, 3-, and 12-lead ECGs.

The analysis of this database in terms of TWA analysis using MAS-MHOSVD is reported in Sections 5.4 and 5.5 as an example of application to a publicly available dataset.

2.6 ECG Performance Evaluation Measures

2.6.1 Distortion measures

Cardiac signal processing aims at extracting significant information from signals for diagnosis, therapy and monitoring. The ECG signal processing should not be done at the cost of clinical significant information and relative diagnostic features. Hence, it is important to measure any distortion of diagnostic features. Distortion measures are classified in two ways: 1) subjective error measures, 2) objective error measures. In subjective measures, signal quality is evaluated by visually inspecting amplitudes, durations and shape of the diagnostic features. Cardiologists/experts give their opinion on diagnostic feature qualities according to mean opinion score (MOS) scale. The MOS is a mapping of the level of diagnostic features of the ECG signal into either descriptive terms like bad, not bad, good, very good and excellent or into equivalent numerical ratings from 1-5. Finally, the scores are averaged across the subjects to obtain the final MOS value. This measure is correlated with the diagnostic information in the signal but it is time-consuming and expensive. On the other hand, the objective error measures are classified as either diagnostic or non-diagnostic distortion measures [96]. In this thesis work, we have used two objective, non-diagnostic (e.g. PRD) and diagnostic (e.g. WDD and WEDD), distortion measures.

- *Percentage Root mean square Distortion (PRD)*

  PRD is the most widely used method for its simplicity structure and is given by:

$$PRD = \sqrt{\frac{\sum_{n=1}^{N}(x(n) - \tilde{x}(n))^2}{\sum_{n=1}^{N} x(n)^2}} \times 100 \tag{2.28}$$

  where N is the number of samples, $x(n)$ and $\tilde{x}(n)$ are the original and compressed signals, respectively.

  Although PRD has been widely used for distortion measures, PRD may not be a good measure of quality of the compressed signal. Also, a low PRD value does not necessarily mean clinical acceptance

- *Weighted Diagnostic Distortion (WDD) [118]*

  Zigel et al. [118] proposed the WDD measure to access the relative preservation of the diagnostic information in the compressed signal. It compares the PQRST morphological features of the original and the compressed signals. The WDD measure uses a diagnostic feature vector that consists of 18 features (six each from durations, amplitudes and shapes of morphological features). Figure 1.1 shows some amplitude and duration of the morphological features. The

WDD (in percentage) is defined as

$$WDD(\beta, \hat{\beta}) = \Delta\beta^T \cdot \frac{\Lambda}{tr[\Lambda]} \cdot \Delta\beta \times 100 \tag{2.29}$$

where β and $\hat{\beta}$ denote the diagnostic feature vectors of the original and the compressed signal, respectively. $\Delta\beta$ is the normalized difference vector and Λ is a diagonal weighting matrix.

Although the WDD measure correlates well with visual inspection, it suffers from high computational complexity due to the requirement of accurate evaluation of all diagnostic features and the calculation of optimal weights for the significant features. Also, the nonstationary nature of ECG signal and the artifacts may lead to a false detection of morphological features. The source error due to the classification and the comparison of irregularity of the wave shapes may degrade the accuracy of the WDD measure.

- *Wavelet Energy-based Diagnostic Distortion (WEDD) [96]*:
  In wavelet domain, the WEDD measure is defined as

$$WEDD = \sum_{j=1}^{M+1} w_j^{'} WPRD_j \tag{2.30}$$

where $w_j^{'}$ is the weight calulated based on energy in a subband and is defined as

$$w_j^{'} = \frac{\sum_{k=1}^{N_j} w_{(j,k)}^2}{\sum_{j=1}^{M+1}\sum_{k=1}^{N_j} w_{(j,k)}^2} \tag{2.31}$$

$$WPRD = \sqrt{\frac{\sum_{k=1}^{N_j}(w_{j,k} - \tilde{w}_{j,k})^2}{\sum_{k=1}^{N_j} w_{j,k}^2}} \times 100 \tag{2.32}$$

where $w_{j,k}$ is the original wavelet coefficient, $\tilde{w}_{j,k}$ is the filtered wavelet coefficient and N_j is the number of coefficients within subband j.

2.6.2 Classification performance measures

For evaluation of the classifier performance, different parameters like sensitivity, specificity, and accuracy [119] are measured by comparing the actual and predicted output. Sensitivity (Sen) is the probability that refers to the positive test result of MI, and is given as

$$Sen(\%) = \frac{TP}{TP + FN} \times 100 \tag{2.33}$$

It shows how good the classifier is at discriminating the MI cases. Specificity (Spe) is the probability that refers to the negative outcomes of MI, and is calculated as

$$Spe(\%) = \frac{TN}{FP + TN} \times 100 \tag{2.34}$$

It suggests how good the classifier is at identifying normal conditions. Accuracy (Acc) of a classifier represents the proportion of true results, and is calculated as

$$Acc(\%) = \frac{TP + TN}{TP + FP + FN + TN} \times 100 \tag{2.35}$$

where TP, FP, TN and FN are true positives, false positives, true negatives and false negatives.

2.7 Motivation of the Thesis

Recent advances in digital technologies have influenced the designing of ambulatory or remote or cloud-based ECG monitoring systems that can diagnose the cardiac patients effectively. These systems not only require large memory for storing the ECG data but also need to send instant feedback to the cardiac patients [120]. For this, the incoming patient data has to be tested with the large database at the test-centers. A fast, accurate detection and instantaneous reply with effective memory requirement are some elemental concerns in these systems. It is therefore necessary to extract discriminant features from the reduced dimension MECG data.

Simultaneous study on the spatio-temporal dynamics of heart may reveal extra information that can enhance performances of different ECG/MECG data processing applications. It is, however, evident from the literature that most of the methods study temporal (either intra-beat or inter-beat) correlation of the ECG signal, and very few consider two types (both intra- and inter-beat) of correlations. Two issues in these methods are: 1) to exploit both types of correlations, a 1-D ECG signal is converted into a 2-D matrix, 2) preservation of diagnostic information of ECG morphological features need to be improved. The recent works [16,68] were proposed to solve these issues, yet exploited only the spatial correlation of MECG data.

In another perspective, most of the existing ECG feature extraction methods for MI classification are unable to reflect the global ECG information completely. Physicians diagnose the MI patients based on multiple ECG cycles and multiple ECG leads. Time-domain-based ECG/MECG feature extraction techniques, for example, as in [66] are time consuming and may not perform better under noisy conditions. Also, some methods do not treat ECG morphological features properly. A recent transform-domain-based technique considers both multiple leads and cycles for the ECG feature ex-

traction [68]. However, simultaneous analysis of both temporal and spatial correlations has not been addressed in the literature.

The later stage of acute MI may cause irreversible heart tissue damage which may lead to inevitable sudden cardiac death [121, 122]. After detection of acute MI and localizing position of infarct in the myocardium wall, the *progression of MI in different leads* using TWA analysis can be a prognosticative study, which is a limitation in literature studies. Another limitation regarding TWA analysis is that, there is still need of robust methods which can characterize the presence of TWA and measure its magnitude more accurately in noisy conditions. In a recent work, TWA analysis was improved by exploiting spatial correlations using PCA or πCA. It is expected that the performance can be improved by developing such techniques which account both temporal and spatial correlations.

The data dependent transformation techniques that account *simultaneous* analysis of information present in multiple cycles and multiple leads of MECG data can be a promising direction to handle these issues. These methods extract information differently depending on the way ECG signal(s) is/are arranged. The wavelet coefficients of all leads at a particular scale show similarity in terms of morphology and beat patterns, i.e. they are spatially and temporally correlated (Figure 2.1). So, there is a scope of applying multivariate data analysis at a wavelet scale by arranging the wavelet coefficients as subband data matrix. Also, it is anticipated to have a similar pattern of multiscale energy for these matrices. Based on these information, it is expected that SVD and its higher derivative, higher-order SVD (HOSVD), can able to exploit different types of correlations. Furthermore, the diagnostic information concerning the ECG morphological features can be handled effectively, if multiscale decomposition and synthesis are added to these schemes. This motivates to develop multiscale SVD (MSVD) and multiscale HOSVD (MHOSVD) for MECG data. The hypothesis of this work is that, issues addressed in this thesis can be improved by exploiting all types of correlations using SVD and HOSVD in multiscale domain.

2.8 Work Plan of the Thesis

The contribution of the present thesis is schematized in Figure 2.2. The main outer circle represents different ECG/MECG data processing methods, whereas the inner one represents works carried out in this thesis. Six ellipses represent six applications of ECG signal processing discussed earlier in this chapter. It is worth noting that although these applications are not independent and should therefore exhibit some overlap, this is not displayed in this figure for the sake of clarity. Since noise elimination is considered as a preprocessing tool in today's any ECG processing and no specific techniques have

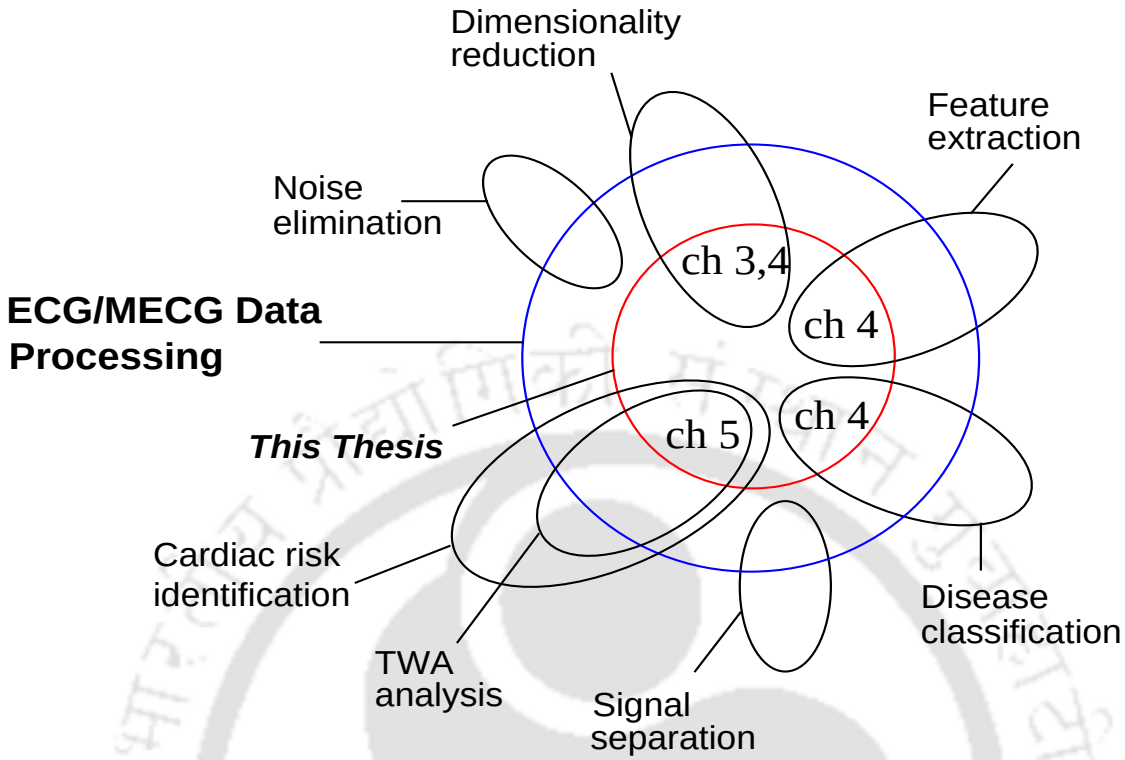

Figure 2.2: Schematic representation of the contribution of the thesis.

been proposed for noise elimination in this thesis, it is placed outside to the circle 'this thesis'.

The proposed investigations in this thesis, in short, are planned as:

- To develop a fast processing and storage efficient method: SVD models two-factor (both row- and column space) variations of the data. SVD can be directly applied to the MECG data without any beat delineation and period normalization as the timing information across all leads is same. This may help exploit both intra-beat and inter-lead correlations of the MECG data. In addition, to make the algorithm execute faster, the correlated wavelet coefficients can be used as the elements of subband matrices under consideration. In Chapter 3, the proposed MSVD method is applied to these subband matrices. The MSVD on multivariate data like MECG reduces dimension and removes the redundant information present in the original data. The proper selection of SVs gives fair representation of original data, and the selected SVs represent the diagnostic information. After reconstruction of MSVD processed multilead signals, distortion measures are evaluated.

- To extract features for detection and localization of MI: Detection and localization of MI is performed by extracting features and providing these to a classifier, which classifies the incoming signal to different classes. Chapter 4 attempts to exploit all three types of correlations simultaneously for dimensionality reduction and feature extraction. Feature extraction is related to

dimensionality reduction, and the later process helps select discriminative features and reduce feature set dimension. It is not possible to extract these correlations efficiently from the 2-D represented MECG data. The data need to be represented in a third-order tensor form. Like to the earlier case, MHOSVD is applied to the subband tensors. The mode SVs (MSVs) at different wavelet scales not only capture the energy of the signal but also they vary according to diagnostic information. The significant MSVs and their corresponding orthonormal vectors represent the diagnostic information of the original data. After dimensionality reduction, mode features, derived and selected from the low frequency subbands, are used as the features to the SVM classifier to separate MI from healthy signals.

- To study the progression of MI in post-MI cases using TWA analysis: TWA measure can be used to identify post-MI patients at increased risk for arrhythmic events. Chapter 5 proposes a new method to improve the TWA analysis performance by exploiting both spatio-temporal correlations using HOSVD. As stated in [74], validation of a new technique is a prior step to clinical evaluation of any kind of risk stratifier. Hence, first, the method is validated by detecting and estimating TWA amounts in semi-synthetic and real datasets. Multiscale analysis-by-synthesis (MAS) of lower frequency subbands can be used to get the T-wave information accurately. Unlike to the earlier two cases, here, HOSVD is applied to the subband reconstructed signals rather to the wavelet coefficients.

3

Multiscale SVD Analysis for Multilead ECG Data

Contents

The purpose of this chapter is to introduce multiscale singular value decomposition (MSVD) for the MECG data. The SVD is an indispensable statistical technique used in many scientific fields, such as neuroimaging [123], complex systems [124], text reconstruction [125], genetics [126], and signal processing applications that include ECG, EEG, speech and image processing systems. Also, different extensions or modifications of SVD like sparse SVD [127], HOSVD [128], etc. were developed in the past. The SVD is so broadly used because it is the core of many multivariate statistical techniques. It transforms the data matrix by maximizing both row- and column-wise variations and hence exploits two types of correlations. In temporal domain, SVD transforms MECG data dimension (leads$\times$samples) to a new space by maximizing both variations and reduces its dimension by considering most significant singular values (SVs). The very first few SVs capture the correlation between the leads (row-wise) and samples (column-wise).

In wavelet domain, it is shown in Section 2.1.2 that both spatial and temporal correlations are reflected in the wavelet coefficients of all leads at each scale. The earlier work [107] attempted on exploitation of only spatial correlation of the MECG data using PCA in multiscale domain. Due to the inherent property (modeling two-factor variations) of the SVD, morphological features of the MECG data in different wavelet subbands can be analyzed using SVD. For implementation of SVD, single lead ECG samples are represented in a 2-D matrix data, where successive ECG periods are arranged in rows or columns of the 2-D matrix. However, the MECG is a 2-D matrix data, and the timing information across all the leads is same. Therefore, SVD can be directly implemented on this data without any period normalization. Such an implementation can help exploit both intra-beat and inter-lead correlations, and this is the motivation of this present work. The MRA property has been added prior to SVD so that morphological features can be handled effectively.

Also, a variable thresholding technique for selecting SVs of subband matrices is proposed. This technique selects SVs based on diagnostic importance of subbands. In this way, diagnostic fidelity of the MECG data is retained. For validation purpose, both objective and subjective distortion measures are evaluated. Furthermore, the effectiveness with regard to fast processing nature of the proposed method for WBSN-enabled applications is studied. Recently, compressive sensing (CS) based compression methods [101, 129–131] for single lead ECG and fetal ECG signals were evaluated in WBSN system. The proposed method is validated by comparing with these methods.

Rest of the Chapter is organized as follows: A general description on SVD for the MECG data and the way it exploits two types of correlations are discussed in Section 3.1. The proposed MSVD method for the MECG data and a new thresholding technique for SVs are presented in Section 3.2. Section 3.3

describes the compression performance and comparison with existing methods. Simulations study on transmission of the MECG data by encoding generated bit streams for WBSN applications is presented in Section 3.4. Also the computational complexity of the proposed method is carried out.

3.1 SVD on Multilead ECG Data

The SVD was applied on both single lead in [21, 22] and multilead in [22] using cut-and-align and lead piling process. With single lead ECG, both intra- and inter-beat correlations have been exploited. In [22], efforts for exploiting inter-lead along with intra-beat correlation were made but using a complex lead piling process. SVD can be applied directly on multivariate the MECG data matrix as the timing information across all the leads is same. The the MECG data matrix $\mathbf{X}_{m\times p}$ can be represented as

$$\mathbf{X} = \begin{bmatrix} x_{11} & x_{12} & \cdots & x_{1p} \\ x_{21} & x_{22} & \cdots & x_{2p} \\ \vdots & \vdots & \ddots & \vdots \\ x_{m1} & x_{m2} & x_{m3} & x_{mp} \end{bmatrix} \tag{3.1}$$

where x_{ls} is the sth sample of the lth lead ($1 \leq l \leq m$ and $1 \leq s \leq p$), and m and p represent number of leads and corresponding samples in each lead, respectively. In this matrix, leads are represented in rows whereas samples of each lead are that in columns. We can say that rows depict temporal information of the heart and each column gives an idea about spatial information at a particular instant as elements of a column are from different sections of the heart.

To demonstrate the presence of inter-lead and intra-beat correlations in the MECG data, correlation coefficients between samples along row-wise and column-wise are evaluated. Table 3.1 shows correlation coefficients that demonstrate inter-lead correlation. Correlation coefficient values closer to ± 1 indicates strong relationship between two leads like in between V1 and V2 (0.863), V2 and V3 (0.925), V1 and V5 (-0.802), V1 and V6 (-0.943), I and II (0.898), and so on. This entails that there are strong inter-lead correlations among some leads. Although it is not always the same pattern observed in each and every ECG data, one can observe the presence of high correlations among the leads. In other case, the column-wise correlation coefficients are shown in Figure 3.1. Subplots of this figure correspond to an ECG signal that is shown in Figure 3.2 (left panel, Lead I, dataset: *s0005_rem*, PTB database). It is not possible to show/tabulate all column-wise correlation coefficients due to the large size of the correlation matrix ($p \times p$). Hence, histogram plots of correlation coefficients for two segments (15 samples from a section of P-wave and rest 15 samples that from QRS segment) are shown. Each

Table 3.1: Inter-lead correlation of the MECG data

	V1	**V2**	**V3**	**V4**	**V5**	**V6**	**I**	**II**
V1	1	0.863	0.615	-0.135	-0.802	-0.943	-0.850	-0.934
V2	0.863	1	0.925	0.351	-0.395	-0.671	-0.498	-0.732
V3	0.615	0.925	1	0.676	-0.0269	-0.363	-0.169	-0.441
V4	-0.135	0.351	0.676	1	0.676	0.360	0.526	0.301
V5	-0.802	-0.395	-0.0269	0.676	1	0.926	0.956	0.850
V6	-0.943	-0.671	-0.363	0.360	0.926	1	0.945	0.944
I	-0.850	-0.498	-0.169	0.526	0.956	0.945	1	0.898
II	-0.934	-0.732	-0.441	0.301	0.850	0.944	0.898	1

histogram plot corresponds to the correlation of a sample (say, 51st sample of P-wave) to all sample values of the ECG signal. For example, correlation coefficients between 51st sample of P-wave and all samples of lead I are calculated and are shown in 1st subplot of this figure. Similar procedure is followed for other above said samples and shown in rest of the subplots. High amount of correlation is observed around isoelectic line and low frequency regions. From the first 25 subplots, it is clear that amount of redundant information is high as correlation coefficient value is close to ± 1 for most of the samples. It indicates strong presence of intra-beat correlation in the low-frequency regions. In some subplots among other 15 plots, correlation coefficient value lies in the range -0.6 to 0.8 for most of samples, and we can say that amount of redundant information in the high-frequency region is low. This overall demonstrates presence of intra-beat correlations. These results correspond to a single beat of subject *s0005_rem* from PTB database.

It is expected that these two types of correlations can be exploited by applying SVD directly on the MECG data. As stated in Chapter 2, the key idea of the SVD is to project the MECG data to a new uncorrelated space by removing both row- and column-wise redundancies, without discarding any diagnostic information. Writing (2.10) again, SVD is an algebraic tool to deconstruct any given matrix $\mathbf{X}$ into its basic structure as

$$\begin{aligned} \mathbf{X}_{m\times p} &= \mathbf{U}_{m\times m}\mathbf{\Sigma}_{m\times p}\mathbf{V}^T_{p\times p} \\ &= \mathbf{U}_{m\times m}\hat{\mathbf{\Sigma}}_{m\times m}\hat{\mathbf{V}}^T_{m\times p} \end{aligned} \tag{3.2}$$

where $\mathbf{U}_{m\times m}$ and $\hat{\mathbf{V}}_{p\times m}$ are orthonormal matrices with rank equal to the original matrix $\mathbf{X}$, and $\hat{\mathbf{\Sigma}}_{m\times m}$ is a diagonal matrix with positive SVs. The vectors of $\mathbf{U}$ and $\hat{\mathbf{V}}$ are termed as the left and the right singular vectors and represent the column spaces and the row spaces of the MECG data, respectively [112]. In MECG case, if we consider m rows as observations and p columns as variables, the eigen

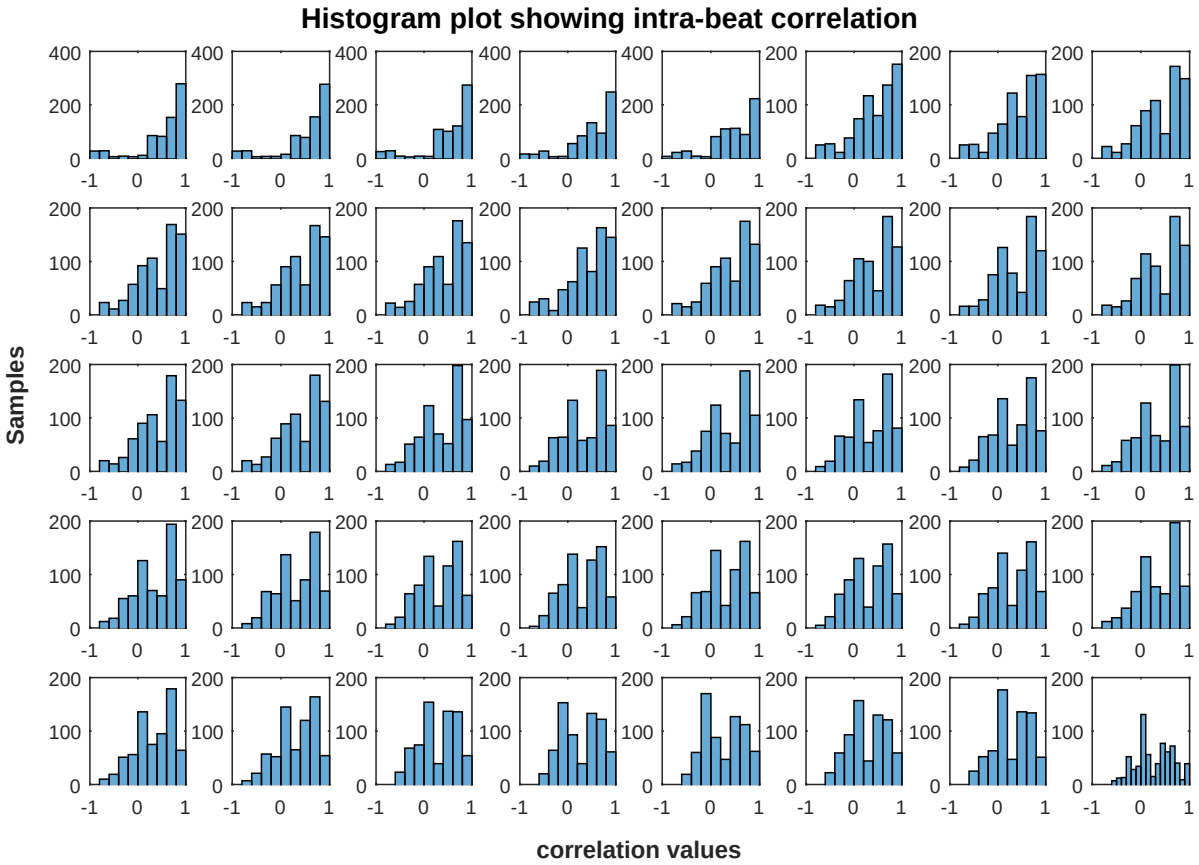

Figure 3.1: Histogram plots showing intra-beat correlations of 40 samples (25 samples are from P-wave region and 15 are from QRS-complex) Dataset: $s0005\_rem$, PTB Diagnostic Database

decomposition of the 'leads $\times$ leads' covariance matrix $\mathbf{R_{x1}} = \mathbf{X}\mathbf{X}^T$ results

$$\mathbf{R_{x1}} = \mathbf{X}\mathbf{X}^{\mathbf{T}} = \mathbf{U}\hat{\mathbf{\Sigma}}\hat{\mathbf{V}}^{\mathbf{T}}\hat{\mathbf{V}}\hat{\mathbf{\Sigma}}^{\mathbf{T}}\mathbf{U}^{\mathbf{T}} = \mathbf{U}(\hat{\mathbf{\Sigma}}\hat{\mathbf{\Sigma}}^{\mathbf{T}})\mathbf{U}^{\mathbf{T}} \tag{3.3}$$

Similarly, if we consider p columns as observations and m rows as variables, the eigen decomposition of the 'samples $\times$ samples' covariance matrix $\mathbf{R_{x2}} = \mathbf{X}^T\mathbf{X}$ results

$$\mathbf{R_{x2}} = \mathbf{X}^{\mathbf{T}}\mathbf{X} = \hat{\mathbf{V}}\hat{\mathbf{\Sigma}}^{\mathbf{T}}\mathbf{U}^{\mathbf{T}}\mathbf{U}\hat{\mathbf{\Sigma}}\hat{\mathbf{V}}^{\mathbf{T}} = \hat{\mathbf{V}}(\hat{\mathbf{\Sigma}}^{\mathbf{T}}\hat{\mathbf{\Sigma}})\hat{\mathbf{V}}^{\mathbf{T}} \tag{3.4}$$

From the above discussions, it is clear that the covariance matrix $\mathbf{R_{x1}}$ characterizes the inter-lead correlation. In this case, the SVs are computed for each sample. The left singular vector matrix $\mathbf{U}$ contains the eigenvectors of $\mathbf{X}\mathbf{X}^T$ corresponding to each SV. In other words, the $\mathbf{U}$ matrix contains the spatial information. Similarly, the covariance matrix $\mathbf{R_{x2}}$ characterizes the intra-beat correlation. In this case, the SVs are computed for each lead. The right singular vector matrix $\hat{\mathbf{V}}$ contains the eigenvectors of $\mathbf{X}^T\mathbf{X}$ corresponding to each SV. In other words, the $\hat{\mathbf{V}}$ matrix contains the temporal information i.e. the ME36 data matrix is encoded in the $\hat{\mathbf{V}}$ matrix [132]. To validate these, simulations on most of

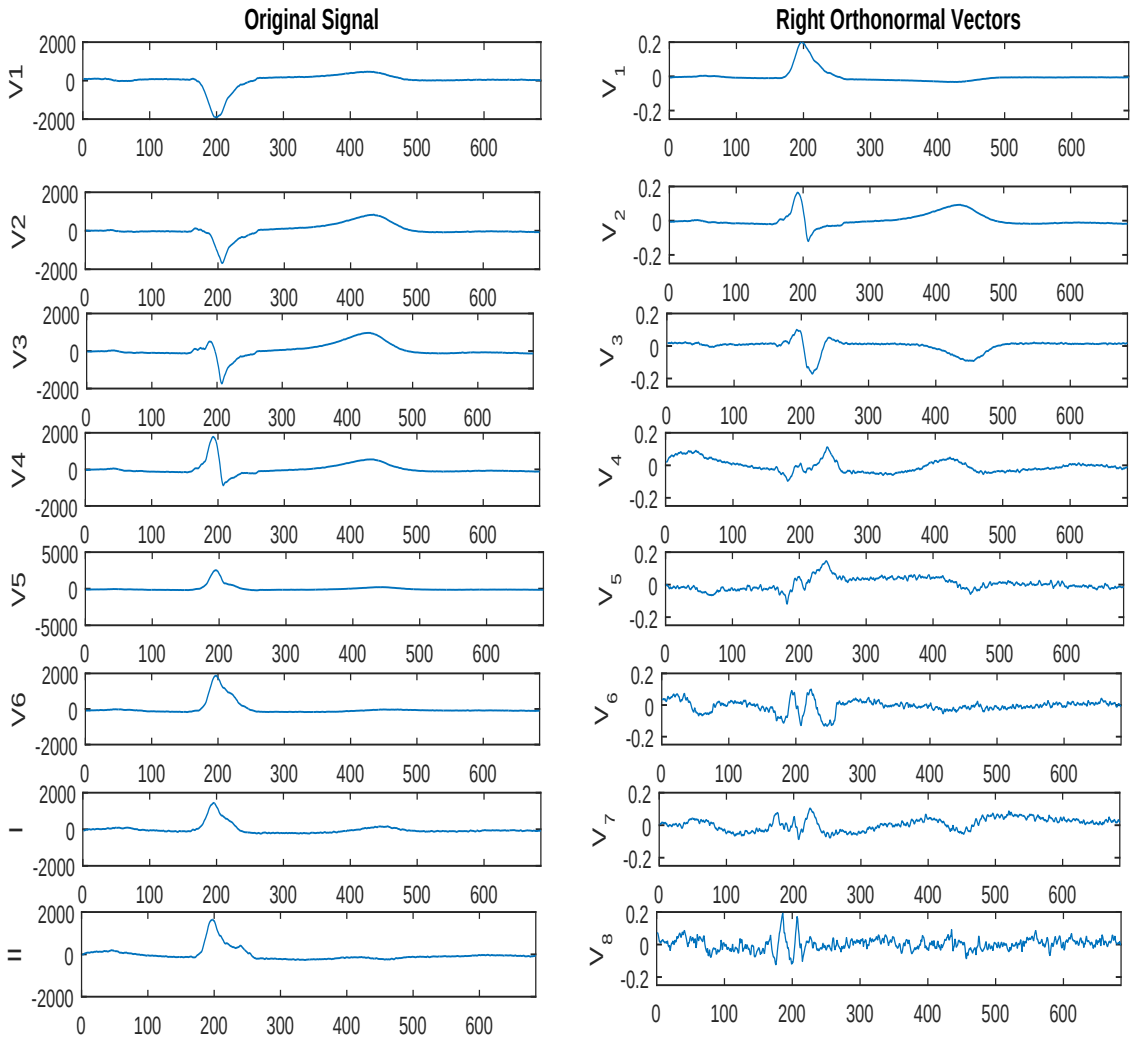

Figure 3.2: Plots of original and left orthonormal vectors. (a)-(h): V1−V6, I, and II, (i)-(p): Right orthonormal vectors after SVD. Dataset: *s0005_rem*, PTB Diagnostic Database. One should appreciate the differences in notations for leads (V1−V6) and orthonormal vectors (V_1−V_8).

the datasets were performed, and graphical results for a single dataset are presented here. Figure 3.2 shows plots of original leads of a real the MECG data and its orthonormal column vectors after SVD. Left panel corresponds to original leads whereas right panel that to right orthonormal vectors. Information in right orthonormal vectors $\mathbf{v}_i$ does not relate directly to original leads $\mathbf{x}_i$. Generally, first three to four left singular vectors concentrate maximum variance of data. However, subplots in right side of this figure suggest that, fifth, sixth and seventh right singular vectors contain some part of low frequency components from P- and T-waves. This proves that direct SVD application on time-domain data may not preserve diagnostic relevant information, which is stated earlier in this chapter. It is difficult to observe lead variations in left singular vector matrix and hence has not been provided here.

It is expected that higher correlations or redundancies with preservation of diagnostic information can

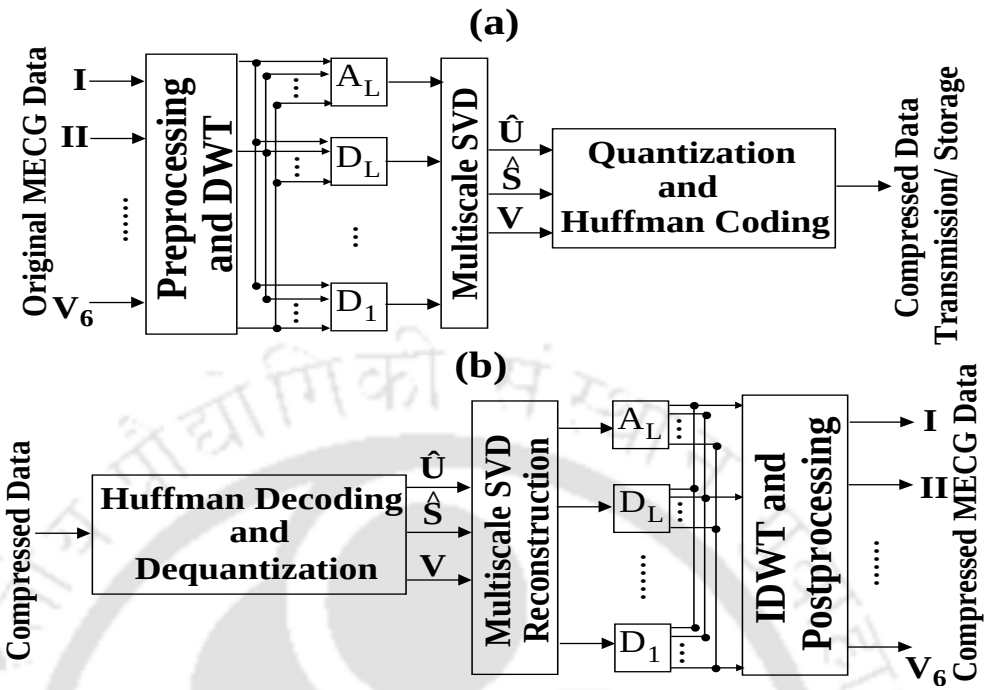

Figure 3.3: Block diagram of MECG correlation exploitation for (a) compression and (b) reconstruction process using MSVD.

be achieved if the MECG data is decomposed to multiscale levels using MRA, prior to applying SVD.

3.2 Proposed Multiscale SVD Method for MECG Data

In this Section, the MSVD-based scheme for simultaneous exploitation of both intra-beat and inter-lead correlations of the MECG data is proposed. As discussed in Chapter 1, correlation exploitation is carried out for various purposes, and dimensionality reduction is one of them. Figure 3.3 shows the block diagram of the proposed scheme. This method consists of preprocessing, MSVD using DWT, and coding. The MECG data is rearranged to get maximum correlation, first the six precordial leads ($V_1, \cdots, V_6$), then I and II [48]. The preprocessing stage prepares the ECG signal for posterior stages and includes operations such as baseline cancellation, amplitude normalization [9, 16]. Normalization guarantees that all significant coefficients be less than one. These operations alleviate further processing. The normalized amplitude factor can be stored or transmitted to the receiver site, if necessary, which is helpful during reconstruction. The proposed MSVD technique has three major steps: MSD of the MECG data, SVD on subband matrices and thresholding of the SVs to reduce dimensionality of orthogonal and SV matrices. Coding stage consists of quantization and Huffman encoding. A detail description on each stage is discussed below. Reconstruction consists of reverse process i.e. decoding, MSVD restoration using IDWT and postprocessing.

3.2.1 Multiscale subband matrix formation

The subband wavelet coefficients are spatially and temporally correlated (Section 2.1). Hence, without reconstructing subband signals, SVD is applied directly on the wavelet coefficients with a hypothesis that it will still exploit both intra-beat and inter-lead correlations.

In this work, dyadic DWT with Daubechies 9/7 Biorthogonal wavelet filters as the mother wavelet is used. It is implemented using a multiresolution pyramidal decomposition technique. The MRA property of DWT is applied to each lead of the preprocessed the MECG data ($\mathbf{X}_{m\times p}$) individually, where *m* and *p* represent number of leads and ECG samples of each lead, respectively. Daubechies 9/7 Biorthogonal wavelet filters are used for wavelet decomposition because of its linear phase and symmetric characteristic. Also these wavelets allow perfect reconstruction at the starting and ending of ECG frames [18]. Another advantage is that the shape of decomposed scaling and wavelet functions of these filters resemble with the ECG signal [133]. After decomposition, the wavelet transformed coefficients corresponding to a particular subband of each lead are arranged to form a subband matrix. This results in $L+1$ subband matrices, where L (2.7) is the number of decomposition levels. Based on different sampling frequencies, Al-Fahoum heuristically derived the value of L that satisfies the frequency span of the ECG morphological features [104]. However, a scientific proof on derivation of this information is not presented in [104] or in follow-up articles. The rationale behind this formula is presented in Appendix A. Above resulted $L+1$ subband matrices consist of one approximation subband matrix ($\mathbf{A_L}$) and L number of detail subband matrices ($\mathbf{D_L},\ \mathbf{D_{L-1}}, \cdots,\ \mathbf{D_1}$). Each row of these multiscale matrices contains grossly segmented information of the original signals. The dimensions of these subband matrices, $\mathbf{A_L}$ and $\mathbf{D_j}$, $j = L, \cdots 1$, are given as $m \times p/2^L$ and $m \times p/2^j$, respectively. The decomposition coefficient ($\mathbf{DEC}$) matrix is formed by uniting $\mathbf{A_L}$ and $\mathbf{D_L},\ \mathbf{D_{L-1}}, \cdots,\ \mathbf{D_1}$, and can be represented as

$$\mathbf{DEC}_{m\times p} = \left[\ \mathbf{A_L};\ \mathbf{D_L};\ \mathbf{D_{L-1}};\ \cdots;\ \mathbf{D_1}\ \right]^{\mathbf{T}}. \tag{3.5}$$

3.2.2 SVD on subband matrices

After constructing the subband matrices, each one is decomposed using SVD as follows

$$\begin{aligned} \mathbf{A_L} &= \mathbf{U_{A_L}}\mathbf{\Sigma_{A_L}}\mathbf{V}_{\mathbf{A_L}}^{T} \\ \mathbf{D_j} &= \mathbf{U_{D_j}}\mathbf{\Sigma_{D_j}}\mathbf{V}_{\mathbf{D_j}}^{T} \end{aligned} \tag{3.6}$$

where $\mathbf{U_{A_L}}, \mathbf{V_{A_L}}, \mathbf{U_{D_j}}, \mathbf{V_{D_j}}$, $j = 1, ..., L$ are unitary matrices and $\mathbf{\Sigma_{A_L}}, \mathbf{\Sigma_{D_j}}$ are SV matrices. The columns of $\mathbf{U_{A_L}}, \mathbf{U_{D_j}}$ and $\mathbf{V_{A_L}}, \mathbf{V_{D_j}}$ are left and right singular vectors of $\mathbf{A_L}$ and $\mathbf{D_j}$, respectively. The

left and right singular vectors are the basis functions that represent the lead-wise data and coefficient-wise variability in wavelet-domain, respectively. After applying the SVD on the multiscale matrices, it is expected that the grossly segmented morphological features do appear in the eigen space.

Let $\mathbf{U}$ contains the unitary matrices of all approximation and detail subband matrices i.e. $\mathbf{U} = [\mathbf{U_{A_L}}; \mathbf{U_{D_L}}; \cdots; \mathbf{U_{D_1}}]$, $\mathbf{U} \in \mathbb{R}^{(L+1)m \times m}$. As the singular value ($\mathbf{\Sigma}$'s) and the right singular vector ($\mathbf{V}$'s) matrices of different subbands have different dimensions, these can be concatenated by appending $p - p'$ number of zero column vectors to each, where *p'* is the number of wavelet coefficients in a particular subband. Hence, $\mathbf{\Sigma}$ and $\mathbf{V}$ can be represented as $\mathbf{\Sigma} = [\mathbf{\Sigma_{A_L}}; \mathbf{\Sigma_{D_L}}; \cdots; \mathbf{\Sigma_{D_1}}]$, $\mathbf{\Sigma} \in \mathbb{R}^{(L+1)m \times p}$ and $\mathbf{V} = [\mathbf{V_{A_L}}; \mathbf{V_{D_L}}; \cdots; \mathbf{V_{D_1}}]$, $\mathbf{V} \in \mathbb{R}^{p \times p}$, respectively. Each singular matrix of $\mathbf{\Sigma}$ has m nonzero values. For example, the approximation subband singular value matrix can be represented as $\mathbf{\Sigma_{A_L}} = [diag\{\sigma_{A_{L_1}}, \sigma_{A_{L_2}}, \cdots, \sigma_{A_{L_m}}\} : \mathbf{0}] = [\hat{\mathbf{\Sigma}}_{\mathbf{A_L}} : \mathbf{0}]$, $\sigma_{A_{L_1}} \geq \sigma_{A_{L_2}} \geq \cdots \geq \sigma_{A_{L_m}} > 0$. Consequently, the $p - m$ rows of the unitary matrix will have no effect in the product of unitary matrix with the singular value matrix (3.6). Hence, $\mathbf{V}$ can be replaced with $\hat{\mathbf{V}}$ by removing $p - m$ columns. The reduced SVD can be expressed as

$$\begin{aligned} \mathbf{A_L} &= \mathbf{U_{A_L}} \hat{\mathbf{\Sigma}}_{\mathbf{A_L}} \hat{\mathbf{V}}^T_{\mathbf{A_L}} \\ \mathbf{D_j} &= \mathbf{U_{D_j}} \hat{\mathbf{\Sigma}}_{\mathbf{D_j}} \hat{\mathbf{V}}^T_{\mathbf{D_j}} \end{aligned} \tag{3.7}$$

where $\hat{\mathbf{V}}_{\mathbf{A_L}}, \hat{\mathbf{V}}_{\mathbf{D_j}} \in \mathbb{R}^{p' \times m}$ and $\hat{\mathbf{\Sigma}}_{\mathbf{A_L}}, \hat{\mathbf{\Sigma}}_{\mathbf{D_j}} \in \mathbb{R}^{m \times m}$. The reduced right singular matrix is represented as $\hat{\mathbf{V}} = [\hat{\mathbf{V}}_{\mathbf{A_L}}; \hat{\mathbf{V}}_{\mathbf{D_L}}; \cdots; \hat{\mathbf{V}}_{\mathbf{D_1}}]$, $\hat{\mathbf{V}} \in \mathbb{R}^{p \times m}$. This reduction in the dimension of $\mathbf{V}$ helps improve the processing speed.

The DEC matrix is encoded in the $\hat{\mathbf{V}}$ matrix [112]. $\mathbf{U}$ represents the space onto which the DEC matrix in $\hat{\mathbf{V}}$ is projected i.e. it contains orthonormal singular vectors of the transposed DEC matrix [132, Ch. 5, pp. 151]. Dimension reduction in $\mathbf{U}$ and $\hat{\mathbf{V}}$ can be achieved by exploiting the inter-lead and the intra-beat correlations present in the wavelet transformed the MECG data. The truncation of σ_i's of each singular value matrix, on the basis of their energy message, induced to discard the redundant column vectors of $\mathbf{U}$ and $\hat{\mathbf{V}}$.

The energy of a data matrix is represented as the sum of squared SVs. The energies of the approximation and the detail subbands are hence given as $E_{A_L} = \sum_{i=1}^{m} {\sigma_{A_{L_i}}}^2$ and $E_{D_j} = \sum_{i=1}^{m} {\sigma_{D_{j_i}}}^2$, respectively. The relative energy of a subband can be used as a measure to discriminate ECG information and noise contained in the subbands. In this regard, multiscale relative energy density (MRED) for the approximation and the details subbands can be defined as

Table 3.2: Multiscale Relative Energy Density

Subbands	$\mathbf{A_6}$	$\mathbf{D_6}$	$\mathbf{D_5}$	$\mathbf{D_4}$	$\mathbf{D_3}$	$\mathbf{D_2}$	$\mathbf{D_1}$
Max. Freq. (in Hz)	3.906	7.812	15.625	31.25	62.5	125	250
Healthy	39.36	18.52	27.74	11.45	2.75	0.175	≈ 0
Pathological	45.53	20.58	19.77	11.21	1.82	1.089	≈ 0

values show the average MRED of 80 healthy (1^{st} row) and 469 pathological (2^{nd} row) datasets for PTB

$$MRED_{A_L} = \frac{E_{A_L}}{E_{A_L} + \sum_{j=1}^{L} E_{D_j}}$$
$$MRED_{D_j} = \frac{E_{D_j}}{E_{A_L} + \sum_{j=1}^{L} E_{D_j}} \tag{3.8}$$

Table 3.2 shows the average MRED values for different subband matrices. It is estimated for normal and pathological datasets. Decomposition level is chosen as $L = 6$. Maximum frequency of the subband matrices $\mathbf{A_6}, \mathbf{D_6}, \cdots, \mathbf{D_1}$ are 3.906, 7.812, ..., 250 Hz, respectively. The subband matrices $\mathbf{A_6}, \mathbf{D_6}, \cdots, \mathbf{D_3}$ together contribute 98.91% of total energy. It indicates that the energy content in these subband matrices is due to the presence of morphological ECG features. The frequency contents of D_1 and D_2 subbands are outside the normal ECG spectrum [96]. At the same time, the MRED value of $\mathbf{D_2}$ subband matrix for pathological cases (1.089) is high compared to normal cases (0.175). It may be due to pathological high frequency QRS components, and notches and slurs of J-point. Low or almost zero MRED values of $\mathbf{D_1}$ for both normal and pathological data are due to absence of the major diagnostic components. The dimension of these subband matrices may be truncated to eliminate redundancies and noise components. An optimal reduction or compression will, in turn, require a suitable threshold of the SVs.

3.2.3 Thresholding of singular values

By selecting the singular vectors corresponding to the K highest SVs, dimensionality reduction with maximum retention of the information could be achieved. These singular vectors form the bases of desired low dimensional subspace. Wei *et al.* [21] used a hard threshold technique for selecting SVs. Truncating SVs based on energy information of time-domain signal may lose ECG morphological features as discussed earlier in this section. This is also clearly reflected from the reconstructed ECG signals in [21, cf. Figs 8 and 12]. Later, some subband energy-based thresholding techniques were proposed [16, 18, 96, 97]. The relative diagnostic information across the subbands is assumed to

be constant [96, 97]. Challenge is still there to select the K number of SVs for different subband matrices such that pathological information is retained fully. In view of the relative significance of diagnostic information in subbands, a subband energy-based threshold for eigen values was proposed [16]. In that paper, the principal components (PCs) selected for high frequency subband matrices ($\mathbf{D_1}$, $\mathbf{D_2}$ and $\mathbf{D_3}$) are more compared to other subband matrices ([16, cf. TABLE II]) though these have less significant information. It requires more floating point operations if selected PCs are more from high frequency subbands. This is because number of wavelet coefficients in these subbands is more compared to low frequency subbands. It would be advantageous if number of PCs can be reduced from these high frequency subband matrices without disturbing diagnostic information. Also, it has been discussed in Table 1 that the relative energy of subbands varies in pathological conditions. Hence, in some sense, existing thresholding techniques are not based on the variation of relative energy across the subbands. It will be useful to have a threshold which can account for the variations in different subbands. Sharma et al. [16] proposed the AFEC thresholding technique to threshold the eigenvalues of different subbands (Ref: 2.16). To overcome the issues discussed above, in this work, a new thresholding technique based on multiscale root fractional energy contribution (MRFEC) is introduced with a purpose to threshold the SVs depending on the variation of energy in different subbands. The MRFECs of the Lth approximation and the jth details subband matrices are defined as

$$\eta_{A_L} = \left[\frac{1}{m}\left(\frac{\sum_{i=1}^{m}\sigma_{A_{L_i}}^2}{\sum_{i=1}^{m}\sigma_{A_{L_i}}^2 + \sum_{j=1}^{L}\sum_{i=1}^{m}\sigma_{D_{j_i}}^2}\right)\right]^{1/\nu} \tag{3.9}$$

$$\eta_{D_j} = \left[\frac{1}{m}\left(\frac{\sum_{i=1}^{m}\sigma_{D_{j_i}}^2}{\sum_{i=1}^{m}\sigma_{A_{L_i}}^2 + \sum_{j=1}^{L}\sum_{i=1}^{m}\sigma_{D_{j_i}}^2}\right)\right]^{1/\nu} \tag{3.10}$$

where ν is the threshold parameter, $\nu = 1,\ 2,\ 3,\ \cdots$. Due to energy variations in different subbands, the value of ν has been altered. The SVs are selected if they are greater than η_{A_L} or η_{D_j}. During thresholding process, the number of SVs selected depends on the value of ν. Figure 3.4 shows the average number of SVs selected for different value of ν. With increase in value of ν, the drop in selected SVs is quite high in case of high frequency subband matrices. For $\mathbf{D_1}$ $\mathbf{D_2}$ and $\mathbf{D_3}$, the selected SVs drop from 7.09, 6.47 and 6.41 to 0.00, 0.13 and 3.02, respectively. In contrast to this, the decay of selected SVs for low frequency subband matrices $\mathbf{A_6}$ $\mathbf{D_6}$ and $\mathbf{D_5}$ is marginal and is from 6.82, 6.53 and 6.93 to 5.70, 5.19 and 5.18, respectively. The proposed thresholding technique selects the SVs based on the variation of energy contents across the subband matrices. In other words, less number of SVs is selected from the high frequency subbands and vice versa. The energy content of the high frequency subband matrices is comparatively very low than the total subband

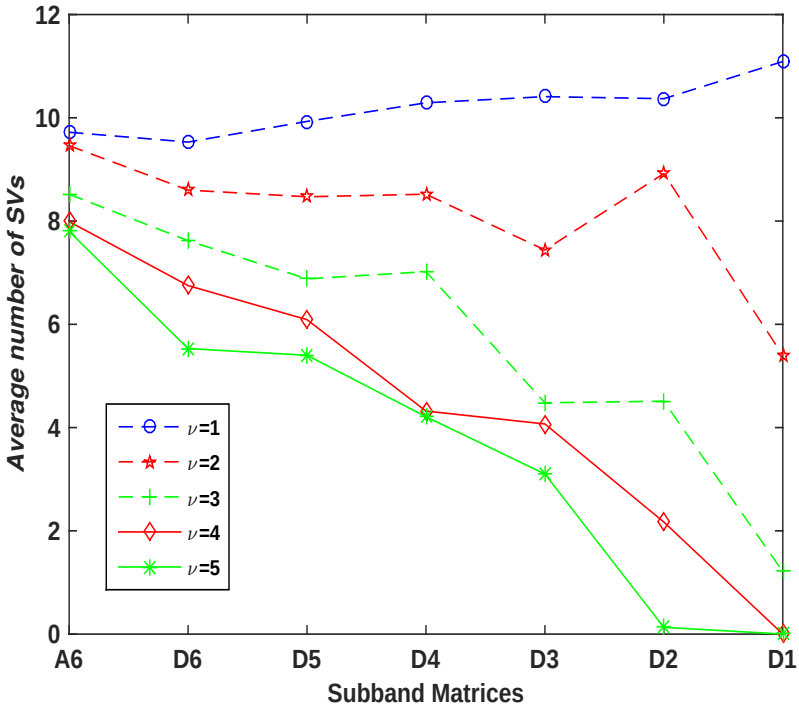

Figure 3.4: Average number of SVs selected for different values of ν. With increase in ν, the drop in selected SVs for low frequency subband matrices $\mathbf{A_6}$, $\mathbf{D_6}$ and $\mathbf{D_5}$ is marginal and is opposite to high frequency subband matrices $\mathbf{D_1}$, $\mathbf{D_2}$ and $\mathbf{D_3}$, where the decay of selected SVs is quite high.

energy. On increasing the value of ν, the MRFEC values grow faster for these matrices than that of low frequency subband matrices. This thresholding technique helps discard more number of SVs and their corresponding singular vectors of the former subband matrices. Consequently, the on-board computations will decrease due to reduction in large number of samples. Another advantage of using this variable thresholding technique is that the value of ν can be altered to control the CR and the diagnostic distortion measures. The comparison performances of the proposed thresholding method with some existing threshold techniques are discussed in Sections 3.3 and 3.4.

The MSVD transformed coefficients are quantized and encoded according to the requirement of the application. All thresholded nonzero coefficients corresponding to unitary matrix $\mathbf{U}$ of all subbands are collected in one vector. The same procedure is used for the unitary matrix $\hat{\mathbf{V}}$ and the singular matrix $\hat{\mathbf{\Sigma}}$. This results in three vectors containing nonzero elements only. These are uniformly quantized and Huffman encoded. As these vectors contain only nonzero coefficients, it is required to encode their indexes in a separate codebook. For this, only minimum and maximum values of each nonzero zone of each subband are determined. On the other hand, if original matrices (coefficients with zeros) are encoded directly, memory requirements and computation time to encode these coefficients would be more. Algorithm 3.6 briefly describes the steps of the compression method.

Algorithm 1 Multiscale SVD Compression

Input: Preprocessed the MECG data matrix $\mathbf{X}$, threshold parameter ν (=5), F_s (=500 Hz)
Output: Compressed Huffman encoded bits
begin
Stage 1: Wavelet decomposition
Determine number of levels, $L = \lfloor log_2 F_s - 2.96 \rfloor$
Perform the 1-D DWT of each lead or column of $\mathbf{X}$ at level L
$[\mathbf{A}_1, \mathbf{D}_1] = \text{dwt}(\mathbf{X}, \text{'bior4.4'})$ % Biorthogonal wavelet filter
for $i = 2 : L$
$[\mathbf{A}_i, \mathbf{D}_i] = \text{dwt}(\mathbf{A}_{i-1})$
end
Stage 2: Apply SVD and reduced SVD on each subband matrix
$[\mathbf{U}_{\mathbf{A_L}}, \hat{\mathbf{\Sigma}}_{\mathbf{A_L}}, \hat{\mathbf{V}}_{\mathbf{A_L}}] = \text{svd}(\mathbf{A_L}, \text{'econ'})$; % Produces reduced SVD directly in MATLAB
$[\mathbf{U}_{\mathbf{D_j}}, \hat{\mathbf{\Sigma}}_{\mathbf{D_j}}, \hat{\mathbf{V}}_{\mathbf{D_j}}] = \text{svd}(\mathbf{D_j}, \text{'econ'}); \quad j = 1, 2, \cdots L$
Stage 3: Thresholding
Select the SVs of $\hat{\mathbf{\Sigma}}_{\mathbf{A_L}}$ and $\hat{\mathbf{\Sigma}}_{\mathbf{D_j}}$ based on MRFEC (Eqs. 3.9 and 3.10)
Select columns of each orthonormal subband matrix corresponding to selected SVs
Stage 5: Collect all thresholded nonzero coefficients of left orthonormal matrix of all subbands in a single vector
Repeat Stage 5 for right orthonormal matrix and singular value matrix of all subbands
Stage 6: Perform quantization and Huffman encoding for the above generated three vectors
end

After recovering the MECG data, the other dependent leads (III, aVR, aVL and aVF) can be reconstructed from leads I and II using the mathematical relations as $III = II - I$, $aVR = -(I + II)/2$, $aVL = I - II/2$ and $aVF = II - I/2$. Performance of the proposed method is evaluated using diagnostic distortion measures like weighted diagnostic distortion (WDD) [134, 135] and wavelet energy based diagnostic distortion (WEDD) [96] and non-diagnostic measures like percentage root mean square difference (PRD) [104].

3.3 Performance Measures and Comparative Analysis

In this section, data dimensionality reduction performance of the proposed method in terms of CR and different distortion measures with a comparative study on few existing compression methods are presented. For evaluation purpose, the MECG data is taken from the PTB Diagnostic ECG database [136]. Details about the database is discussed in Chapter 2.6.1. Each ECG data has been resampled to 500 Hz as the effectiveness of the proposed method will be compared with existing CS-based methods, and sampling frequency seldom exceeds 500 Hz in these methods [131]. To make a fair comparison, ECG signals are resampled. Only eight independent leads with a data dimension of 8×4096 are processed.

The dimensionality reduction performances in terms of CR and distortion measures are assessed

Table 3.3: Average number of singular values selected for $p = 5$

Diagnostic Class	Subjects	$\mathbf{D_6}$	$\mathbf{D_5}$	$\mathbf{D_4}$	$\mathbf{D_3}$	$\mathbf{D_2}$	$\mathbf{D_1}$
Healthy Control	80	3.9	4.3	3.9	2.3	0.09	10^{-4}
Myocardial Infarction	367	5.5	5.4	4.2	3.1	0.13	10^{-3}
Other Pathologies	102	5.1	5.1	4.0	3.2	0.1	10^{-3}
Average	**549**	**5.19**	**5.18**	**4.12**	**3.00**	**0.12**	$\mathbf{10^{-3}}$

for number of frames of each dataset over the entire signal. The resulting frame-wise the MECG data are concatenated, and then compared with the original the MECG data. The results, henceforth, shown are the average values of all frames.

3.3.1 Dimensionality reduction performance

Singular value decomposition is carried out for subband matrices. To avoid any loss of diagnostic information, all SVs are considered for $\mathbf{A_6}$ subband matrix as it contains more than 45% of energy (Ref: Table 3.2). For $\mathbf{D_6}, \cdots, \mathbf{D_1}$ subband matrices, the SVs are selected using the proposed thresholding technique. The compression performance is evaluated for different values of the threshold parameter (ν). Table 3.3 shows the average number of SVs selected with ν = 5 for all datasets. It is observed that, the SVs are selected depending on the diagnostic importance of the subbands i.e. more number of SVs is selected from the low frequency detail subband matrices ($\mathbf{D_6}$, $\mathbf{D_5}$: > 5) and less number of SVs is selected from the high frequency subband matrices ($\mathbf{D_3}$, $\mathbf{D_2}$: < 3). A few SVs corresponding to high frequency subband matrix $\mathbf{D_1}$ are chosen for some datasets (67 out of 549). This is so because, it does not carry any diagnostic information and has almost zero MRED value. Overall diagnostic information of the processed signal will not be affected by discarding this subband information if the threshold parameter is chosen appropriately. This also helps fast processing as a minimum of 50% of wavelet transformed coefficients are eliminated which are present in this subband. Hence, during real-time transmission, there is no need to perform SVD of $\mathbf{D_1}$ subband matrix. Reduction in number of SVs with corresponding left and right singular vectors of the high frequency subbands will result in faster processing during encoding and transmission. This thresholding technique gives a significant sample-wise reduction of 2.43:1, 3.15:1, 4.27:1 and 6.22:1 before coding for ν = 2, 3, 4, 5. For lossless compression, the selected MSVD transformed coefficients are uniformly quantized with varying quantization bits/sample followed by Huffman encoding. [1]

[1] Huffman encoding has been adopted for comparison purpose as it is being used for WBSN systems by different authors [130, 137].

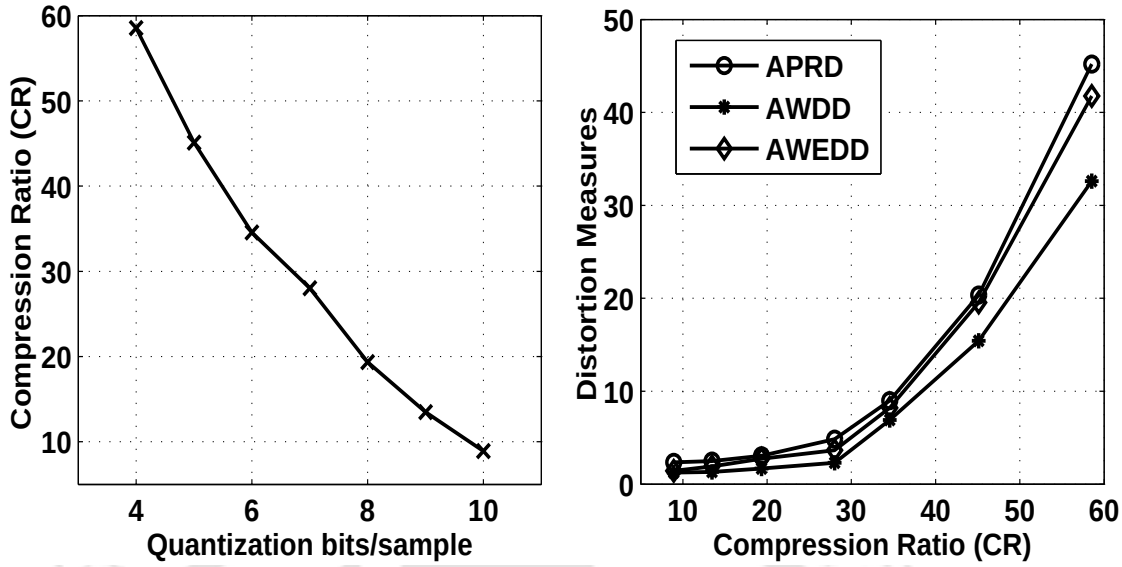

Figure 3.5: Compression ratio, quantization bits/sample and distortion measures, (a) CR vs quantization bits/sample (b) APRD, AWEDD vs CR

3.3.1.1 Compressed MECG performance measure

The compression performance is evaluated using average CR and aforementioned distortion measures like PRD, WDD, and WEDD. CR is given as

$$CR = \frac{B_o}{B_c} = \frac{B_o}{B_{NZSVD} + B_{dict} + B_{sm} + B_h} \tag{3.11}$$

where B_o and B_c are the total number of bits required to represent the original and the compressed signal, respectively, B_{NZSVD} is the number of bits required to represent nonzero MSVD coefficients, B_{dict} is the number of bits used to represent the dictionary information (symbols information with length of codeword to represent each symbol), B_{sm} and B_h are the number of bits used to code the significance map and the header, respectively. The header consists of minimum and maximum values of three vectors (Ref: Subsection 3.2.3, last paragraph), and the maximum value of each lead.

The significant singular vector coefficients (vectors containing nonzero elements of $\mathbf{U}, \hat{\mathbf{\Sigma}}$ and $\hat{\mathbf{V}}$) are uniformly quantized with number of quantization bits (q) ranging from 4 to 10, and corresponding CR values are calculated. To minimize the quantization error, the vector containing nonzero indices of $\hat{\mathbf{\Sigma}}$ matrix is quantized with 13 bits. The variation of CR value with quantization bits/sample is shown in Figure 3.5 (a). As the value of q increases, CR decreases significantly. At the same time, the average distortion measures (PRD, WDD and WEDD) increase with CR values as shown in Figure 3.5 (b). Therefore, a trade-off among quantization bits, CR and distortion measures is required. The CR value depends on the number of quantization bits. During the simulation, it is observed that the computation time increases drastically beyond q = 9 which may not be suitable for WBSN applications. Hence, the

maximum number of quantization bits is selected as q = 8.

3.3.1.2 Distortion measure evaluation

It is required to evaluate the compression performance in diagnostic terms with respect to the threshold parameter ν. To verify how well the diagnostic morphological features are preserved after compression, the diagnostic distortion measures namely WDD and WEDD along with a non-diagnostic distortion measure (PRD) are evaluated for three different values of ν. For WDD evaluation, same features (the duration, the shape and the amplitude parameters) and penalty matrices with same diagonal matrix of weights are considered as in [135]. It is evaluated for each beat. Then, for any specific lead (of a dataset), this measure is averaged over all beats. The average values of the distortion measures for whole datasets are listed in Table 3.4. An 8 bit quantization level is used for these evaluations. It is observed that the chest leads (V_2–V_6) have very low PRD values. For ν = 4 and ν = 5, these values fall under either 'excellent' or 'very good' category [104]. The PRD values of bipolar leads are higher compared to the chest leads. This may be due to the presence of motion artifacts or noise. The WDD values falling in the 'very good' category ($0 - 2.3$ [135]) suggest the preservation of diagnostic information. The high WDD values (> 2.3) corresponding to leads II (2.45), aVR (2.63) and V_1 (2.38) fall in the 'good' category. The inaccurate detection of P-wave characteristics due to the presence of noise leads to high WDD values in these leads. There is a small difference in WEDD values between the bipolar and the chest leads. This small difference indicates that the loss of diagnostic information is similar for both types of leads. These WEDD values are in the 'excellent' category [96]. This suggests that the proposed method with the thresholding technique can help the retention of diagnostic information. From these results, it is observed that there are significant changes in PRD and WEDD values while moving from ν = 5 to ν = 6. This is because a few SVs are selected for ν = 6. Hence, ν = 5 is appropriate to threshold the SVs at multiscale level.

Subjective measure is also important as these give the true quality of the compressed signal. It is carried out using the mean opinion score (MOS) of five evaluators. They include two medical doctors and three researchers who are working in the ECG signal processing area. MOS represents the visual inspection comparison of the original and the compressed signals. A semiblind test is conducted for MOS evaluation [16, 104, 135]. A detail procedure on how to conduct this test can be found in [135]. In this evaluation, the compressed signals with $\nu = 5$ are compared with the original signals. Features considered for this test include P-wave, PR-segment, QRS-complex, ST-segment, QT-interval and T-wave. Evaluators were asked to give a score based on the likeliness of these features between the original and the compressed signal. Quality ratings are 5 (excellent), 4 (very good), 3 (good), 2 (not

Table 3.4: Distortion measures with CR for $p = 4, 5, 6$ (PTB Database)

ν	Metric	I	II	III	aVR	aVL	aVF	V1	V2	V3	V4	V5	V6	CR
4	PRD	3.85	5.98	3.92	7.75	4.07	3.87	5.18	3.25	3.49	2.99	3.78	3.52	15.54 (93.56%)
	WDD	1.57	2.45	1.78	2.63	2.07	1.59	2.38	0.99	1.39	0.83	1.53	1.31	
	WEDD	2.08	2.27	2.74	2.30	2.90	2.30	2.69	2.15	2.24	2.05	2.49	2.23	
5	PRD	4.01	6.18	3.92	7.87	4.59	4.11	5.61	3.67	3.79	3.09	4.01	3.85	19.34 (94.83%)
	WDD	1.61	2.74	1.80	2.89	2.09	1.63	2.57	1.35	1.39	1.01	1.59	1.43	
	WEDD	2.11	2.29	2.80	2.39	2.92	2.37	2.75	2.27	2.31	2.06	2.49	2.27	
6	PRD	6.02	8.37	6.10	10.15	6.91	6.69	7.39	6.48	6.88	5.49	6.77	5.92	22.10 (95.47%)
	WDD	1.95	4.55	2.27	5.29	2.68	2.21	4.01	1.97	2.05	1.58	1.96	1.54	
	WEDD	2.59	2.63	3.27	2.93	3.27	2.82	3.43	2.57	2.59	2.29	2.61	2.65	

The values shown in the table are for 8 bit quantization level.

bad) and 1 (bad).

The MOS of an ECG signal is defined as follows

$$MOS = \frac{1}{N_e N_f} \sum_{e=1}^{N_e} \sum_{f=1}^{N_f} Q(e,f) = \frac{1}{N_f} \sum_{f=1}^{N_f} \left(\frac{1}{N_e} \sum_{e=1}^{N_e} Q(e,f) \right) \tag{3.12}$$

where N_e is the number of evaluators and N_f is the number of features considered. $Q(e,f)$ is the quality rating of the fth feature by the eth evaluator. The factor inside the bracket in (3.12) represents the MOS value of the fth feature, i.e. $MOS(f) = \frac{1}{N_e} \sum_{e=1}^{N_e} Q(e,f)$. The gold standard diagnostic MOS errors for each feature and overall ECG signal are given as

$$\begin{aligned} MOS_{fe} &= \left(1 - \frac{MOS(f)}{5}\right) \times 100\% \\ MOS_{e} &= \left(1 - \frac{MOS}{5}\right) \times 100\% \end{aligned} \tag{3.13}$$

Table 3.5 shows the MOS errors for selected ECG features and overall compressed signals for leads I, III, aVF and V5. Some features like P-wave, PR-segment and QRS-complex of lead III have MOS_{fe} of 9.33, 9.33 and 8.00, respectively. Presence of noise in this lead (Ref: Figure 3.7 (a)) may be the reason for low rating by the evaluators which implies high errors. Also, leads I and V_5 have the lowest MOS_e. Finally, based on the MOS error criteria, the values related to MOS errors of compressed ECG features and overall leads fall under 'excellent' category [96].

Table 3.5: MOS error (in %) for compressed ECG

MOS error for selected ECG features				
Features	**I**	**III**	**aVF**	**V5**
P-wave	4.00	9.33	8.00	4.00
PR-segment	2.67	9.33	5.33	4.00
QRS-complex	4.00	8.00	1.33	5.33
ST-segment	5.33	6.77	6.77	2.67
QT-interval	2.67	2.67	5.33	6.67
T-wave	6.67	4.00	6.67	2.67
MOS error for ECG signal				
Overall ECG	4.22	6.67	4.56	4.22

3.3.2 Comparison with existing methods

Performances of the proposed method and the existing compression techniques are compared as shown in Table 3.6. CR depends on factors such as number of leads, F_s, and quantization bits/sample, and types of correlations exploited, etc. Compression methods exploiting intra- or inter-beat correlation for single lead ECG result in high CR and less PRD. But, the computational complexity in processing the MECG data using single lead ECG compression schemes will increase as sequential period normalization of each lead is required. To the best of our knowledge, a robust and fast MECG compression algorithm has not been developed. Hence, it is difficult to compare the compression performance of the proposed method with others. For fairness in the comparison, same amount of samples from the PTB database are processed by implementing the existing algorithms. Its effectiveness for WBSN has been evaluated in the next Section.

It is observed that the CR value decreases when the MECG data is processed. The linear transform based KLT and DCT methods by Cetin *et al.* obtained a CR value of 7.25:1 with a PRD value of 3.81% for eight leads [48]. An average CR and PRD values of 7.68:1 and 2.96% are obtained using MSPCA method [16] for twelve lead ECG data. These (single- or multi-lead compression) methods may not be suitable for the MECG data in WBSN applications as these require more computations. The computational timing characterization of different methods are discussed in the Subsection 3.4.2. The proposed method achieved an average CR and PRD values of 19.34:1 and 3.05% respectively. The high CR value may be due to exploitation of both intra-beat and inter-lead correlation present across the samples and among the leads respectively.

3.4 Simulation Study of the Proposed Method for WBSN Applications

This Section discusses the effectiveness of the proposed method in terms of fast processing nature for WBSN applications. Transmission of the generated bit-streams, after Huffman encoding of the MECG data from the central control unit (CCU) to the personal server (Figure 3.6, dotted mark) is carried out. This figure represents a typical telemedicine system. Wireless sensors, placed on the human body, acquire and send the biomedical data to the CCU which is placed on or close proximal to the human body. It processes and sends the data to a personal server for further processing and transmits to doctors' site.

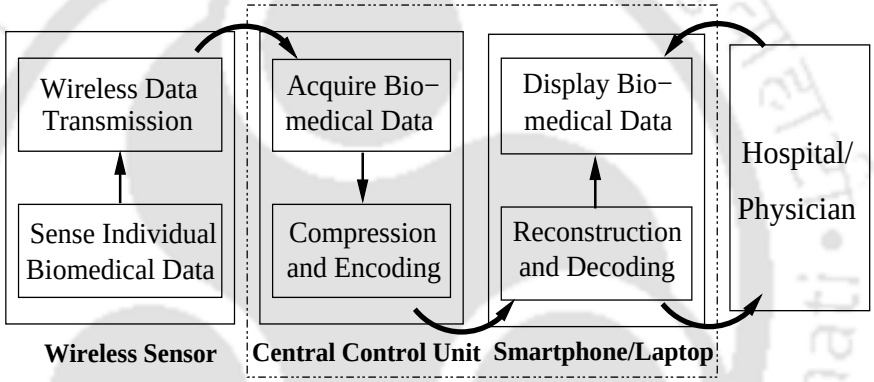

Figure 3.6: Block diagram of a typical telemedicine system

3.4.1 Transmission of Huffman encoded MECG bit-stream

Each bit of the compressed ECG binary bit-stream is represented as number of pulses. For transmission of these bits, pulse amplitude modulated (PAM) direct sequence UWB[1] (DS-UWB) technique is adopted [141], which can be stated as

$$s(t) = \sum_{j=-\infty}^{\infty} (2\boldsymbol{a}_j - 1)\, \boldsymbol{c}_j\, g(t - jT_s) \tag{3.14}$$

where each bit of the original binary stream is represented by number of repeated pulses for N_p times and is symbolized as $\boldsymbol{a}$, $\boldsymbol{c}$ composed of ± 1's and T_s is the average pulse repetition period. Every bit is represented by a Gaussian doublet pulse, $g(t)$ [140], which at any time t is given as

$$g(t) = \left[1 - 4\pi\Big(\frac{t}{\tau_m}\Big)^2\right] e^{-2\pi(t/\tau_m)^2} \tag{3.15}$$

[1]UWB technology is suitable for physiological signals as it requires lower transmission power than Bluetooth, Zigbee, WLAN [138,139]. It has less interference [140] which is highly essential while dealing with different physiological signals.

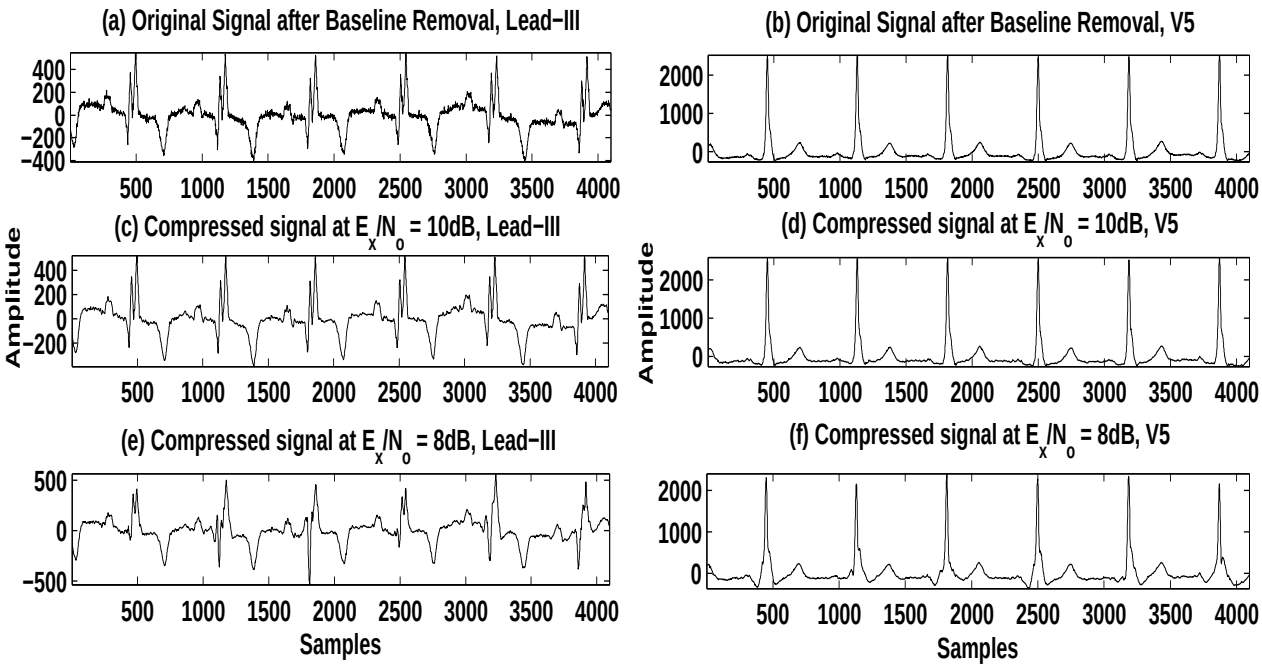

Figure 3.7: (a), (b): Original signals and (c), (d) (e) and (f): Reconstructed Signals at $E_x/N_o = 8$ dB and 10 dB of Lead-III and V5 respectively, Dataset: $s0008\_rem$, PTB Diagnostic ECG Database. Description: Female, Age 81, Acute myocardial infarction

where τ_m is the spreading factor or duty cycle. Each pulse duration is considered to be T_s ns with a very small duty cycle. The bit-stream of each data block can be transmitted using burst transmission technique. After each data block transmission, CCU sensor node will go into an inactive mode until the next data block transmission which will save energy [139]. To transmit the compressed binary bit-stream using PAM DS-UWB, the following parameters are considered: T_s = 2 ns (3.14), τ_m=0.25 ns (3.15) and N_p = 3.

During real-time transmission, signals get corrupted due to presence of noise. It will be useful to evaluate the performance of compression scheme with noisy data. In order to estimate the minimum energy of the signal at the transmitter for reliable reception, additive white Gaussian noise (AWGN) with zero mean is added to the bit-stream. Different values of E_x/N_o (in dB) where E_x is the received single pulse energy and N_o is the standard deviation of the AWGN are employed. The value of E_x/N_o resulting an error free bit-stream is chosen to be optimal. As the quantized coefficients are produced by Huffman encoding method, a complete error free binary bit-stream is mandatory at the receiver. To estimate the bit-stream at the receiver, the following two steps are employed. First a correlator mask is generated; then each bit is detected over a bit period of time N_sT_s [141]. The compressed the MECG data is recovered by following the reverse procedure as shown in Figure 3.3(b).

Figure 3.7 shows the original and the compressed ECG signals (Dataset: $s0008\_rem$, Lead-III

Table 3.6: Comparison of compression performance and average computational timing characterization

Method	Data Processing	$\mathbf{N_s}$	Quantization & Encoding	DS-UWB Transmission	Total	CR	PRD (in %)
No Compression	-	3.276E4	16.3 s	41.9 s	58.2 s	3.01	-
Proposed Method	$\mathcal{O}(MN^2)$ 23.5 ms	5.27E3	1.05 s	1.82 s	2.90 s	19.34	3.05
Sharma [16]	$\mathcal{O}(MN^2)$ 31.7 ms	1.66E4	7.45 s	15.01 s	22.49 s	7.68	2.96
Cetin [48]	m$\mathcal{O}(N^2)$ 20.1 ms	1.83E4	7.91 s	16.47 s	24.40 s	7.25	3.81
CS_{BP} [130]	$8\mathcal{O}(N)$ 8×1.6 ms	8×1.64E3	3.67 s	7.51 s	11.19 s	8.74	-
CS_{BSBL} [131]	$8\mathcal{O}(N)$ 8×0.59 ms	8×1.56E3	2.84 s	5.22 s	8.066 s	9.39	-

† All algorithms computed in same environment (MATLAB, i5 CPU, 3.2 GHz processor) with **same number of MECG samples (8×4096)** of PTB database

† Example: $\mathbf{N_s} = 3.276\text{E}4 = 3.276{\times}10^4$

and V5) when E_x/N_o is 8 dB and 10 dB. The AWGN distribution prevails over the ECG signal for modest E_x/N_o values which causes high bit error probability. The received bit-stream is completely error free for 10 dB [Figure 3.7(c, d)]. High distortion in Figure 3.7(e, f) are due to the fact that few wrongly estimated bits decode new symbols during Huffman decoding. Hence, it is necessary to receive an error free bit-stream at the receiver. Simulation studies on different MECG records indicate that a minimum of 10 dB is required for better performance. It can be noticed that the proposed method eliminates the high noise artifacts present in the original ECG signal as in Lead-III. It preserves the pathological information like biphasic QRS complex, T-wave inversion. One of the issues in the proposed method is the initial delay during the first frame data acquisition.

3.4.2 Computational complexity measure

The proposed method comprises of data processing steps like preprocessing, DWT, MSVD, quantization with Huffman encoding, and DS-UWB. This requires more on-board memory and computations prior to quantization compared to CS based techniques [101, 130, 131]. Also, this method discards a large number of components from high frequency subbands and some non-diagnostic components from low frequency subbands. It reduces the computation burden during quantization, Huffman en-

coding, and transmission.

The complexity is evaluated by implementing the proposed method in MATLAB environment in a personal computer (i5 CPU, 3.2 GHz processor). The decompressed the MECG data of 4096 $\times$ 8 samples (corresponding to a duration of 8 s and F_s = 500 Hz) takes about 58.2 s for encoding and DS-UWB modulation technique. This is because a large amount of samples are to be encoded and the encoded bits are to be transmitted using the modulation technique. The execution time indicates the necessity of large number of on-board computations, and consequently, will increase the energy consumption. The proposed method helps in transmitting the data with fewer bits, and with less computations by compressing the MECG data. The DWT using Daubechies Biorthogonal filter takes about 9.7 ms to estimate the DEC matrix with 6 decomposition levels. The computational complexity of SVD of a matrix $\mathbf{X}_{m\times n}$ is $\mathcal{O}(4m^2n + 8mn^2 + 9n^3)$ [142, Ch. 7, pp. 392] for $m \gg n$. It takes about 14 ms (MSVD: 4.2 ms, thresholding: 1.8 ms, matrix dimension reduction: 7.7 ms) to compute the MSVD and formation of dimension reduced matrices after thresholding. The computational complexity for uniform quantization of the three reduced singular matrices of size $m \times n$ would be $\mathcal{O}(mn \log mn)$. However, this can be solved efficiently with complexity $\mathcal{O}(N_s \log N_s)$ by collecting significant nonzero coefficients of each singular matrix in a single vector, where N_s ($N_s \ll mn$) is the number of nonzero coefficients before encoding. It takes about 1.05 s for quantization and Huffman encoding of the three vectors. The individual time requirement from three stages (DWT, MSVD, quantization with encoding) suggests that more computations are required during quantization and encoding.

In the DS-UWB modulating technique, each bit of the binary bit-stream is represented as number of pulses. In (3.14), $s(t)$ is the convolution of an exponential function with the function representing the number of pulses. With the aforementioned parameters, there are 12 coefficients to represent the Gaussian doublet pulse. This modulation technique has computational complexity of $\mathcal{O}(12N_P)$; $N_P = N_p \times N_b$ is the total number of pulses to be transmitted for each frame, where N_b is the number of bits required to represent N_s non-zero coefficients. Hence, it is certain that the number of computations increases with number of non-zero coefficients to be encoded (N_s). It takes about 1.82 s for DS-UWB modulation process after Huffman encoding.

On an average, our non-optimized MATLAB program takes approximately 2.90 s for transmitting the encoded bit-stream, starting from the DWT computation. This time complexity can be further reduced by an efficient implementation of the proposed algorithm. In the following, we present a comparative study based on code execution time with other methods.

Table 3.6 shows the average execution time comparison among MECG and CS-based single lead

ECG compression algorithms. As mentioned earlier, more computations are needed during the encoding and bit transmission stages as this depends on the number of samples to be encoded, N_s. In other words, number of computations will increase with the number of samples. It may be one of the reasons why most of the energy consumption takes place during the communication process. The code execution time suggests that it takes more than 70% of total time for DS-UWB modulation for decompressed data, and is well in accordance with the literature [129]. From the table, it is clear that the proposed method performs better than the existing MECG compression techniques [16, 48] in terms of code execution time (24.40 s, 22.49 s) and storage volume capacity (7.68, 7.25). In the literature, the CS based ECG compression techniques [130, 131] are widely used for telemonitoring systems. But these methods require a lot of computations during encoding and transmission, and may consume more energy for MECG compression at the CCU. The results presented in this work indicate that the proposed method can be executed at least 2.7 times faster than the existing CS-based techniques with better storage volume capacity.

3.5 Summary

In this chapter, the MECG data dimensionality reduction was carried out by exploiting both intra-beat and inter-lead correlations present across samples and among leads, respectively, in wavelet domain. For fast and effective computation, the MECG data was represented in a 2-D array. After decomposing the MECG data into different subbands, subband matrices were constructed by considering wavelet coefficients as matrix elements. The proposed MSVD method was applied on these subband matrices. A new variable thresholding technique for selecting SVs of subband matrices was also suggested. A simulation study was carried out to show the fast processing nature, by evaluating timing characterization of individual steps, of the proposed method. A CR of 19.34 with average PRD value of 3.05 % is obtained. One of the limitation in this work is that inter-beat correlation present in the MECG data, which is a huge source of redundancy, has not been exploited. Next chapter focuses this by introducing a new representation of the MECG data. Also features are extracted from the dimension reduced data for MI classification.

4

MECG Analysis and MI classification using Multiscale HOSVD

Contents

This chapter introduces a third-order tensor representation of MECG data, decomposition of MECG tensor using multiscale higher-order SVD (MHOSVD) and a feature extraction technique for classification (both detection and localization) of MI. Tensors (multidimensional arrays) are used to represent and analyze multidimensional data simultaneously [143, 144]. Though there are several tensor-based applications for different purposes in chemometrics, psychometrics, numerical analysis, data mining, computer vision, target detection, signal and image processing, and many more for high-dimensional data analysis [128, 145–154], its application for ECG signal is limited in the literature [93, 155–158]. Use of tensors for the MECG data allows to combine and analyze the information present in heartbeats of all leads. There are three types of correlations, namely intra-beat, inter-beat and inter-lead correlations present in the MECG data. In the previous chapter, efforts were made to exploit both intra-beat and inter-lead correlations using MSVD method, but not all. This is one of the objectives of this third-order tensor representation for the MECG data.

It was observed in the previous chapter that, SVD on multiscale matrices has advantages in dimensionality reduction and faster processing while preserving diagnostic information. The HOSVD, an analogue of SVD, has been applied on multidimensional array (as SVD cannot be used directly on the same) in different branches of science for dimensionality reduction [144, 148], texture synthesis [146], detection [150], classification [145], etc. In this work, HOSVD has been adopted to decompose third-order multiscale tensors. Dimensions along different modes of subband tensors are truncated based on energy content of mode singular values (MSVs). Details about modes, MSVs, and other terms related to tensor are discussed in subsequent Sections.

Further, in addition to exploitation of all types of correlations, a feature extraction technique for MI detection and localization from the reduced MECG tensor is proposed. From Chapter 2, we can observe that most of the articles focused for detection of MI only, and very few articles were proposed for both detection and localization. Also, extraction of features in two stages (for detection and then for localization) as was in [68], may require more computations. The proposed algorithm selects features from the subband core tensors that are formed after dimensional reduction of the MECG tensor, and features for both stages are extracted simultaneously which makes it more efficient than other algorithms. The objectives in this work are data dimensionality reduction by exploiting all types of correlations and feature extraction for MI classification using set of more discriminative features.

The rest of this chapter is organized as follows. A brief review on tensor notations and conventions is presented in Section 4.1, followed by HOSVD in Section 4.2. Proposed method for dimensionality reduction and feature extraction is discussed in Section 4.3. Sections 4.4 and 4.5 present experimental

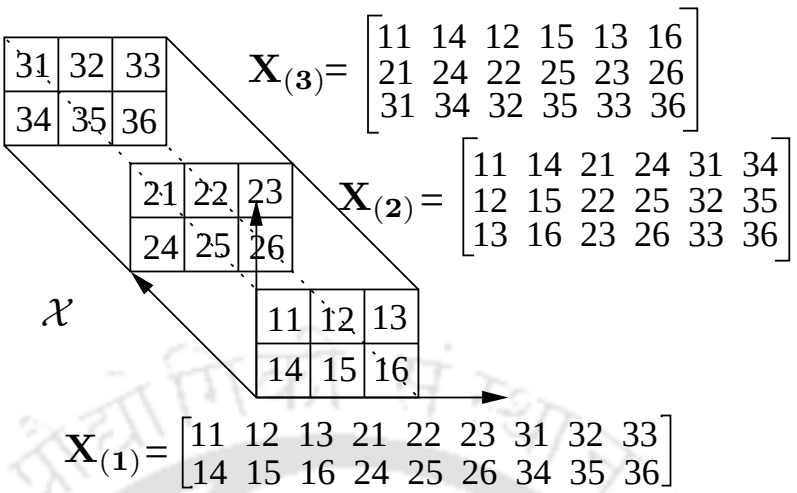

Figure 4.1: A 3-array representation and its flattening into three slices (matrices)

observations for dimension reduction and classification performances, respectively. Also, comparisons with the state-of-the-art methods are discussed in these sections. Finally, summaries are drawn in Section 4.6.

4.1 Tensor Notations and Conventions: A Preview

Before applying different signal processing tools on tensors, it is worthwhile to discuss what is a tensor and related notations used henceforth. A tensor is a multidimensional Nth order array where the order is the number of its modes or dimensions. A third-order tensor of size $I \times J \times K$ is written with a calligraphic letter $\mathcal{X}$, and its elements as x_{ijk}, $i = 1, \cdots, I$, $j = 1, \cdots, J$ and $k = 1, \cdots, K$.

The other two terminologies, which are used extensively in this thesis, associated with a tensor are *fibers* and *slices*. A fiber is defined by fixing the index in all modes except one. The mode-1 fiber of a tensor is the column vector and denoted as $\mathbf{x}_{:jk}$. Mode-2 and mode-3 fibers are the row and the tube vectors and are represented as $\mathbf{x}_{i:k}$ and $\mathbf{x}_{ij:}$, respectively.

Slices of a tensor are obtained by fixing all but two indices, and its structure is similar to a matrix. A third-order tensor comprises of three types of slices, namely 'horizontal', 'vertical' and 'frontal' slices. The 'horizontal' slice where index i is fixed is denoted as $\mathbf{X}_{i::}$. Other two slices, keeping j and k fixed, are represented as $\mathbf{X}_{:j:}$ and $\mathbf{X}_{::k}$, respectively.

Two common operations associated with a tensor are flattening and mode-n product. Flattening is transforming a tensor into matrix and is a very useful operation during decomposition. A tensor of order N can be unfolded or flattened in N different ways. Flattening of a tensor $\mathcal{X}$ in its mode-n is symbolized by the matrix $\mathbf{X}^{(n)}$[1]. An example to show the flattening process of a third-order tensor is

[1]superscript n inside a bracket indicates mode-n

Table 4.1: Basic tensor notations

$\mathcal{X}_{I\times J\times K}$	Third-order tensor
x_{ijk}	Tensor elements
$\mathbf{x}_{:jk}$	Fibers (analogous to vectors) of $\mathcal{X}$ obtained by fixing all but one index
$\mathbf{X}_{::k}$	Matrix slice of $\mathcal{X}$ obtained by fixing all but two indices
$\mathcal{Y}=\mathcal{X}\times_n \mathbf{A}$	n-mode product of a tensor $\mathcal{X}$ with a matrix $\mathbf{A}$

shown in Figure 4.1. The mode-n flattening is adopted from [147]. The mode-n fibers are columns of the mode-n flattened matrix.

The mode-n product of a tensor $\mathcal{X}\in\mathbb{R}^{I_1\times I_2\times\cdots I_n}$ with a matrix $\mathbf{A}\in\mathbb{R}^{J\times I_n}$ is represented as $\mathcal{Y}=\mathcal{X}\times_n\mathbf{A}$. In terms of the flattened tensors, the product can be expressed as $\mathbf{Y}^{(n)}=\mathbf{A}\mathbf{X}^{(n)}$. A summary on basic tensor notations are given in Table 4.1.

4.2 Higher-Order SVD

In the last Chapter, we have seen that SVD decomposes a matrix $\mathbf{X}$ into two orthonormal matrices and a diagonal matrix as $\mathbf{X}=\mathbf{U}\mathbf{\Sigma}\mathbf{V}^{\mathbf{T}}$. Considering the matrix as a second-order tensor, SVD in terms of n-mode product can be rewritten as $\mathbf{X}=\mathbf{\Sigma}\times_1\mathbf{U}\times_2\mathbf{V}$.

The SVD of a matrix can be generalized to a tensor of any order using HOSVD [128,153]. HOSVD, an analogue of SVD, is used to decompose a multidimensional array. We have limited our discussion to a third-order tensor $\mathcal{X}_{m\times n\times p}$, which can be decomposed using HOSVD as

$$\mathcal{X}=\mathcal{S}\times_1\mathbf{U}\times_{\mathbf{2}}\mathbf{V}\times_{\mathbf{3}}\mathbf{W} \tag{4.1}$$

where $\mathbf{U}\in\mathbb{R}^{m\times m}$, $\mathbf{V}\in\mathbb{R}^{n\times n}$ and $\mathbf{W}\in\mathbb{R}^{p\times p}$ are orthonormal matrices. For quick understanding purpose, visualization and approximation of HOSVD is presented in Figure 4.2. These matrices ($\mathbf{U}$, $\mathbf{V}$ and $\mathbf{W}$) as they represent the left singular matrices of $\mathbf{X}^{(n)}$, $n=1,2,\cdots,3$ are computed using SVD as follows

$$\begin{aligned}\mathbf{X}^{(1)}&=\mathbf{U}\mathbf{\Sigma}^{(1)}{\mathbf{V}^{(1)}}^T\\ \mathbf{X}^{(2)}&=\mathbf{V}\mathbf{\Sigma}^{(2)}{\mathbf{V}^{(2)}}^T\\ \mathbf{X}^{(3)}&=\mathbf{W}\mathbf{\Sigma}^{(3)}{\mathbf{V}^{(3)}}^T\end{aligned} \tag{4.2}$$

without forming the $\mathbf{V}^{(j)}$'s explicitly. This saves a large number of floating point operations. After obtaining the orthonormal matrices, the core tensor $\mathcal{S}$ is computed as $\mathcal{S}=\mathcal{X}\times_1\mathbf{U}^T\times_2\mathbf{V}^T\times_3\mathbf{W}^T$.

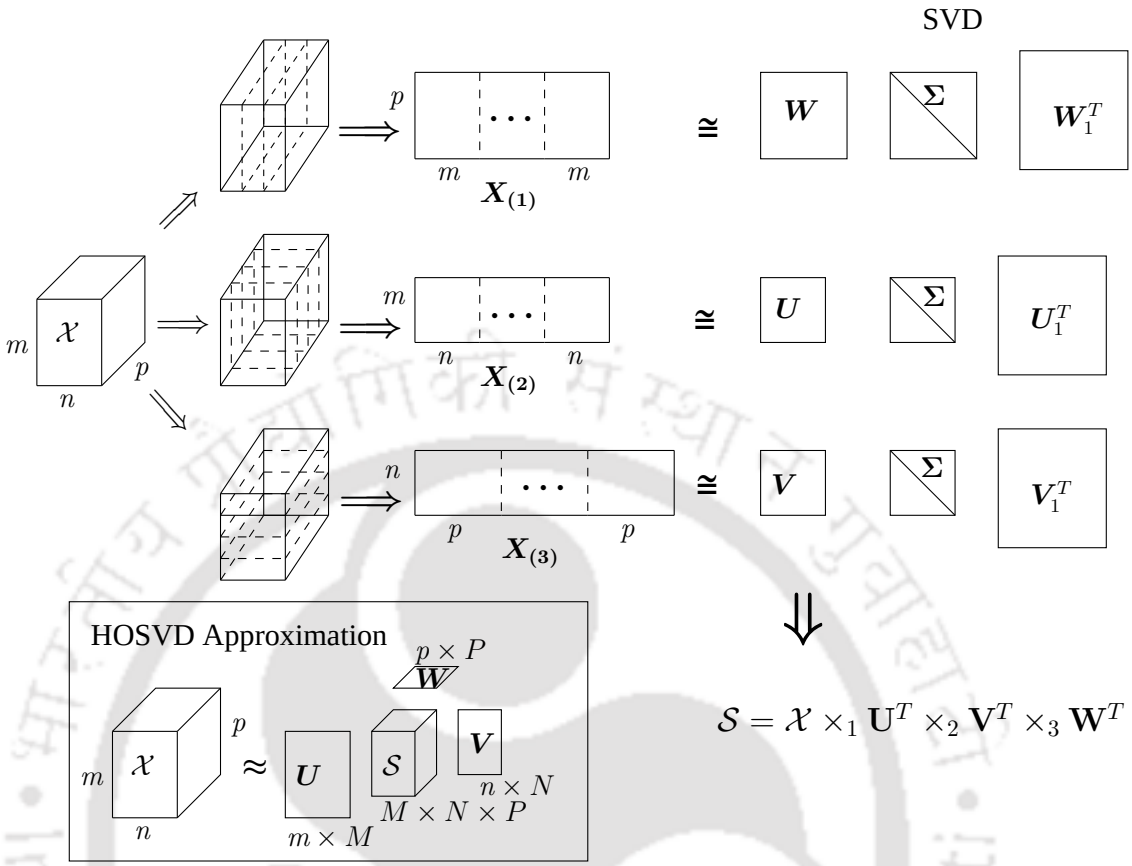

Figure 4.2: HOSVD visualization and approximation for a third-order tensor)

Although it corresponds to the singular value matrix of conventional 2-D SVD, it does not have a simple diagonal structure [112].

The core tensor $\mathcal{S}$ has the dimension as that of $\mathcal{X}$. Typical rank of a tensor ($\mathcal{X}$) of size $m \times n \times p$ with $mn \leq p$ is mn [147]. Hence, first $p' = mn$ frontal slices of the core tensor have significant nonzero values, and rest $p - p'$ frontal slices have entries in the order of 10^{-12} or less, which can be set to zero. The effective dimension of core tensor $\mathcal{S}$ is $m \times n \times p'$, and it satisfies following properties [128]:

- *all-orthogonal*, i.e. any two slices in a fixed mode are orthogonal.
- *ordered*, i.e. the norms of the slices along any mode are ordered in decreasing manner. For example,

$$\begin{aligned} 1^{st}\ mode:&\ ||\mathcal{S}(1,:,:)|| \geq ||\mathcal{S}(2,:,:)|| \geq \cdots \geq 0 \\ 2^{nd}\ mode:&\ ||\mathcal{S}(:,1,:)|| \geq ||\mathcal{S}(:,2,:)|| \geq \cdots \geq 0 \\ 3^{rd}\ mode:&\ ||\mathcal{S}(:,:,1)|| \geq ||\mathcal{S}(:,:,2)|| \geq \cdots \geq 0 \end{aligned} \tag{4.3}$$

The above ordered property informs about the energy of the core tensor that is concentrated in the s_{111} element. This is the reason why HOSVD is used for data dimension reduction.

As discussed earlier for SVD case, the mode matrices $\mathbf{U}$, $\mathbf{V}$ and $\mathbf{W}$ contain the orthonormal

vectors. These vectors span the column space of three different types of slices that resulted from the flattening of $\mathcal{X}$ along different modes. For example, the left orthogonal matrix $\mathbf{U}$ is calculated by applying SVD on the $m \times np$ matrix, which is obtained by mode-1 flattening of $\mathcal{X}$. These mode matrices are regularized by the core tensor $\mathcal{S}$.

One of the motives in this work as stated earlier is the low rank approximation of the tensor $\mathcal{X}$, which makes use of the redundancies present in different modes. To have the core tensor $\mathcal{S}$ as a compressed form of $\mathcal{X}$, reduced dimensions can be chosen as $M \ll m$, $N \ll n$ and $P \ll p'$. Hence, $\mathcal{X}$ can be approximated as

$$\mathcal{X} \approx \hat{\mathcal{S}} \times_1 \hat{\mathbf{U}} \times_{\mathbf{2}} \hat{\mathbf{V}} \times_{\mathbf{3}} \hat{\mathbf{W}} \tag{4.4}$$

where $\hat{\mathcal{S}} \in \mathbb{R}^{M \times N \times P}$, $\hat{\mathbf{U}} \in \mathbb{R}^{m \times M}$, $\hat{\mathbf{V}} \in \mathbb{R}^{n \times N}$ and $\hat{\mathbf{W}} \in \mathbb{R}^{p' \times P}$ respectively.

4.3 Proposed MHOSVD-based Method

The overall block diagram of the proposed MHOSVD-based method for third-order MECG tensor is sketched in Figure 4.3(i). It comprises of number of steps including dimensionality reduction, feature extraction, and detection and localization of MI. A detailed block diagram for tensor dimensionality reduction is shown in Figure 4.3(ii). The encoder part comprises of preprocessing, MECG tensor formation, multiscale HOSVD. Exploitation of three types of correlations is achieved by representing MECG data in third-order tensor form. Then MHOSVD is applied on MECG tensor. This turns out to achieve a high data reduction volume without loss of any clinical information. Figure 4.3(ii)(b) shows the decoder part of the proposed method. It follows the reverse process i.e. decoding, HOSVD restoration, IDWT, third-order tensor representation followed by period recovery and postprocessing. Details on these steps are discussed in following subsections.

4.3.1 Signal preprocessing

In the preprocessing stage, all leads are preprocessed to remove baseline-wander which helped all ECG leads bring to their iso-electric level. Isoelectric line is the baseline that is recorded in the TP interval. It is necessary to detect onset and offset of the fiducial points accurately. The isoelectric line for other portion of the heartbeat except the TP interval was estimated using cubic-spline interpolation technique in most of the articles. Problem with this interpolation technique is that, if some of the end points just before the onset of P-wave are monotonically increasing or decreasing, then the baseline cancellation process using cubic-spline interpolation gives erroneous results. In this work, baseline-wander removal is performed by passing each ECG signal through a digital Butterworth high-pass filter

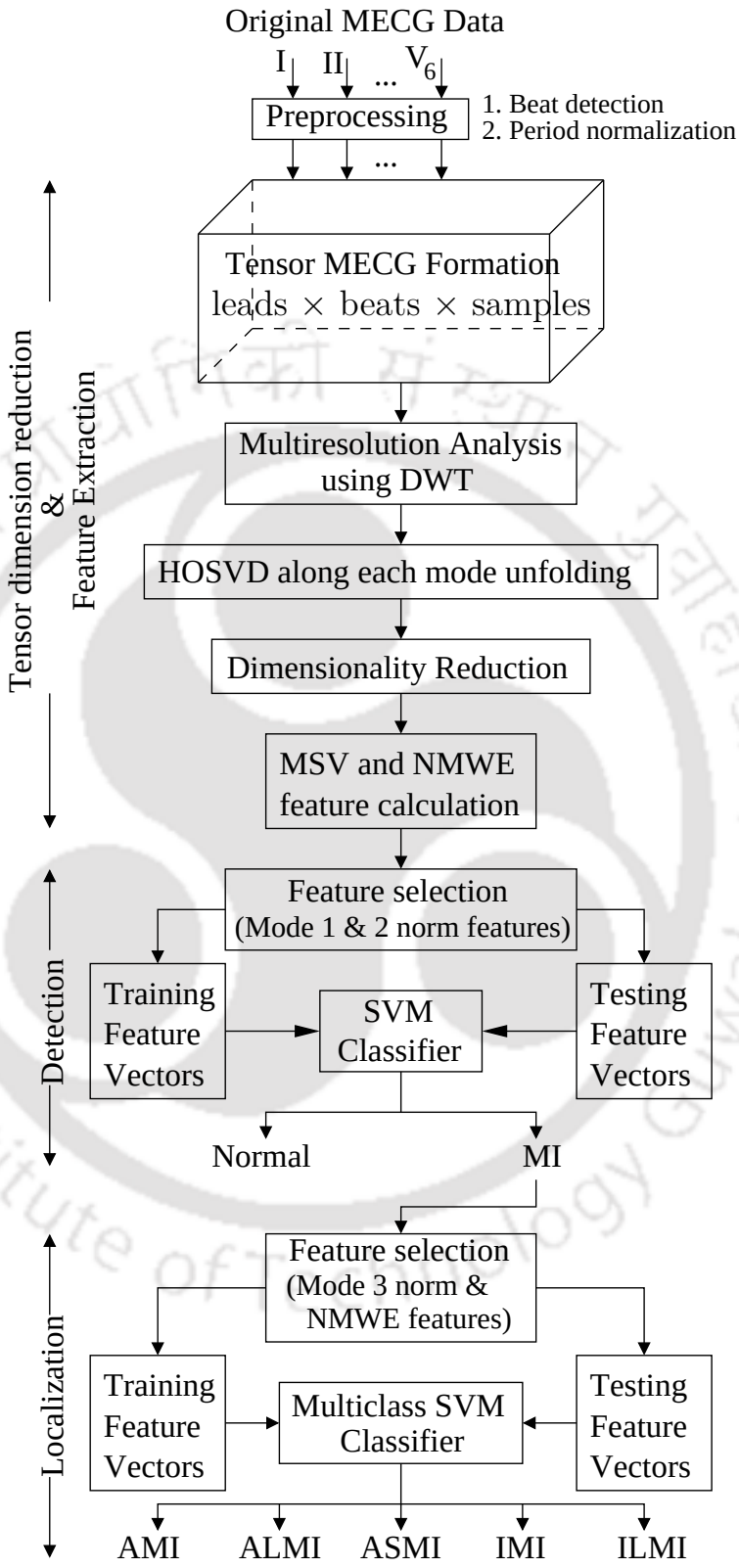

Figure 4.3: (i) Block diagram of MECG tensor dimension reduction and feature extraction for MI detection and localization

with cut-off frequency f_c = 0.5 Hz. To get zero-phase shift, the filtered signal is passed through the "Zero-phase forward and reverse digital filter" [100].

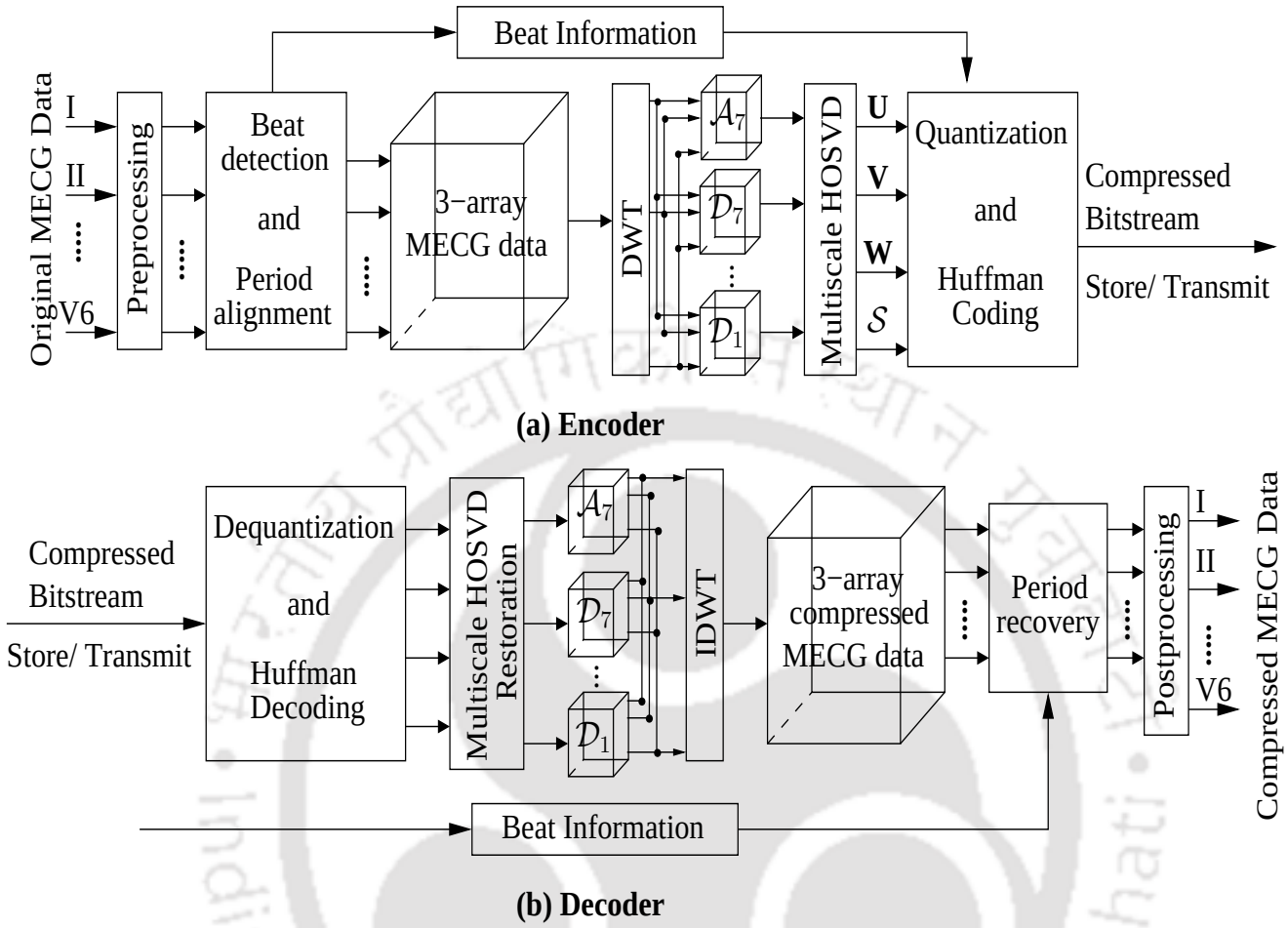

Figure 4.3: (Contd...) (ii) Block diagram of MECG tensor (a) Compression and (b) Reconstruction

4.3.2 Construction of third-order MECG tensor

The MECG data is a 2-D matrix data where rows represent number of leads and samples of each lead correspond to number of columns. It can be laid out, however, as a third-order tensor by stacking vertical slices side-by-side, since the timing information across all the leads is same. Each vertical slice represents a beat period of all leads. This is done by following R-peak detection, segmentation and period normalization. To reduce the computational complexity, R-peaks of two leads (V2 and V10) are detected by following the Pan-Tompkin's algorithm [13]. Reason behind choosing these leads is that the PTB database, considered in this work, has less noise in the precordial leads. The R-peak detection of a single lead may be sufficient, but two leads are processed to avoid detection of missing R-peaks in some pathological cases.

An ECG beat period comprises of a P-wave, followed by a QRS-complex, and finally a T-wave. The duration of PR interval (on-set of P-wave to the beginning of the QRS complex) is 120 to 200 ms. Each beat period has length of consecutive R-peaks, but segmenting beats just at R-peaks is not an effective

way to represent an ECG beat. Hence, each beat in the tensor is spanned 200 ms (200 samples) left from the current R-peak to 200 ms left from the next R-peak. After detection of R-peaks, each lead is segmented and normalized to number of beat periods. In literature, cubic spline interpolation and cut-and-align [19] beats techniques were used widely for period normalization. Problem with cubic spline technique is the same what we encountered during baseline cancellation, i.e. if some of the samples before end of the segment of a beat are monotonically increasing or decreasing, then amplitude of end samples of the resulting normalized segment is quite high that suppress the ECG signal. This outcomes poor performance and requires more computations. Hence, the cut-and-align technique is used in this work. Each beat period of a lead (V2 or V5), followed by beat periods of other leads, is normalized to same length (p). While following the cut-and-align method, appropriate number of zeros are padded to end of each beat to match their lengths. Then, the MECG data is arranged as a third-order tensor $\mathcal{X} \in \mathbb{R}^{m \times n \times p}$, where the dimensions m, n, and p correspond to number of leads, heart beats, and consecutive samples of period normalized heartbeat, respectively. The horizontal slices of $\mathcal{X}$ (keeping index m fixed, while other indices, n and p, are free) represent each ECG lead, and each vector of a horizontal slice represents the consecutive beats of a lead. For example, the horizontal slice $X_{1::}$ represents Lead I while the vector $x_{11:}$ represents the first beat period of Lead I and so on. However, for visualization of a third-order MECG tensor with each frontal slice that corresponds to a beat period of all leads is shown in Figure 4.4, but in the proposed work, each vertical slice contains a beat period of all leads as mentioned earlier.

4.3.3 Multiscale decomposition of the MECG tensor

It was discussed in the last chapter that the WT has better time-frequency resolution property and can segment ECG morphological features into different subbands, and hence, same is applied in this work also. The third-order MECG tensor $\mathcal{X}_{m \times n \times p}$ is wavelet decomposed using 1-D DWT. It is applied on the mode-3 fibers ($\mathbf{x}_{mn:}$) (by varying m and n with fixed p) to generate p-dimensional wavelet coefficients. Note that the 1-D DWT can be applied on a vector only. The resulted $L+1$ subband tensors comprised of one approximation ($\mathcal{A}_L$) and L number of details ($\mathcal{D}_L, \cdots, \mathcal{D}_1$) subband tensors. The dimensions of these tensors, $\mathcal{A}_L$ and $\mathcal{D}_j$, $j = L, \cdots 1$, are given as $m \times n \times p/2^L$ and $m \times n \times p/2^j$, respectively.

4.3.4 HOSVD application on subband tensors

After constructing the subband tensors, HOSVD (Section 4.2) is applied on these subband tensors for dimensionality reduction. Discussions and properties of HOSVD presented earlier are applicable for

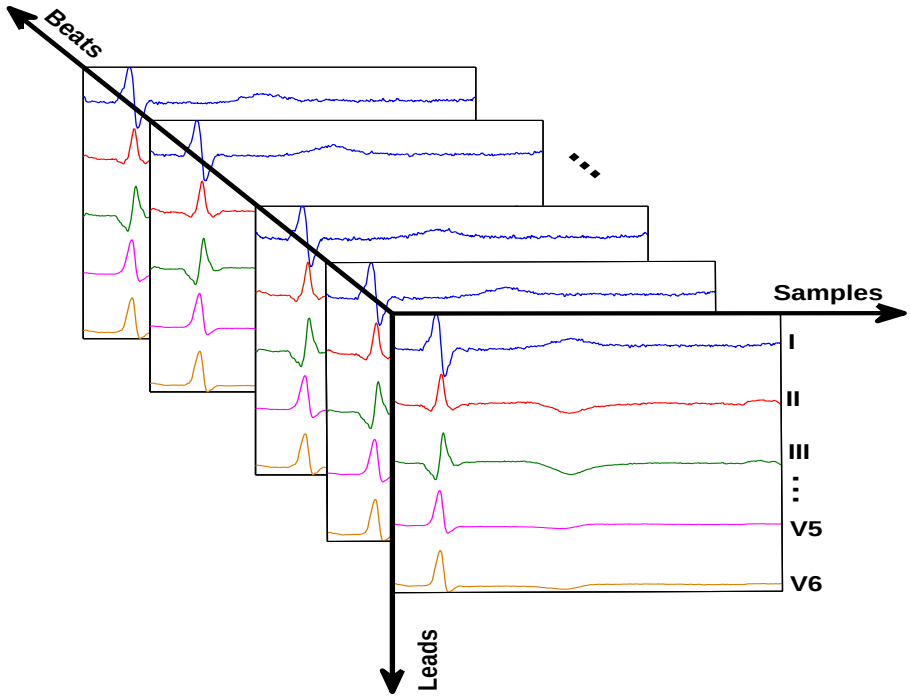

Figure 4.4: Visualization of tensor represented MECG Data ($Leads \times Samples \times Beats$). However, unlike the way tensor MECG is shown in this figure, each vertical slice contains each beat period of all leads in our work.

each subband tensor. HOSVD decomposes these subband tensors as

$$\mathcal{A}_L = \mathcal{S}_{A_L} \times_1 \mathbf{U}_{\mathbf{A_L}} \times_2 \mathbf{V}_{\mathbf{A_L}} \times_3 \mathbf{W}_{\mathbf{A_L}} \tag{4.5}$$

$$\mathcal{D}_j = \mathcal{S}_{D_j} \times_1 \mathbf{U}_{\mathbf{D_j}} \times_2 \mathbf{V}_{\mathbf{D_j}} \times_3 \mathbf{W}_{\mathbf{D_j}} \tag{4.6}$$

where $\mathbf{U}_{\mathbf{A_L}}$, $\mathbf{V}_{\mathbf{A_L}}$, and $\mathbf{W}_{\mathbf{A_L}}$ are orthonormal matrices of approximation subband tensors, and $\mathbf{U}_{\mathbf{D_j}}$, $\mathbf{V}_{\mathbf{D_j}}$, and $\mathbf{W}_{\mathbf{D_j}}$ are that of details subband tensors. These correspond to mode-1, mode-2, and mode-3, respectively.

Due to multiresolution property of DWT, the morphological features of ECG signal are grossly segmented into different wavelet subbands depending on their frequency content. Hence, the significant information of each beat of different leads are encoded in different orthonormal subband matrices. The column vectors of $\mathbf{U}_{\mathbf{A_L}}$ and $\mathbf{U}_{\mathbf{D_j}}$ span the lead space in respective subbands. The column vectors of $\mathbf{V}_{\mathbf{A_L}}$ and $\mathbf{V}_{\mathbf{D_j}}$ span the beat space, and the column vectors of $\mathbf{W}_{\mathbf{A_L}}$ and $\mathbf{W}_{\mathbf{D_j}}$ span each beat samples space in respective subbands [112]. This can be verified by considering, say, approximation

subband tensor. Computation of three orthonormal matrices ($\mathbf{U}_{\mathbf{A_L}}, \mathbf{V}_{\mathbf{A_L}}$ and $\mathbf{W}_{\mathbf{A_L}}$) is given as

$$\begin{aligned} \mathbf{A_L}^{(1)} &= \mathbf{U}_{\mathbf{A_L}} \mathbf{\Sigma}^{(1)} \mathbf{V}_{\mathbf{A_L}}^{(1)\ T} \\ \mathbf{A_L}^{(2)} &= \mathbf{V}_{\mathbf{A_L}} \mathbf{\Sigma}^{(2)} \mathbf{V}_{\mathbf{A_L}}^{(2)\ T} \\ \mathbf{A_L}^{(3)} &= \mathbf{W}_{\mathbf{A_L}} \mathbf{\Sigma}^{(3)} \mathbf{V}_{\mathbf{A_L}}^{(3)\ T} \end{aligned} \tag{4.7}$$

Rows of the matrix $\mathbf{A_L}^{(1)} \in \mathbb{R}^{m \times np'}$ consist of wavelet coefficients corresponding to leads whereas columns consist of wavelet coefficients of all beat samples. Hence, the matrix $\mathbf{A_L}^{(1)}$, as discussed in Section 3.1, is encoded in the left orthonormal matrix $\mathbf{U}_{\mathbf{A_L}}$. Similarly, rows of the matrices $\mathbf{A_L}^{(2)} \in \mathbb{R}^{n \times p'm}$ and $\mathbf{A_L}^{(3)} \in \mathbb{R}^{p' \times mn}$ consist of wavelet coefficients corresponding to beats and samples, respectively. And hence, matrices $\mathbf{A_L}^{(2)}$ and $\mathbf{A_L}^{(3)}$ are encoded in the left orthonormal matrices $\mathbf{V}_{\mathbf{A_L}}$ and $\mathbf{W}_{\mathbf{A_L}}$. In this way, these three matrices span the lead space, the beat space, and the samples space in approximation subband. Similar deductions are also applicable to other (details) subbands.

4.3.5 Thresholding of mode singular values

After performing MHOSVD on subband tensors and obtaining core subband tensors, dimensionality reduction is performed using an energy based thresholding technique. Energy of a tensor that corresponds to the squared Frobenius-norm of core tensor is calculated for all subband tensors. These subband tensors ($\mathcal{D}_5 \cdots \mathcal{D}_2$) are processed further for dimensionality reduction. This has been performed by measuring the quality of approximation of these tensors. The decreasing nature of the MSVs along different modes of each subband tensor can be used as a measure for the approximation [128, Property 10]. Frobenius-norm based dimensionality reduction was used in [144]. Likewise, the squared MSVs (that represent energy of a subband tensor) along different modes are proposed here for the thresholding process.

The MSVs, denoted as $\sigma^{(n)}$, for all decomposed tensors $\mathcal{A}_L$ and $\mathcal{D}_j$'s are given by

$$\begin{aligned} \sigma_k^{(1)} &= \sqrt{\sum_{i=1}^{p}\sum_{j=1}^{q} s_{ijk}^2}, \quad k = 1, \cdots r \\ \sigma_j^{(2)} &= \sqrt{\sum_{i=1}^{p}\sum_{k=1}^{r} s_{ijk}^2}, \quad j = 1, \cdots q \\ \sigma_i^{(3)} &= \sqrt{\sum_{j=1}^{q}\sum_{k=1}^{r} s_{ijk}^2}, \quad i = 1, \cdots p \end{aligned} \tag{4.8}$$

where p, q and r are size of n-mode dimensions, and s_{ijk}'s are elements of each subband core tensor. Value of r varies depending on the size of core subband tensor. Because of the ordering property (4.3) of the norms of slices, each multiscale tensor can be approximated by discarding non-significant SV

of core tensors and corresponding vectors of orthonormal matrices. Hence, the values of M, N and P (Section 4.2) for each multiscale tensor can be chosen using the following thresholding technique:

$$\eta_j^{(k)} = \frac{\sum_{i=1}^{I_k} \left(\sigma_i^{(k)}\right)^2}{||\mathcal{S}_{D_j}||_F^2} > 0.95 \tag{4.9}$$

where j = 1, 2, $\cdots$, 7 for respective subband tensors, $I_k = M$ or N or P depending on the mode and $||\mathcal{S}_{D_j}||_F^2 = \sum_i^m \left(\sigma_i^{(1)}\right)^2 = \sum_i^n \left(\sigma_i^{(2)}\right)^2 = \sum_i^{p'} \left(\sigma_i^{(3)}\right)^2$; p' is the 3rd-order dimension of each multiscale tensor. The value of *p'* depends on the value of *p* and is equal to $p/2^L$ or $p/2^j$, $j = 1, 2, \cdots L$ for approximation and details subbands, respectively.

4.3.6 Feature selection

After obtaining core subband tensors ($\mathcal{S}_{A_L}$ and $\mathcal{S}_{D_j}$'s), MSVs of selected subband tensors were computed. We learned in last chapter how the 'PQRST' morphological changes reflected by sum of squared SVs. Similarly, the MSVs (4.8) carry the information of different subband tensors in wavelet domain. Figure 4.5 shows the variation of MSVs for a healthy control (HC) case and two MI (antero-septal and inferior) cases. In case of HC (1st row panels), subband tensor $\mathcal{D}_6$ has highest MSV along any mode, followed by $\mathcal{A}_7$, $\mathcal{D}_5$, and so on. This is because QRS complex being the highest amplitude, is more dominant in D_6 subband. In case of ASMI (2nd row panels), we can observe few things: a large drop of MSVs between $\mathcal{D}_6$ and $\mathcal{D}_5$, and unlike in case of HC, $\mathcal{D}_7$ and $\mathcal{D}_5$ have higher magnitude than $\mathcal{A}_7$. This is because of pathological Q-wave, whose energy spectrum prevails over D_7, D_6 and D_5. In IMI case (3rd row panels), MSVs of $\mathcal{A}_7$ attains highest value, and $\mathcal{D}_7$ has higher magnitude than $\mathcal{D}_5$. This is due to ST-segment elevation in the dataset. Hence, it is expected that the morphological variations in different pathological conditions are reflected by MSVs.

Also, we can observe that the decreasing trend of MSVs for HC follow a particular trend. The general trend of MSVs for HC case is $D_6 > A_7 > D_5 > D_7 > D_4$ for 1st set of SVs, and trends for other set of SVs can be depicted from Figure 4.5 (a-c). However, this trend is deviated in MI cases depending on the change in morphologies (pathological Q-wave, ST-segment elevation or depression and T-wave inversion) in different subbands. For instance, in case of ASMI and IMI, MSVs follow the trend $D_6 > D_5 > D_7 > A_7 > D_4$ and $A_7 > D_6 > D_7 > D_5 > D_4$ for 1st set of MSVs, respectively. These trends follow in most cases. Comparing these results, the mode-1 and the mode-2 (Figure 4.5 (a, d, g) and (b, e, h)) SVs can be used as discriminating features for MI and HC.

Also, these values, as expected, decay fast for mode-2 indicating presence of high inter-beat correlations because of high similarity in beat morphologies. Slow fall-off of mode-1 and mode-3 SVs

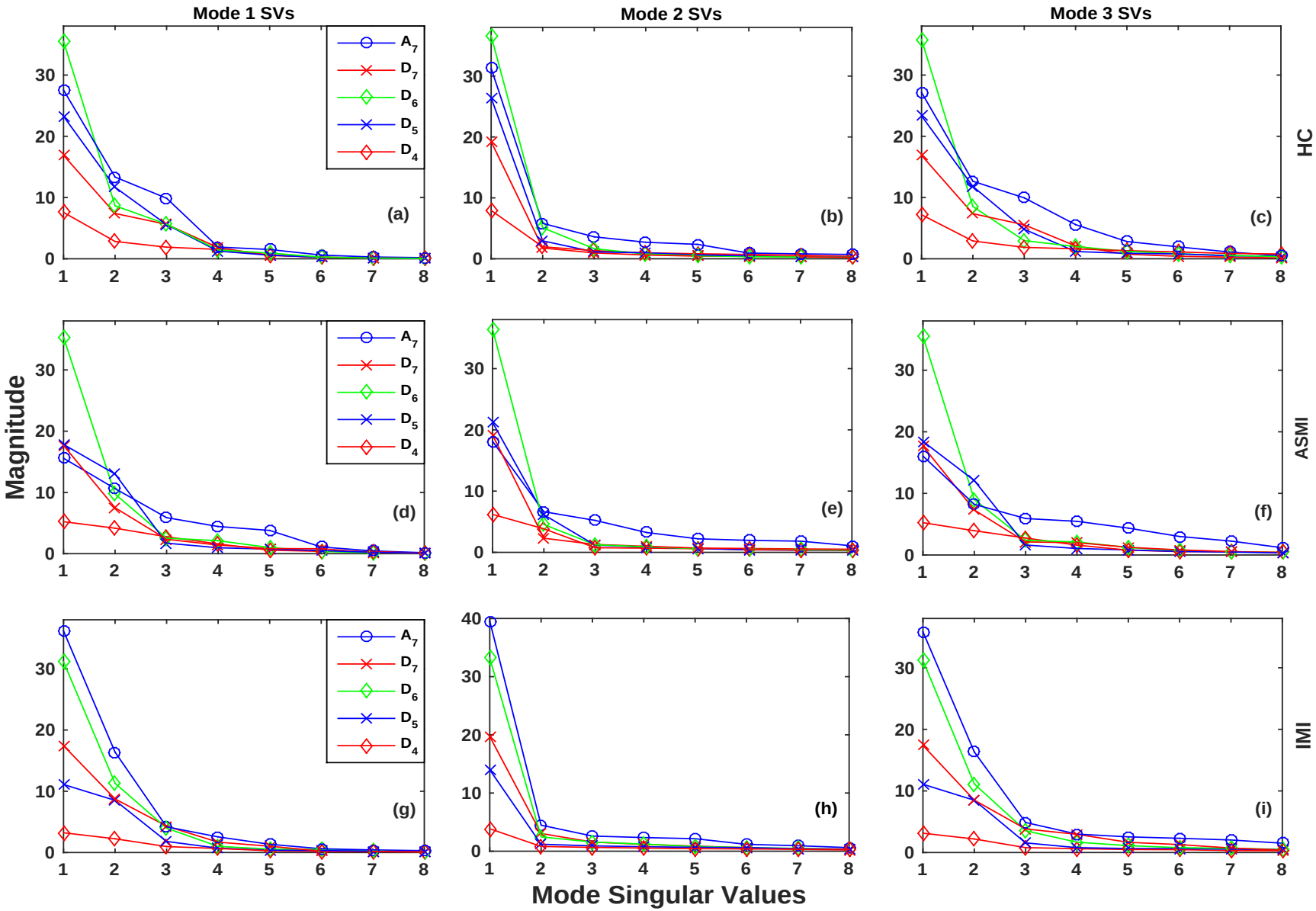

Figure 4.5: Mode 1, 2 and 3 Frobenius norms of SVs for different subbands. Panels (a)-(c) represent for HC (*s0273lrem*) case, and (d)-(f) and (g)-(i) represent for ASMI (*s0179lrem*) and IMI (*s0177lrem*) cases, respectively.

Table 4.2: Average MSVs selected along different modes of subband core tensors

Modes	$\mathcal{S}_{A_7}$	$\mathcal{S}_{D_7}$	$\mathcal{S}_{D_6}$	$\mathcal{S}_{D_5}$	$\mathcal{S}_{D_4}$
mode-1 (P=)	3.7	3.2	3.4	4.3	5.2
mode-2 (Q=)	3.6	3.4	3.8	4.7	4.7
mode-3 (R=)	3.6	3.5	4.4	5.3	6.3

suggest large morphologic variability due to variation among different leads and significant change in wave shapes (P-wave, QRS-complex, and T-wave), respectively. Average MSVs selected along different modes of subband core tensors, after approximation of subband tensor (Section 4.2), are shown in Table 4.2. For a particular subband tensor, the average MSV along a mode is calculated as the ratio between sum of the number of selected MSVs along that mode of all frames and total number of frames. The average results shown in this table are of all considered frames of all records. Selection of MSVs are based on the energy contribution in a particular subband tensor and is based on the results from earlier sections. Hence, for the feature vector that is to be used during training and testing, we have considered the floor[1] value of these average values. For example, first three, three, three, four, and five mode-1 SVs of $\mathcal{S}_{A_7}$, $\mathcal{S}_{D_7}$, $\mathcal{S}_{D_6}$, $\mathcal{S}_{D_5}$ and $\mathcal{S}_{D_4}$, respectively, are being selected. Similarly, in case of mode-2 and mode-3, the respective dimensions are three and three, three and three, three and four, four and five, and four and six, respectively for above subband core tensors. Reason behind choosing these subbands (A_7, $D_7, \cdots D_4$) is that these contain 'PQRST' segmented information, and rest hardly contain any useful information.

For localization, the normalized multiscale wavelet energy (NMWE) and mode-3 SVs are considered as features. This is because only MSV features are not able to localize subgroups of MI accurately. Reason behind choosing mode-3 SVs as features is that these convey the message of sample space variability. However, mode-1 and mode-3 SVs can be used as feature vectors alternately for detection and localization process, but during simulation we observed 2% higher accuracy if former one is chosen for detection process. The NMWE of the approximation or the details subband tensors along mode-3 is given as

$$E_{s,l}^{(3)} = \frac{\sum\sum[W_{l::}]^2}{qr} = \frac{\sum_{j=1}^{q}\left(\sum_{k=1}^{r} w_{l,j,k}^2\right)}{qr}, \quad l = 1, \cdots, 12 \tag{4.10}$$

where $W_{l::}$ contains wavelet coefficients of a particular lead and each vector w represents wavelet representation of a beat. In this equation, r corresponds to number of wavelet coefficients in a particular

[1] round the element to the nearest integer towards minus infinity

subband, and $s = 1, \cdots, 5$ stands for selected subbands (Table 4.2), used for classification purpose. This forms a $60(= 12 \times 5)$-dimensional NMWE feature set. Due to the presence of different types of correlations in the MECG signal, it is certain that the resulting NMWE features are also correlated. Also, a high-dimensional feature set requires more computations, thus by increases computational time. The student's t-test, a filter-based feature selection algorithm, can be used to reduce the feature length dimension, based on feature correlation criteria, to remove redundant features [159, 160]. The dimension of NMWE features is reduced to $6 \times 5 = 30$, after performing this test. Then these NMWE and mode-3 SVs are used as features for discriminating different subgroups of MI.

4.4 Dimensionality Reduction Performance Evaluation

In this section, dimensionality reduction performance of the proposed method and a comparative study with few existing methods are presented. For evaluation purpose, the MECG data from the PTB database is used. The MECG data of standard 12-leads are used. This work is a frame-wise processing of ECG beats where each frame contains $B = 10$ number of beats, and frames of limited records have been considered as shown in Table 4.4. Reason behind considering 10 beats in a frame is discussed in next section. Number of frames considered from different diagnostic classes for this analysis is shown in this table.

The MHOSVD is applied on each subband tensor as described in Section 4.3.4. To avoid any loss of low frequency characteristics in ECG, dimension of core tensors corresponding to $\mathcal{A}_7$, $\mathcal{D}_7$ and $\mathcal{D}_6$ are kept as it is. This is because these tensors contribute approximately 84% ($\mathcal{A}_7$: 36.47%, $\mathcal{D}_7$: 24.82%, and $\mathcal{D}_6$: 22.61%) altogether of the total relative energy. This is based on the relative energy of a particular tensor with respect to the total energy. It is observed that the relative energy of core tensor $\mathcal{D}_1$ is 0.06% as this subband has frequency information from 250 Hz to 500 Hz and hardly contain any significant information. Hence, this subband core tensor is discarded, and overall diagnostic information of the processed signal has not been affected much by discarding this subband tensor. This also helps fast processing as a minimum of 50% of wavelet transformed coefficients are eliminated which are present in this subband tensor. The dimension of other core tensors are reduced using the thresholding technique given in (4.9). It is observed that the mode-1 and the mode-2 dimensions of core tensors ($\mathcal{S}_{D_5}, \cdots \mathcal{S}_{D_2}$) reduce to 7.3 and 6.7 (on an average) from 12 and 10 respectively. Also there is a large dimensional reduction in mode-3 dimension of $\mathcal{S}_{D_3}$ and $\mathcal{S}_{D_2}$ core tensors.

Let us discuss with an example. Say, the original ECG tensor size is $12 \times 10 \times 867$, (number of

Table 4.3: An example showing tensor dimension size during MHOSVD decomposition

Original tensor	Subband core tensors	Expected dimensions	Actual dimensions due to rank property	Dimensions after thresholding
$\mathcal{X}_{12\times10\times867}$	$\mathcal{S}_{A_7}$	$12\times10\times15$	$12\times10\times15$	$12\times10\times15$
	$\mathcal{S}_{D_7}$	$12\times10\times15$	$12\times10\times15$	$12\times10\times15$
	$\mathcal{S}_{D_6}$	$12\times10\times22$	$12\times10\times22$	$12\times10\times22$
	$\mathcal{S}_{D_5}$	$12\times10\times35$	$12\times10\times35$	$8\times7\times6$
	$\mathcal{S}_{D_4}$	$12\times10\times62$	$12\times10\times62$	$8\times6\times7$
	$\mathcal{S}_{D_3}$	$12\times10\times116$	$12\times10\times116$	$7\times6\times8$
	$\mathcal{S}_{D_2}$	$12\times10\times223$	$12\times10\times120$	$7\times5\times5$
	$\mathcal{S}_{D_1}$	$12\times10\times438$	$12\times10\times120$	None

† The above numbers are taken directly from MATLAB for the record $s0004\_rem$ of the PTB database. Theoretically, D_1 subband has 434 coefficients if 867 samples are wavelet decomposed using multiscale analysis. Similarly, 217 coefficients in D_2 subband, and so on. But in MATLAB, these values go up to 438 in D_1 and 223 in D_2, and so on

leads: 12, frames processed: 10, and maximum length of a single beat period: 867). Table 4.3 shows dimension of each core tensor. We can observe that dimension along mode-3 of $\mathcal{S}_{D_2}$ and $\mathcal{S}_{D_1}$, due to rank property, is reduced to 120 (=12×10) from 223 and 438, respectively. However, after thresholding the MSVs, there is great reduction in dimensions (from 35, 62, 116 and 223 to 6, 7, 8 and 5) along mode-3 of $\mathcal{S}_{D_5}, \cdots, \mathcal{S}_{D_2}$. Number of samples in original tensor is $12\times10\times867 = 1,04,040$. After thresholding, number of coefficients in all subband core tensors is $12\times10\times(15+15+22)+3\times8\times7\times6+7\times5\times5 = 7423$. Effective number of coefficients in orthonormal matrices ($\mathbf{U}_{\mathbf{A_L}}$, $\mathbf{V}_{\mathbf{A_L}}$ and $\mathbf{W}_{\mathbf{A_L}}$) is $12\times10+10\times15+15\times12 = 450$. Similarly, effective number of coefficients in orthonormal matrices corresponding that to other subbands is $450+604+146+146+146+95 = 1587$. Total number of coefficients required to represent the original tensor after thresholding is $7423+450+1587 = 9460$. The proposed MHOSVD technique gives a sample-wise reduction of approximately 11:1 before coding stage. For lossless compression, selected MHOSVD transformed coefficients are uniformly quantized with 8 quantization bits/sample followed by Huffman encoding. Then the reverse procedure to reconstruct the MECG data is performed as shown in Figure 4.3. It follows Huffman decoding, MHOSVD restoration, inverse DWT, compressed MECG tensor formation, and period recovery.

Figure 4.6 shows the original (upper row) and the compressed (lower row) ECG signals of leads I, aVR and V6. It is clear that ECG characteristic waves are well preserved. Also, in leads I and aVR, noise has been reduced significantly in the compressed signals. This is due to application of multiscale

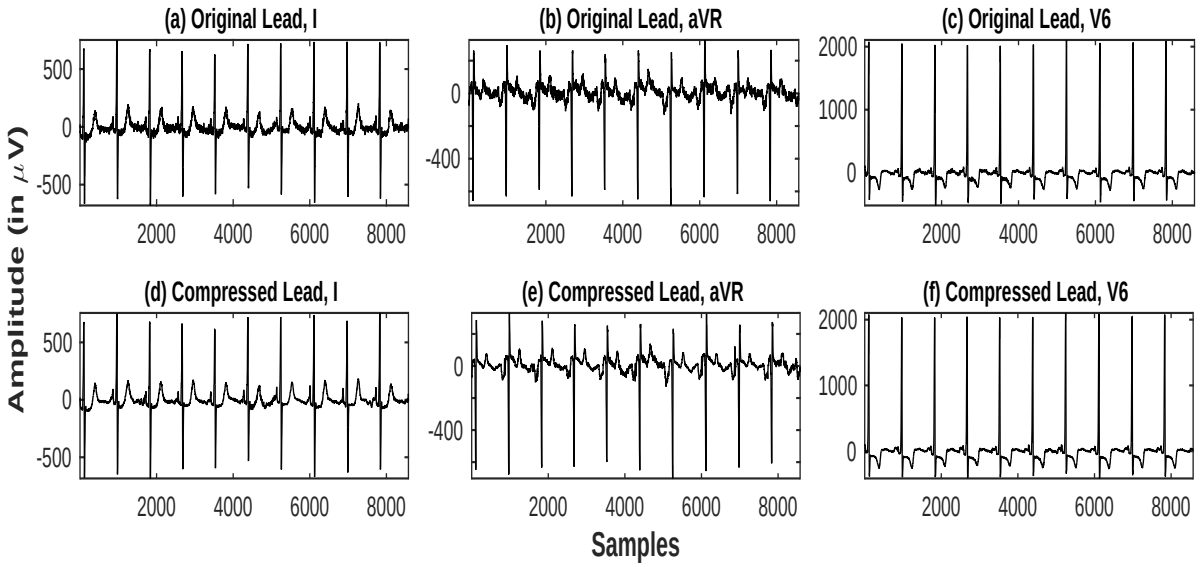

Figure 4.6: (a)-(c): Original and (d)-(f): Compressed ECG signals of Leads I, aVR and V6

DWT where noise content in high frequency subband tensors has been reduced.

4.4.1 Performance measures

To evaluate the dimensionality reduction performance of the proposed method, different quantities like average CR and three distortion measures (PRD, WDD and WEDD) are assessed. Bits for reduced data size include the number of bits required to represent nonzero coefficients, dictionary information, corresponding significance map and header information [161]. The significant singular vector coefficients (vectors containing nonzero elements of $\mathbf{U}$, $\mathbf{V}$, $\mathbf{W}$ and $\mathcal{S}$) are uniformly quantized with 8-bit quantization level, and corresponding CR values are calculated. The vector containing nonzero indices of core tensor $\mathcal{S}$ are quantized with 14 bits whereas the vectors containing nonzero indices of $\mathbf{U}$, $\mathbf{V}$, $\mathbf{W}$ are quantized with 8 bits.

To verify how well the clinical morphological features are preserved after compression, the distortion measures, namely PRD, WDD and WEDD are evaluated. In [118], authors considered eighteen features (six each from the duration, the shape and the amplitude parameters) and a penalty matrices with a weighted diagonal matrix for WDD evaluation. Same procedure has been adopted in this work. First, WDD is evaluated for each beat. Then these values are averaged for different leads. The average values of the distortion measures with CR for some datasets are enlisted in Table 4.4. Data shown here are of average values from different diagnostic classes. It is observed that chest leads (V2-V6) have less PRD and WEDD, and fall under 'excellent' (0-4.33) or 'very good' (4.33-7.8) category [104]. In any diagnostic class, we can observe that the PRD values of bipolar and augmented

Table 4.4: Average CR and distortion measures of different diagnostic classes

Diagnostic classes	frames	Metric	I	II	III	aVR	aVL	aVF	V1	V2	V3	V4	V5	V6	CR
Myocardial Infarction	20	**PRD**	11.85	5.98	3.92	28.75	7.07	24.87	5.18	3.25	3.49	2.39	4.23	3.52	46.3
		WEDD	4.39	2.56	2.29	6.57	2.64	5.48	3.51	2.37	2.91	1.88	2.27	2.92	
Cardiomyopathy	17	**PRD**	9.71	4.53	2.49	27.42	3.72	23.19	3.82	2.54	2.96	2.99	3.77	3.28	42.6
		WEDD	3.81	2.51	2.17	6.79	2.44	5.26	3.07	2.16	2.43	1.99	2.11	2.81	
Bundle branch block	17	**PRD**	10.55	4.13	2.19	27.56	4.72	25.47	4.19	2.64	3.28	2.97	3.61	3.34	45.7
		WEDD	4.07	2.60	2.15	6.03	2.06	5.20	3.14	2.14	2.29	2.10	2.31	2.02	
Dysrhythmia	16	**PRD**	12.81	5.84	3.29	29.53	4.28	26.71	4.17	3.57	3.91	2.94	3.76	3.94	26.3
		WEDD	4.79	4.36	3.85	8.72	4.84	5.41	3.68	3.49	3.82	2.74	2.90	3.05	
Healthy control	17	**PRD**	9.12	3.97	2.89	27.18	4.11	26.69	3.26	3.13	2.41	2.38	4.19	3.17	49.1
		WEDD	3.24	2.16	2.08	5.61	2.33	4.66	2.74	1.91	2.04	1.42	1.83	2.62	

The values shown in the table are for 8 bit quantization level.

leads are higher than the chest leads which may be due to the presence of motion artifacts and noise. The high PRDs ($>$ 24) in leads aVR and aVF does not signify poor reconstruction quality rather it is due to removal of noise in these leads (Figure 4.6). Discussing about the WDD, values those are smaller than 2.3 suggest the preservation of clinical information. These fall under 'very good' category ($0 - 2.3$ [118]). Some leads (I, aVR and aVF) have high WDD values that fall under 'good' category. These high values are due to the inaccurate detection of some characteristic features in those noisy leads. The low WEDD values in these leads indicate the good reconstruction quality. These values fall in the 'very good' (4.51-6.91) category. With this acceptable distortion ranges, the CR in different diagnostic classes is more than 45:1. However, for dysrhythmia class, CR reduced to approximately 25:1. This may be due to irregular nature of heart beat where the QRS detection algorithm fails to detect the exact R-peaks. This causes the number of beats to be very high, considering the same number of ECG samples i.e. value of becomes more than 70 instead of 8 to 20. This problem can be solved by an efficient QRS detection algorithm for dysrhythmia or similar type of diagnostic classes.

4.4.2 Comparison with existing data reduction methods

Comparison performance of the proposed method and the existing compression techniques is carried out and is shown in Table 4.5. CR depends on factors such as correlation, number of leads, sampling frequency, and quantization bits/sample. There are limited work available in literature for the MECG data. The compression performance has been carried out with different databases. Hence, direct comparison of the proposed method with others may not be appropriate. For fairness in comparison, same number of frames are processed by simulating the existing algorithms. Values shown in this table are average of 87 subjects (from different diagnostic classes of the PTB database). The average PRD and WEDD measures shown in this table are of a single lead (V4). During simulation, it is observed that CR value decreases when number of ECG signals are increased. The KLT and DCT based method has a CR of 7.25 with a PRD and WEDD of 3.18% and 3.10% respectively. The truncated SVD algorithm has a CR of 15.7 with a PRD and WEDD of 2.83% and 2.73% respectively. But one can mark significant deviations in characteristic waves like P-wave, ST-segment and T-wave of original and compressed signal [21]. This may be due to poor handling of ECG characteristic waves. Wavelet based LP model [40] has a good data reduction capability (CR = 22.70) but has high distortion errors (PRD = 10.25% and WEDD = 6.81%). The multiscale based PCA algorithm has less CR (12.61%) but has a good reconstruction quality with PRD and WEDD of 2.66% and 2.18% respectively. From this table, it is clear that our proposed method outperforms the existing techniques [16, 48]. It achieved a minimum CR value of 45 (except dysrhythmia class) with PRD and WEDD of 2.71% and 2.09%

Table 4.5: Comparison with existing ECG compression methods

Method	Type of Correlation	CR	PRD (in %)	WEDD (in %)
Cetin et al. [48] (KLT and DCT)	intra-beat	7.25:1	3.18	3.10
Wei et al. [21] (Truncated SVD)	inter-beat	15.7:1	2.83	2.73
Ramakrishnan et al. [40] (Wavelet based LP)	inter-beat	22.70:1	10.25	6.81
Sharma et al. [16] (DWT based MSPCA)	inter-lead	12.61:1	2.66	2.18
Padhy et al. (MSVD)	intra-beat & inter-lead	19.34:1	3.05	2.92
Proposed Method Multiscale HOSVD	All	> 45:1	2.71	2.01

† All algorithms computed in same environment (MATLAB, i5 CPU, 3.2 GHz processor) with equal MECG frames ($B = 10$)

respectively.

4.5 MI Classification Performance Evaluation

In this section, the MI classification performance is discussed. To evaluate the same, different parameters like Sensitivity (Sen), Specificity (Spe) and Accuracy (Acc) measured. In the literature, most of the authors have considered MIT database for classification. We have considered the PTB database as it has number of well classified (though not annotated) records related to MI. Data of 12-lead ECG corresponding to MI and HC diagnostic classes are used in this work. Out of 549 records available in this database, 369 records are related to MI subjects and 79 records are of healthy subjects. Approximately twelve records including one from healthy subjects are incomplete or irregular (difficult to process), and these have not been considered in this experiment. In cardiac diagnosis, MI has been categorized into different groups depending on the location of infarction in the myocardium [2]. In this experiment, five groups of MI (AMI, ALMI, ASMI, IMI and ILMI) have been considered since other groups have very limited number of ECG records for training and testing the classifier. Number of frames and beats of different MIs and healthy subjects (HS) used in the present experiment are shown

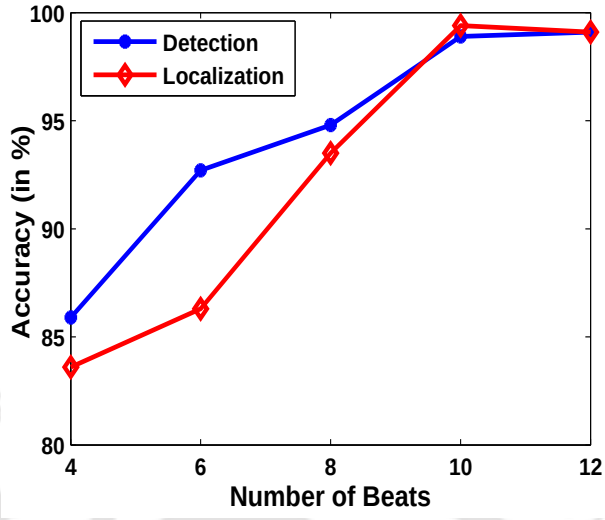

Figure 4.7: Frame size selection

Table 4.6: Number of instances of different types MIs and HC during training and testing

Type	AMI	ALMI	ASMI	IMI	ILMI	HC	Total
#records	49	42	74	92	55	78	390
#beats	6656	5622	10644	12313	6491	9966	51692
#frames	656	546	970	1192	627	982	4973
			Training				
#records	10	9	9	10	11	40	89
#frames	115	104	108	112	106	501	1046
			Testing				
#records	39	33	65	82	44	38	301
#frames	541	442	862	1080	521	481	3927

in Table 4.6. Number of frames depends on the total number of beats of an ECG signal in each dataset and is given as $No.\ of\ frames = \lfloor (total\ no.\ of\ beats)/B \rfloor$. The classification performance degrades when the value of B chosen is less than 10. Figure 4.7 shows the detection and localization accuracy (in %) for different frame sizes. We can observe that the accuracy is more than 97% when the value of $B = 10$ or more (which will be discussed later in this subsection), and it dropped to less than 95% when the value of B is less than 10. It may be due to the fact that 10 beats or more are able to capture the ECG information efficiently. This is the reason why value of B is kept 10 for both dimensionality reduction and classification purpose.

Table 4.7: Cross-validation Result of SVM Classifier for MI Detection

Classifier	Measures	Fold1	Fold2	Fold3	Fold4	Fold5	Avg
Polynomial	Sen(%)	91.3	92.5	89.4	91.8	91.6	91.3
	Spe(%)	91.9	93.3	90.4	92.6	92.8	92.2
	Acc(%)	88.4	90.4	87.5	88.3	89.7	88.9
RBF	Sen(%)	95.3	95.7	96.8	95.7	94.4	96.1
	Spe(%)	95.8	94.7	96.1	96.2	94.3	95.4
	Acc(%)	96.5	95.2	94.3	95.8	96.1	95.6
χ^2	Sen(%)	98.8	99.5	98.1	99.7	99.1	**99.1**
	Spe(%)	98.8	99.4	96.7	98.5	99.1	**98.5**
	Acc(%)	99.1	98.8	97.6	98.6	99.4	**98.7**

4.5.1 MI detection

The detection of MI is considered as a two class classification problem with MI and HC as two classes. LIBSVM, an integrated software for support vector classification is used to classify these two classes [**?**]. The significant MSVs (mode-1 and -2) corresponding to $\mathcal{A}_7$, $\mathcal{D}_7$, $\mathcal{D}_6$, $\mathcal{D}_5$ and $\mathcal{D}_4$ subband tensors are considered as features. In the earlier Section 4.3.6, we discussed about the dimension of feature vector for the classifier. A 35-dimensional feature set (mode-1: 18 and mode-2: 17 MSVs) is considered as the input to the SVM classifier. Each feature set of a frame corresponds to an instance. Total respective number of instances of MI and HC are 3991 and 982 when $B = 10$. These instances are divided into training and testing sets.

As these two classes have different number of instances (heartbeat frames), the classification problem is performed with same number of instances from each class, considering a balanced one. For training purpose, 500 instances, each from MI and HC classes, are selected. Random selection may chose the instances from the same subject during training and testing process. To avoid this over-fitting problem in this work, instances from set of subjects are considered during training. Then remaining instances of other subjects only are used for testing purpose. For example, 500 instances are selected from 40 subjects out of 78 in case of HC. Similar approach is followed for MI instances. Number of instances processed during training and testing are listed in Table 4.6.

Different SVM kernel parameters (*d*, γ, and *C*) are chosen that achieve an optimal performance, by following a grid-search using cross-validation. A five-fold cross-validation process is performed, and the best results for the kernel functions, namely polynomial, RBF and χ^2 are reported in Table 4.7. Parameters for these kernels are set as following $-$ polynomial: $C = 2^6$, $\gamma = 2^{-5}$, $d = 2$, RBF: $C = 2^5$, $\gamma = 2^{-5}$, and χ^2: $C = 2^5$, $\gamma = 2^{-4}$. The SVM classifier with polynomial kernel function has an Acc of

Table 4.8: Confusion matrix and MI Detection performance with optimal kernel parameters; Total instances = 980

Kernel type	Polynomial		RBF		χ^2	
Actual / Predicted	MI	HC	MI	HC	MI	HC
MI	429	57	460	29	473	19
HC	71	423	40	451	27	461
	TPR	FPR	TPR	FPR	TPR	FPR
	85.8%	11.9%	92.0%	6.1%	94.6%	3.9%
	FNR	TNR	FNR	TNR	FNR	TNR
	14.2%	88.1%	8.0%	93.9%	4.4%	96.0%
	Acc		Acc		Acc	
	86.93%		92.95%		95.30%	

88.9%, and Sen and Spe of 91.3% and 92.2%, respectively. The classifier with RBF kernel function achieve Acc, Sen, and Spe of 95.6%, 96.1%, and 95.4%, respectively, and the corresponding values with χ^2 kernel function are 98.7%, 99.1%, and 98.5%, respectively. It is clear from these results that SVM classifier with χ^2 kernel function performs better than the other two kernels. After obtaining the best kernel parameters, the whole training set is trained again to generate the final classifier. Then the classifier is tested with remaining 480 HC and randomly chosen 500 (100 from each subgroup) MI instances, those kept for testing purpose. These instances are from those subjects that have not been considered during training process. The TPR or Sen, TNR or Spe, FPR, FNR, and Acc for different kernels are shown in Table 4.8. The classifier with polynomial and RBF kernels give accuracy of 86.93% and 92.95%, respectively. But χ^2 kernel function outperforms these two in every aspect and gives better Acc of 95.30%. In this case, 473 MI instances have been classified correctly with a Sen of 94.6% and Spe of 96.0%. All experiments in this work are performed using MATLAB R2012b in a personal computer with CPU @3.20 GHz and 8 GB RAM.

4.5.2 MI localization

After detecting the presence of infarction, MI localization is an important task as it informs about the injury on which side of the heart wall or myocardium. In this work, five types of MI, namely AMI, ALMI, ASMI, IMI and ILMI are considered for localization process. It is a multi-class classification problem. The publicly available MSVMpack [162], an open source package dedicated to multi-class support vector machines is used for localization. The MSVs of $\mathcal{S}_{A_7}$, $\mathcal{S}_{D_7}$, $\mathcal{S}_{D_6}$, $\mathcal{S}_{D_5}$ and $\mathcal{S}_{D_4}$ along mode-3, evaluated after applying HOSVD on different subband tensors, are considered as the features for MI

Table 4.9: Performance comparison of subgroups with χ^2 kernel function SVM classifier; Total tested instances = 2922

Actual \ Predicted	AMI	ALMI	ASMI	IMI	ILMI	HC
AMI (500)	489	1	8	0	0	2
ALMI (442)	2	438	2	0	0	0
ASMI (500)	9	2	488	0	0	1
IMI (500)	1	0	2	487	9	1
ILMI (500)	1	2	0	7	490	0
HC (480)	1	1	2	0	0	476

localization. As described in Section 4.3.6, 51-dimensional feature set is considered as the input to the MSVM classifier. This 51-dimensional feature set constitutes 21-MSVs and 30 NMWE features along mode-3.

During training of MSVM classifier, 100 instances each from five subgroups of MI are considered as five classes with same kernel parameters. Remaining unknown instances are tested with the training model. Five MI classes have different instances and are listed in Table 4.6. We considered 500 instances randomly from ASMI and ILMI to make a bias free classifier. Hence, number of instances considered from AMI, ALMI, ASMI, IMI, ILMI and HC are 500, 442, 500, 500, 500 and 480, respectively, with a total of 2922 instances. Table 4.9 shows the localization performance for different MI subgroups with χ^2 kernel function. ALMI and HC classes are accurately classified with Acc equal or more than 99%. In case of AMI and ASMI classes, we can observe more number of mis-classifications. Of 500 AMI testing instances, 8 are classified as ASMI. Similarly, 9 are classified as AMI out of 500 ASMI testing instances. It is due to MI morphological changes in common leads V3 and V4. Similar reason can be concluded for other two MI subgroups, IMI and ILMI.

4.5.3 Comparison performance

A comparative study on Sen, Spe and Acc are presented in Table 4.10. Most of the algorithms reported in the literature are beat-specific [65–67, 72, 163, 164], and focus only on detection of MI from HC. The method described in [66] was able to perform both detection and localization, and achieved a good localization accuracy of 98.8%. Similarly other methods also achieved good classification performance. One of the limitation with these methods [66, 68, 72, 163] is that the experimentation is too over-fitted to the dataset, i.e. the heartbeats from the same subjects have been used during both the training and the testing sets. This, in turn, results high Sen, Spe and Acc. We have performed the experiments with and without over-fitting the training and the testing data. Results of Table 4.10 convey

Table 4.10: Comparison of classification performance with existing methods

Params \ Methods		Proposed				Sharma [68]	Arif [66]	Sun [67]	Jayachandran [72]	Nugent [65]	Heden [164]
		χ^2	χ^2	RBF	RBF	RBF	KNN				
Detection	Sen	94.6	98.2	92.0	97.2	93.0	97.2	92.6	NA	78.0	95.0
	Spe	96.0	98.7	93.9	96.7	99.0	99.6	82.4	NA	97.3	86.3
	Acc	95.3	98.8	92.7	96.9	96.0	NA	NA	95.9	NA	NA
Localization	Acc	98.1	99.3	94.0	98.4	99.6	98.8	NA	NA	NA	NA
Comments		NO	O	NO	O	O	O	NO	O	Not clear	

∗ NO: No over-fitting O: Over-fitting

that Sen, Spe and Acc values got lowered by 4-5% with RBF and 3-4% with χ^2 kernel function when the classifier is performed without over-fitting the data.

Without over-fitting the datasets, we still achieve better classification results. Sen (94.6%) and Spe (96.0%) of the proposed method during detection has been enhanced by 2% and 13% [67] when training and testing datasets are not over-fitted. Similarly, detection Sen and Acc (98.2% and 98.8%) with the recent work (93% and 96%) [68] has been enhanced by 5% and 2.8%, respectively, with over-fitting the datasets. Moreover, this method has two advantages. First, the dimension of feature set for classification is very small which may help fast processing. This is because the feature set has been extracted from the reduced MECG data. This method takes 0.23 s and 0.021 s, on an average, for detection and localization, respectively, during testing compared to 0.44 s and 0.025 s in [68]. Both methods have been executed under same environment. Second, detection and localization of MIs are being done simultaneously.

4.6 Summary

In this chapter, a third-order tensor representation of MECG data was proposed that helped exploit intra-beat, inter-lead with inter-beat correlations. The MHOSVD was applied to reduce the tensor data dimension. The storage efficiency was enhanced 45 times or more with acceptable distortion level using the proposed method.

Also some discriminative features were extracted from the reduced dimension of MECG data for detection and localization of MI. Results showed that the proposed tensor-based method performed better than the existing vector- or matrix-based methods. Another thing that had been followed in this work was that the training and the testing datasets were not over-fitted, i.e. datasets from some set of subjects were reckoned for training purpose, and datasets from other set of subjects, those were

not considered during training, were considered for testing purpose. Also during classification, it was observed that SVM classifier with the chi-square kernel function had better accuracy compared to the polynomial and RBF kernel function based classifier. In the next chapter we will discuss a study on how the MI progresses in different leads over period of time. This study will be performed by analyzing TWA.

5

T-Wave Alternans Analysis for Acute MI Progression

Contents

The development of reliable indicators of the sudden cardiac death (SCD) risk in patients with ischemic heart disease is one of the most important challenges for modern cardiology. Recent reports guide to study of T-wave alternans (TWA) as a promising indicator of an increased risk of life-threatening arrhythmias [165]. TWA is an electro-physiological phenomenon that appears in the ECG as an alternating pattern of ST-T-wave morphologies on alternate beats. TWA magnitude reflects a continuum of cardiac electrical instability; higher TWA levels indicate greater cardiac risk. TWA is considered as a prior prognosticator of SCD after acute MI, and same has been mentioned in [121] that the μ-TWAs are the risk factors for SCD after MI. In other words, it is most often used in patients who have had MI or other heart damage to see if they are at high risk of developing a potentially lethal cardiac arrhythmia. However, there is no quantitative study reported in the literature on how the TWA amplitude progresses in different leads over a period of time. This needs more information regarding the timing of the recording. In Chapter 4, detection and localization of acute MIs was proposed, but not their progression. To study this, first, it is essential to detect presence of TWA and estimate its amplitude and validate with synthetic and real datasets. The objective of this chapter is to introduce a new TWA detection and estimation method, followed by TWA amplitude progression in different leads for different types of acute MI over period of time.

A number of methods have been proposed for TWA detection over the past three decades. These methods range from the widely-used spectral analysis [88] to the recently proposed non-parametric signal processing technique [76] and template matched-filter-based scheme [77]. An excellent classification with a broad methodological review on TWA detection can be found in [74]. The continuous wavelet transform-based method [121] analyzed the TWA detection performance under Gaussian noise at different SNR levels. It results in more false positives or negatives in the presence of high-level of noise. Burattini et al. [75, 166] performed the TWA analysis to investigate the effect of interferences like residual noise, respiration modulation, replaced and missed beats and T-wave misalignments, etc. with synthetic and clinical signals. Some of the limitations of the previous methods as given in [76] are as follows: 1) the performance of the earlier methods requires proper conditioning of the signal before the TWA analysis, 2) the non-optimized parameters of the respective methods need to be tuned for different databases. However, the method in [76] used a number of stages for TWA detection and estimation. Inclusion or exclusion of some processing stages will alter the detection and estimation results for different databases. It is a difficult task to select which processing stages are to be included or excluded for a certain database. Also, these algorithms perform well when the TWA level is high, and they have less sensitivity to low-level TWA [59].

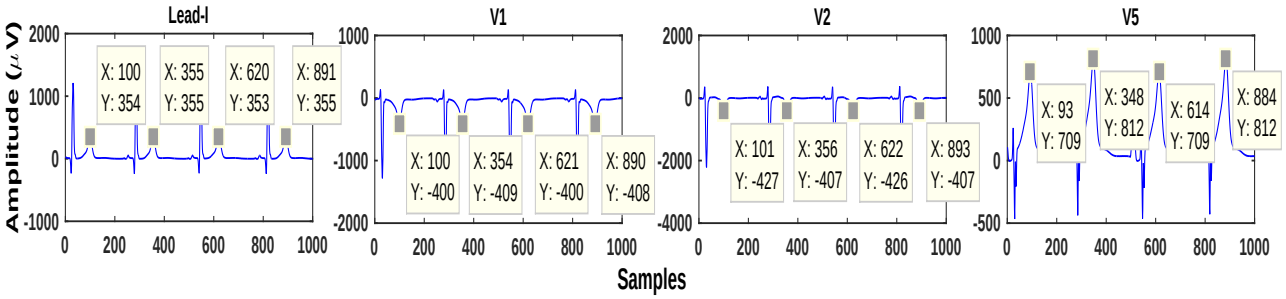

Figure 5.1: Visualization of TWA in some leads (I, V1, V2, and V5). Average heart rate = 113.705 beats/min over a 32-beat analysis window. Sampling frequency = 500 Hz

It is reported in [59, 95] that most of the existing methods proposed earlier either analyzed a single lead ECG or applied to each lead individually. As the TWA level is lead dependent, it may not be identified in a single lead or in a specific lead of the multilead ECG (MECG) system unless it is analyzed in all leads. Authors in [167] demonstrated that TWA analysis in all leads provides better and more reliable results than the single lead system. Figure 5.1 shows varying TWA amplitude levels in different leads of a single subject. In V5, there is a high level of TWA present, whereas a moderate level can be observed in V1 and V2, and less or no TWA in lead-I. Since last decade, authors have put research interest on multilead TWA analysis. Principal component analysis (PCA)-based multilead TWA analysis scheme [59] was proposed to improve the TWA analysis performance by exploiting the spatial redundancy of MECG data. A tensor-based TWA detection in MECG data was proposed in [93]. This method was based on extracting information from the time-domain T-wave signal and was tested with few datasets where either macroscopic TWA or no sign of TWA were considered. It is difficult to find exact locations of fiducial points in adverse conditions while dealing with time-domain-based methods. Also, a benchmark evaluation of study for TWA detection is not presented in [93].

To overcome the issues like parameter tuning and low sensitivity to low-level alternans and to enhance the TWA analysis for MECG data, a simple and robust TWA detection algorithm based on tensor applications, MAS, and HOSVD is proposed in Section 5.1. The first aim is to extract the only T-wave morphology from ECG signal even in noisy conditions. Multiscale analysis alleviates this problem by grossly segmenting the ECG morphological features where signal information and noise are placed into different subbands. The HOSVD is adopted with a hypothesis that TWA analysis can be improved by exploiting both temporal and spatial correlations of MECG data in the wavelet domain. The two types (semi-synthetic and real TWA) of datasets used for this analysis are discussed in Section 5.2. The proposed algorithm is tested with these data sets and experimental results are discussed in Section 5.3 and 5.4. Study on progression of MI in different leads over period of time

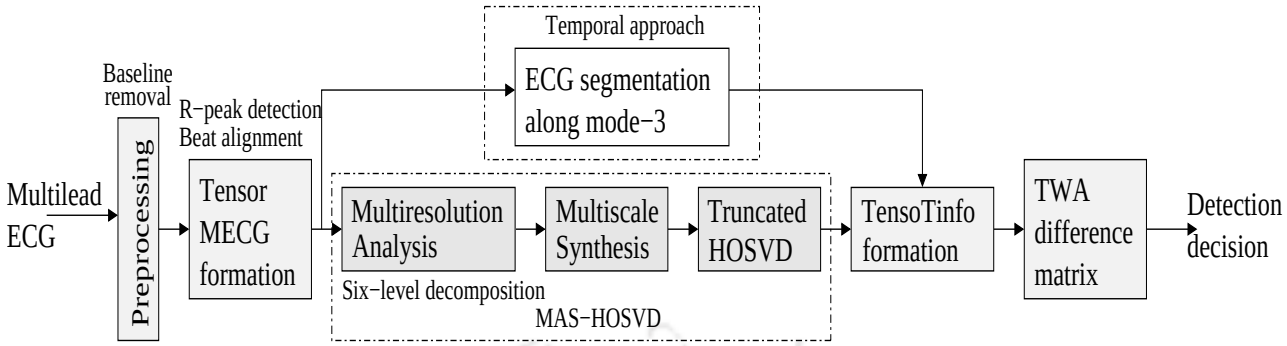

Figure 5.2: Block diagram for TWA detection using multiscale analysis and synthesis with HOSVD

using TWA analysis is carried out in Section 5.5. Finally, summaries are drawn in Section 4.6.

5.1 Proposed MAS-HOSVD-based Method

A block diagram for TWA detection scheme based on MAS-MHOSVD is outlined in 5.2. It consists of steps such as preprocessing, tensor MECG formation, MAS on tensor MECG, HOSVD on subband reconstructed T-wave tensor. These steps have been shown in grey colored boxes, whereas the white color filled box is intermediate step for temporal analysis. Detail procedure is presented in the following subsections. In the detection stage, it is decided whether there is TWA in the signal or not, and in the estimation stage the amplitude and/or the waveform of TWA is estimated. Depending on the specific method, detection and estimation can be performed simultaneously or consecutively, or one of them may be omitted. From here on, we will use the term 'analysis' to denote both detection and estimation as a whole.

5.1.1 Signal preprocessing

In the preprocessing stage, all independent eight leads are preprocessed to remove baseline-wander. During the TWA analysis, baseline-wander cancellation is an essential step and is considered as a major issue for Holter recordings [168]. In literature, baseline-wander was removed using different filtering and interpolation techniques [74]. In the preprocessing stage of the current work, baseline-wander of each lead was removed by passing each ECG signal through a digital sixth-order Butterworth high-pass filter with cut-off frequency f_c = 0.3 Hz. To get the zero-phase shift, the filtered signal was passed through the "Zero-phase forward and reverse digital filter" [16].

5.1.2 Tensor MECG formation

To analyze the beat-to-beat variations, i.e. the 'ABAB' pattern of T-wave, we restructured the 2-D MECG data into a third-order tensor, after R-peak detection and ST-T alignment. This representation helps all ECG leads process simultaneously while looking at different heartbeats. The T-wave alignment of beats was performed by maximizing their cross-correlation [**?**, 74, 168] with the beat having the highest length from a number of beats (frames of 32-beats were used). Then, zeros were padded at the beginning and end of each beat to match their lengths.

5.1.3 T-wave reconstruction using multiscale analysis-by-synthesis

After third-order tensor MECG formation, it is decomposed using discrete wavelet transform (DWT) to know exactly the spectro-temporal distribution of ECG morphologic features. As discussed in earlier chapters, the MRA property of the DWT grossly segments these features into different frequency subbands depending on their frequency content. These morphologic features have different spectral distributions over different subbands. T-waves have significant proportion of their energy only up to 10 Hz. The TWA is associated with the cardiac repolarization, and the ST-T interval (the interval between the starting of ST-segment and the end of the T-wave) represents the repolarization activity of the heart. Hence, the signal of interest, is concentrated in the frequency range of 0.3 and 15 Hz [169].

The DWT is applied on the mode-3 fibers ($\mathbf{x}_{mn:}$) (by varying m and n with fixed p) of the third-order MECG tensor $\mathcal{X}_{m\times n\times p}$. It results in $L+1$ subband tensors with $L=6$ [104] that comprise of one approximation ($\mathcal{A}_L$) and L number of details ($\mathcal{D}_j$, $j=6,\cdots 1$) subband tensors with dimensions $m\times n\times p/2^L$ and $m\times n\times p/2^j$, respectively. The maximum frequency of the subbands $\mathbf{A_6}, \mathbf{D_6}, \mathbf{D_5}, \cdots, \mathbf{D_1}$ are 3.906, 7.812, 15.624, $\cdots$, 250 Hz, respectively, if sampling frequency of the signal is 500 Hz. As discussed in the earlier paragraph, the T-wave information is retained in subbands A_6, D_6, and D_5.

To obtain the T-waves' information only, multiscale synthesis of lower frequency subband tensors $\mathcal{A}_6$, $\mathcal{D}_6$, and $\mathcal{D}_5$ along mode-3 fibers is performed. The recombination of the wavelet coefficients to reconstruct the original signal is basically a synthesis problem. The reconstructed samples are added to obtain the T-wave tensor $\mathcal{R}$ as follows

$$\mathcal{R} = \mathbf{r}_{ij:} = \mathbf{a}_{6ij:} + \mathbf{d}_{6ij:} + \mathbf{d}_{5ij:}, \quad \begin{matrix} i=1:m \\ j=1:n \end{matrix} \tag{5.1}$$

where $\mathbf{a}_{6ij:}$, $\mathbf{d}_{6ij:}$, and $\mathbf{d}_{5ij:}$ are the reconstructed samples of $\mathcal{A}_6$, $\mathcal{D}_6$, and $\mathcal{D}_5$. Note that $\mathcal{A}_6$, $\mathcal{D}_6$, and $\mathcal{D}_5$ have the same dimensions. The resulted mode-3 fibers that contain the T-wave and some part of P-wave information are noise free and suitable for analysis of TWA detection. Durations of PR interval

and QRS complex are, respectively, 120 to 200 ms and 80 to 100 ms. Hence, an interval of 320 ms, after 200 ms from the beginning, is considered. This segment contains the ST-segment and the T-wave of an ECG beat. The dimension of the T-wave tensor $\mathcal{R}$ turns out to be $m \times n \times p'$ where p' is the number of samples corresponding to the only T-wave.

5.1.4 TWA analysis using HOSVD on T-wave tensor

The third-order T-wave tensor $\mathcal{R}_{m\times n\times p}$ can be decomposed using HOSVD as

$$\begin{aligned}\mathcal{R} &= \mathcal{S} \times_1 \mathbf{U} \times_2 \mathbf{V} \times_3 \mathbf{W} \\ &= \sum_{i=1}^{m}\sum_{j=1}^{n}\sum_{k=1}^{p'} \mathcal{S}_{ijk}\mathbf{u_i} \otimes \mathbf{v_j} \otimes \mathbf{w_k}\end{aligned} \tag{5.2}$$

where $\mathbf{U} \in \mathbb{R}^{m\times m}$, $\mathbf{V} \in \mathbb{R}^{n\times n}$ and $\mathbf{W} \in \mathbb{R}^{p'\times p'}$ are orthonormal matrices. $\mathcal{S}$ (analogous to Σ of linear SVD) is the core tensor which controls interaction between orthonormal matrices. Unlike Σ, it does not have a simple, diagonal structure. The matrices ($\mathbf{U}$, $\mathbf{V}$ and $\mathbf{W}$) depict the space variabilities along different modes. In other words, the column vectors of $\mathbf{U}$, $\mathbf{V}$ and $\mathbf{W}$ span the lead, beat and beat samples space variabilities. Details on computing orthonormal matrices and the core tensor are given in [99]. The core tensor $\mathcal{S}$ is calculated as $\mathcal{S} = \mathcal{R} \times_1 \mathbf{U}^T \times_2 \mathbf{V}^T \times_3 \mathbf{W}^T$.

Then the TensorTinfo ($\mathcal{T}$) was determined as

$$\mathcal{T} = \mathcal{S} \times_3 \mathbf{W} \approx \hat{\mathcal{S}} \times_{\mathbf{3}} \hat{\mathbf{W}} \tag{5.3}$$

where $\hat{\mathcal{S}}$ and $\hat{\mathbf{W}}$ are the dimension reduced versions (of the corresponding original core tensor and orthonormal matrix, respectively), after retaining the T-wave information. This truncation process based on the thresholding of mode singular values preserves 95% energy of the tensor along any mode. A detailed discussion can be found in [**?**, 99]. As dimension reduction of a tensor is beyond the scope of this study, readers are encouraged to refer these materials for details. The TensorTinfo describes how the lead and the beat variation parameters interact. The presence of TWA or 'ABAB' pattern across beats of a lead can be recognized from the vector $\mathbf{t}$ which was computed as

$$\mathbf{t}_{lb} = \mathcal{T} \times_1 \mathbf{U}_{:l}^T \times_2 \mathbf{V}_{:b}^T \tag{5.4}$$

where $\mathbf{U}_{:l}$ and $\mathbf{V}_{:b}$ are desired lead and beat representation vectors, respectively. Information in $\mathbf{t}$ was

Algorithm 2 μ-TWA detection using MAS with HOSVD on third-order MECG tensor

Input: Preprocessed MECG data matrix $\mathbf{X}$, F_s (=1000 Hz)
Output: Detect the presence of TWA or not
begin
Stage 1: Form the 3-array MECG tensor, $\mathcal{X}$
Stage 2: T-wave reconstruction using MRA
Apply L-level wavelet decomposition on mode-3 fibers of $\mathcal{X}$ to form $L+1$ subband tensors
Reconstruct the subband tensors using multiscale synthesis on mode-3 fibers of $\mathcal{A}_6$ and $\mathcal{D}_6$
Add the reconstructed samples to get T-wave tensor, $\mathcal{R} = \mathbf{r}_{ij:} = \mathbf{a}_{6ij:} + \mathbf{d}_{6ij:} + \mathbf{d}_{5ij:}$, i = *1:m*, j = *1:n*
Stage 3: HOSVD on T-wave tensor ($\mathcal{R}$)
T-wave tensor is decomposed to provide the lead, beat, and sample space variabilities using HOSVD as $\mathcal{R} = \mathcal{S} \times_1 \mathbf{U} \times_2 \mathbf{V} \times_3 \mathbf{W}$
TensorTinfo is represented as $\mathcal{T} = \mathcal{S} \times_3 \mathbf{W} = \mathcal{R} \times_1 \mathbf{U^T} \times_2 \mathbf{V^T}$
Vector $\mathbf{t}$ that helps recognize the presence of TWA or not is given as $\mathbf{t} = \mathcal{T} \times_1 \mathbf{u}^T \times_2 \mathbf{v}^T$
end

concatenated and presented in a matrix form as follows

$$\mathbf{T} = \left[\underbrace{\mathbf{t}_{11}\mathbf{t}_{21}\cdots\mathbf{t}_{m1}}_{\mathbf{B_1}} \underbrace{\mathbf{t}_{12}\mathbf{t}_{22}\cdots\mathbf{t}_{m2}}_{\mathbf{B_2}} \cdots \underbrace{\mathbf{t}_{1j}\mathbf{t}_{2j}\cdots\mathbf{t}_{mj}}_{\mathbf{B_j}} \right] \tag{5.5}$$

where columns of matrix $\mathbf{B}$ contains T-wave information in $\mathbf{t}$ of respective leads, and j represents the number of beats considered for analysis (here $j = 32$). In [59, 95], TWA detection was performed on the transformed data, whereas in the proposed work, it was performed in the time-domain. The TWA information in tensor $\mathcal{T}$ (5.3) was transformed back to the time-domain in terms of vectors in $\mathbf{t}$ (5.4). As $\mathbf{t}$ is in time-domain, detrending can be applied on it to cancel the ST-T complexes. So, the TWA difference matrix **D** was computed by differencing conjugate beats, i.e. second beat information from the first beat, the third beat that from the second beat, and so on, which is given as

$$\mathbf{D} = [\mathbf{B}_i - \mathbf{B}_{i+1}], \quad i = 1 : j-1 \tag{5.6}$$

This matrix was used for evaluation of detection and estimation. Also, the TWA or 'ABAB' pattern can be distinguished visually by observing the difference matrix. An algorithmic procedure of our proposed method for tensor based TWA is presented in Algorithm 2.

5.1.5 TWA detection decision and estimation

To decide the presence of TWA or not, we measured two parameters, namely the TWA ratio (TWAR) [88] and the probability *p*-value by following the Wilcoxon rank-sum test [121]. TWAR measure is based on the spectral analysis, which has been described elsewhere [88]. In brief, power spectra of each beat-to-beat samples of ST-T complex are computed using the fast Fourier transform. The TWA detection statistic (Z) is given by the composite spectrum of summed power spectral at each time point

whose spectral magnitude is 0.5 cycles/beat (cpb). Mathematically, TWAR is given as

$$TWAR = \frac{Z - \mu}{\sigma} \tag{5.7}$$

where μ and σ are the mean and the standard deviation of the spectral noise measured in the spectral window (0.33-0.48 cpb). The TWAR is compared to a fixed value of the threshold (γ). In this case, $\gamma \geq 3$ signifies the presence of TWA, or otherwise [59, 74, 76, 80, 88, 92, 170]. The estimated TWA amplitude is given as

$$V = \sqrt{Z - \mu}. \tag{5.8}$$

For evaluation of *p*-value, the maximum T-wave amplitude of each T-wave in $\mathbf{T}$ (5.5) was considered for the rank-sum test. These 32 values of a frame were separated into two groups, corresponding to even and odd beats. The Wilcoxon rank-sum test was applied to these two groups, each containing 16 entries, to compute the *p*-value. Then, the groups whether come from the same population or not was decided based on the calculated *p*-value with a confidence level of 95% ($p < 0.05$).

■

In temporal approach (Figure 5.2), the TWA analysis was carried out with the time-domain ECG signal. This approach was being evaluated to compare with the proposed method. After MECG tensor formation, ECG beats along mode-3 were segmented. A segmentation window of 320 ms, after the end of the QRS complex, was selected for the TWA analysis.

5.2 Datasets

5.2.1 Semi-synthetic dataset

To validate and compare the proposed method in different scenarios and with other state-of-the-art methods, a semi-synthetic database by adding known and different amount of alternans to alternate heartbeats of ECG signals is first re-created. These ECG signals are considered from the healthy subjects of the PTB database [171]. This database contains 52 healthy subjects' data with each having one to three records; a single record corresponding to each subject is considered in our work. Each signal is digitized at 1000 samples per second, resolution of 16 bit with 0.5 μV/LSB. To keep a constant sampling frequency over the other database considered in this work, we resampled each ECG signal to 500 Hz. Only eight independent leads out of the 12-lead set were processed.

Different TWA amplitude levels ranging from 0 to 100 μVs are added to every other T-wave of the records under consideration. Addition of alternate waveforms is carried out with selected but randomly

chosen leads rather than with all 8-leads. Further, to experience a high degree of realism, four types of noise are considered: Gaussian (*gs*), Laplacian (*lp*), electrode motion (*em*), and muscular activity (*ma*). Different levels of *gs* and *lp* noise with SNRs ranging from 0 to 50 dB in interval of 5 dB were added to each of ECG leads of all records. Real noises for ECGs such as *em* and *ma*, obtained from the MIT-BIH Noise Stress Test Database [172], are added randomly to MECG records as follows. As the clean and the noise signals are sampled with different sampling frequencies, the noise signals were resampled to 500 Hz. To add the noise signal with the clean signal, a noise segment of length equal to that of the clean signal was extracted. For each MECG record, each noise signal of two-lead noise records are paired with four ECG signals but with different multiplicative scale factors [173].

5.2.2 Physionet TWA database

The other database considered in this work is from the TWA/CinC challenge database. A detailed description on this database is discussed in 2.5.2. In the present analysis, records of the standard 12-lead ECGs only (72 out of 100 records) are considered, and the proposed algorithm is evaluated with independent 8-lead ECG signals.

5.3 Experiments on 8-lead Semi-synthetic Signals

5.3.1 Observations with temporal method

Temporal analysis for TWA detection is carried out as shown in Figure 5.2. The consecutive beats are considered directly after ECG segmentation during temporal analysis. This approach is somehow similar to the temporal analyzing schemes proposed in the literature. Table 5.1 shows the *p*-value and TWAR for different comparative studies. The algorithm classifies correctly with $p < 0.05$ when there is either no TWA present or TWA amount is more or equal to 100 μV. But for other alternan amplitude levels, the classifier performance degrades to 83.9%, 72.5%, and 65.7% when the amplitude levels are 50, 20, and 10 μV, respectively. With TWA amplitude of 10 μV, the value of TWAR (less than 3) signifies the absence of TWA. For TWA amplitude of 20 μV, the results of the TWAR and the *p*-value ($p < 0.05$) are contradictory in nature. We can observe in this case is that the algorithm is able to classify only 72.5% where TWAR is greater than 3. This is because that the noise has prevailed over the low-voltage TWA, and the detection algorithm using the temporal method fails to notice the microscopic TWA.

The TWA detection performance when ECG records are added with different SNRs (30, 20, 10, and 5 dB) is presented in Table 5.1. The study under noisy conditions are shown with two TWA amplitude

levels (20 and 50 μV) for each SNR. We can observe that the detection performance is 71.1% when SNR is 50 dB and added TWA amplitude is 20 μV, and it goes down as the SNR level decreases. Also for a particular SNR, the algorithm performs well when the alternan level is more or equal to 50 μV, but it fails if this level is less than 20 μV.

5.3.2 Observations with MAS method

Similar test analysis is accomplished for multiscale synthesis. For TWA analysis, T-wave information is obtained directly from the T-wave tensor (5.1) without performing HOSVD and used to evaluate the difference matrix $\mathbf{D}$. During this test procedure, the *p*-value and the TWAR are evaluated from consecutive beats directly after multiscale synthesis and before applying HOSVD (Ref: 5.2). The results of Table 5.1 suggests that there is an improvement in TWA detection using the multiscale synthesis over the temporal analysis. This is because the high-frequency noise gets suppressed due to the multiresolution analysis by synthesis. The algorithm able to classify ($p < 0.05$) 50 μV alternans with 95.2%, but it still fails to detect low amplitude alternan levels.

The TWA detection performance gets improved till moderate levels of noise (SNR up to 20 dB) are added. When SNR is 20 dB or below, detection performance is improved by more than 12% compared to the temporal scheme.

5.3.3 Observations with MAS-HOSVD method

We can observe that the multiscale synthesis method is able to detect the TWA presence when the alternan level is 50 μV or more with SNR up to 20 dB. This method fails in adverse conditions like when the alternan amplitude level is 20 or 10 μV, or the SNR goes below 20 dB. As like in [59] where PCA was used for multilead TWA analysis, we adopted HOSVD in this work as 2-D PCA or SVD cannot be applied to the third-order T-wave tensor. Transformation scheme using MAS-HOSVD has improved the TWA detection performance. The algorithm classified ($p < 0.05$) TWA amplitude levels of 50 and 100 μV accurately. The detection performance has been improved significantly for TWA amplitude levels of 10 and 20 μV. Also, the estimated TWA amplitudes are almost same with a maximum deviation of 0.8 μV when added $V_{alt} = 10$ μV. With different levels of noise, the estimation performance is also accurate; the maximum deviation is 2.0 μV for 10 dB SNR signals when added $V_{alt} = 20$ μV. In addition, the mis-classifications with the temporal method has been improved using the MAS-HOSVD method.

Table 5.1: Average Wilcoxon rank-sum test probability (p-value), TWARs and average V_{alt} for different TWA amplitude levels and SNRs of semi-synthetic signals

			temporal analysis			**MAS**			**MAS with HOSVD**		
			p <0.05	TWAR	Avg V_{alt}	p <0.05	TWAR	Avg V_{alt}	p <0.05	TWAR	Avg V_{alt}
Amplitude (μV)		0	100%	0.07±0.003	0.1	100%	0.21±0.008	0.1	100%	0.98±0.004	0.0
		10	65.7%	1.25±0.005	15.6	**79.1%**	**3.58±0.015**	11.5	95.2%	4.93±0.011	10.8
		20	**72.5%**	**3.89±0.017**	25.8	80.6%	4.95±0.013	18.7	98.5%	7.71±0.018	20.5
		50	83.9%	5.03±0.009	45.6	95.2%	8.82±0.019	51.9	100%	15.65±0.022	50.1
		100	99.8%	9.18±0.117	106.1	100%	13.68±0.017	101.5	100%	18.29±0.029	100.1
SNR (dB)	50	20μV	71.1%	5.17±0.020	29.7	96.4%	5.91±0.071	24.4	99.1%	8.28±0.070	20.7
		50μV	81.2%	8.03±0.009	57.1	98.5%	9.73±0.009	53.1	100%	14.16±0.020	49.8
	30	20μV	78.9%	6.42±0.049	32.9	93.1%	8.38±0.020	24.1	96.2%	8.49±0.098	21.3
		50μV	82.6%	9.72±0.068	45.3	94.7%	10.02±0.053	47.2	98.6%	15.01±0.020	50.9
	20	20μV	76.2%	7.09±0.071	33.6	90.1%	8.19±0.290	25.5	94.5%	7.94±0.031	21.6
		50μV	81.5%	10.49±0.025	59.6	93.4%	10.49±0.054	46.7	95.9%	14.88±0.047	51.2
	10	20μV	69.8%	7.48±0.021	32.4	86.9%	9.01±0.008	27.0	92.3%	8.09±0.049	22.0
		50μV	71.7%	10.76±0.034	60.2	88.2%	11.41±0.041	54.8	92.7%	15.18±0.067	51.7

Note: Values shown here are averaged over all 8-leads

5.3.4 Comparison with the state-of-the-art methods

Due to the unavailability of clinical gold standards for TWA, it is difficult to compare and validate the proposed method with most of the existing methods. However, for a fair comparison, the proposed method was compared with three (the classical modified moving average (MMA) [89], the wavelet-based [121] and the multi-PCA [59]) methods, considering the same database. We implemented the wavelet-based [121] and the multi-PCA [59] methods and used the TWAnalyser toolbox [174] for the MMA method. Semi-synthetic signals were processed with these methods using a 32-beat analysis window.

To compare the proposed method with the multi-PCA, parameters like the probability of detection (P_{D}) and probability of false alarm (P_{FA}) were evaluated. Following the conventional definitions of detection theory, the P_{D} and P_{FA} were defined as

$$P_{\mathrm{D}} = \frac{\text{number of positive TWA detections with a given V}_{alt}}{\text{total number of detections}}$$

$$P_{\mathrm{FA}} = \frac{\text{number of positive TWA detections when the added V}_{alt} = 0}{\text{total number of detections}}$$

The detection performance was evaluated from the receiver operating characteristic (ROC) curve as shown in Figure 5.3. It shows the variation between P_{D} and P_{FA} for different detection threshold γ. The P_{D} and P_{FA} were evaluated by considering 194 frames of semi-synthetic dataset described in Section 5.2.1. We can observe that the P_{D} value increases with lowering the γ value, but the P_{FA} value gets increase simultaneously. To have a minimum P_{D} value of 0.95, we chose the P_{FA} = 0.01 and the corresponding threshold γ was selected for detection. This procedure was followed for different added SNR levels for a particular type of noise.

Figure 5.4 shows the comparison plots of the resulting P_{D}s vs input alternans level. For the TWA amplitude range of 10 to 60 μV, the MAS-HOSVD method detects alternans with at least $P_{\mathrm{D}} = 0.197$ higher than the multi-PCA method. With the TWA amplitude of 10 μV, the proposed method attains the P_{D} = 0.857, whereas the multi-PCA method attains the P_{D} = 0.422 for the same level of TWA amplitude. Results with *lp* noise at SNR = 20 dB are also shown in this figure. Decrease in P_{D} for a given V_{alt} of the MAS-HOSVD method is lower than the multi-PCA method. For example, when $\mathrm{V}_{alt} = 10\ \mu V$, the P_{D} changes from 0.857 to 0.627 and 0.422 to 0.147 for MAS-HOSVD and multi-PCA methods, respectively.

To analyze the behavior of the methods under different noise conditions, the above considered four types of noise were added to the semi-synthetic datasets with different SNR levels. For each case, the γ was selected so that P_{FA} = 0.01 and the corresponding P_{D} was evaluated and compared. Figure

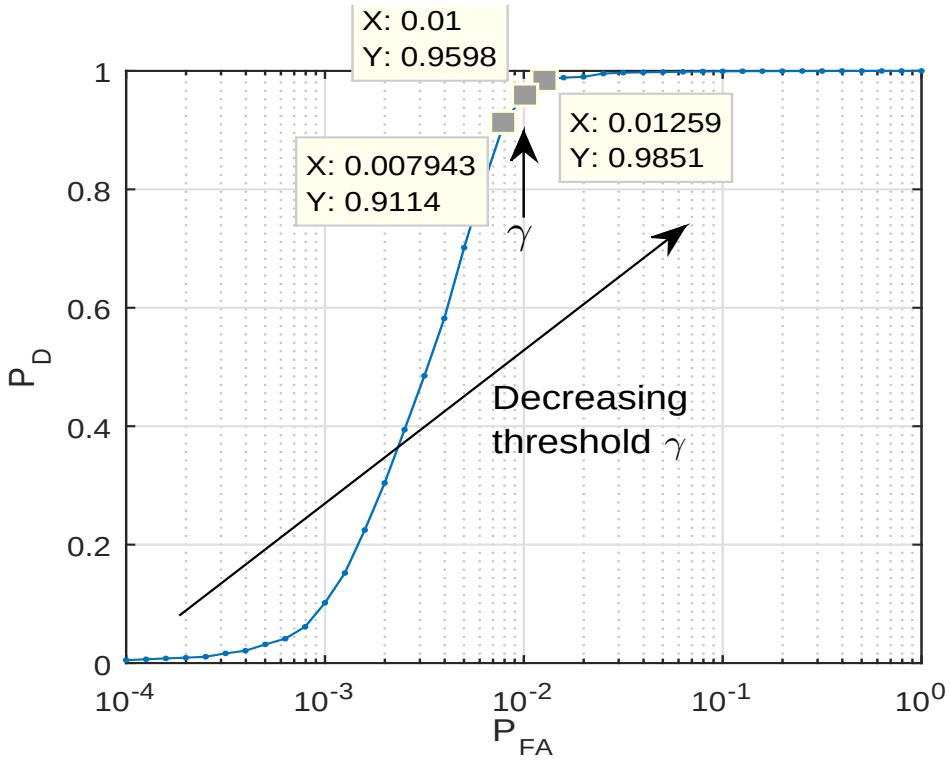

Figure 5.3: Variation of P_{D} vs P_{FA} for SNR = 20 dB

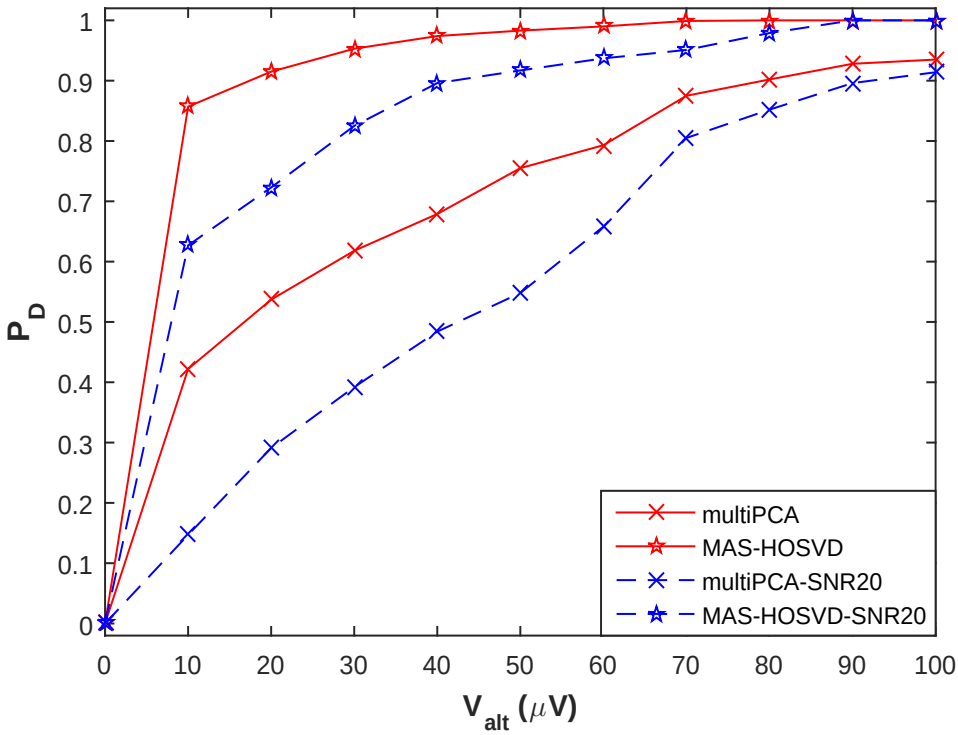

Figure 5.4: Variation of $\mathrm{P_D}$ vs V_{alt} (semi-synthetic datasets with *lp* noise of SNR = 20 dB) for multi-PCA and MAS-HOSVD techniques

5.5 shows P_{D} of the three methods versus SNR for *gs*, *lp*, *em* and *ma* types of noise. For a certain P_{D} (say, $P_{\mathrm{D}} = 0.95$), the SNR level in case of *gs* noise is at least lower by 10 dB for the MAS-HOSVD

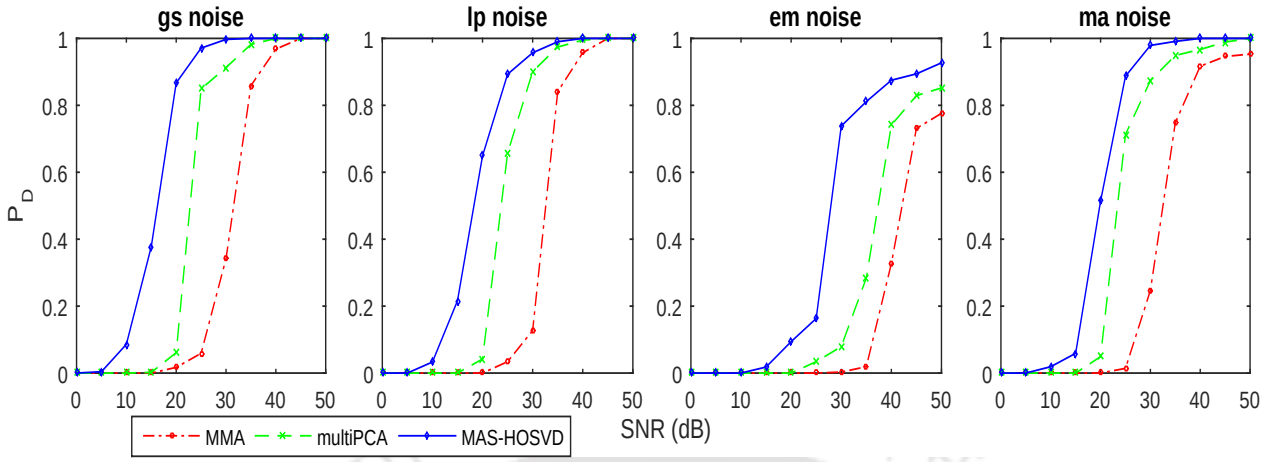

Figure 5.5: Variation of P_D of MMA, multi-PCA and MAS-HOSVD methods under *gs*, *lp*, *em* and *ma* noise with different SNR (dB) levels. $P_{FA} = 0.01$ for all methods

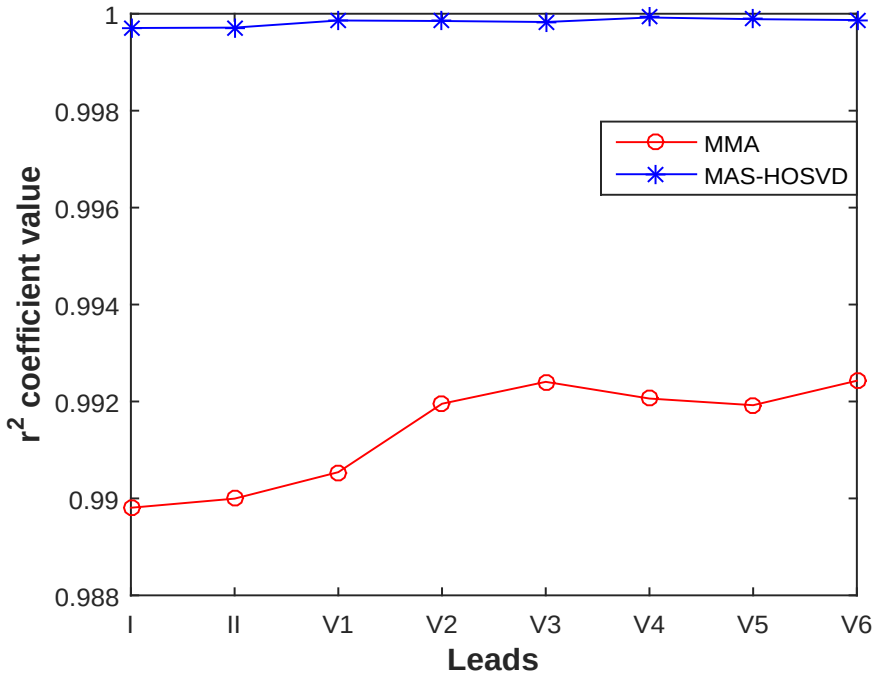

Figure 5.6: Comparison performance of MAS-HOSVD with MMA using the r^2 correlation coefficient values of all leads.

method compared to the multi-PCA method. In case of *lp* and *ma* noises, the proposed method attains the said P_D at the SNR level lower by 5 dB compared to the other method. The detection performance degrades for *em* noise. The proposed method achieves the $P_D \geq 0.9$ for SNR = 45 dB or more, and it performs better than the multi-PCA method.

Further, comparing the *p*-value results with the wavelet-based method [121], a significant improvement in detection performance is observed. The algorithm in [121] classifies ($p < 0.05$) 81%, 86%, 98%, and 100% TWA signals when the alternan amplitude levels are 10, 20, 50, and 100 μV, respectively. The proposed MAS-HOSVD method classifies ($p < 0.05$) 95.2%, 98.5%, 100%, and 100%

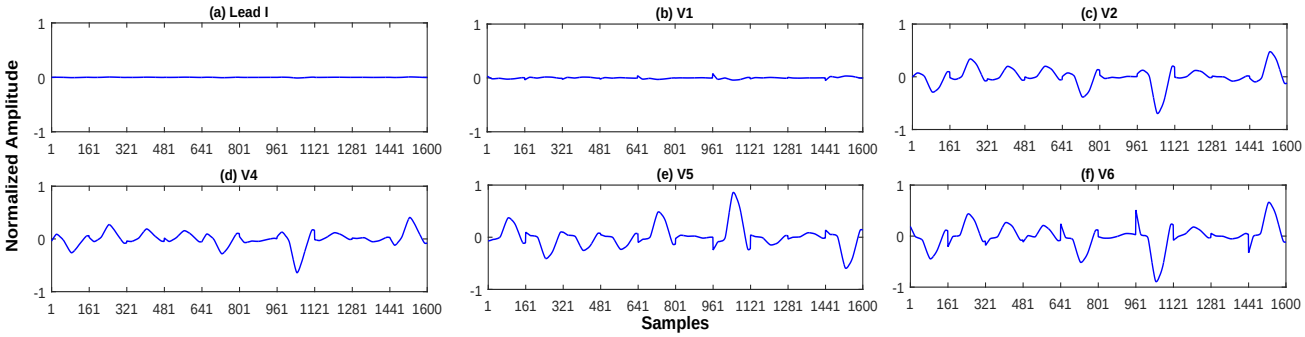

Figure 5.7: Variation in row vectors of **D** for different leads (a) I, (b) V1, (c) V2, (d-f) V4-V6. Note that the normalized amplitude is in the range of ± 1 for all leads.

of TWA signals for the respective alternan amplitude levels. These two methods were executed and compared using the same semi-synthetic signals.

To compare with the MMA method [89], r^2 correlation coefficient between estimated and input alternans level is evaluated. Figure 5.6 shows the r^2 correlation values of all leads for comparison purpose. The MAS-HOSVD method results r^2 values in the range 0.9997 to 0.9999 for all leads. The r^2 values obtained using the MMA method comparatively lower than the MAS-HOSVD method for all leads. It is due to the difference between estimated and input alternans level in the range 10 μV to 40 μV.

5.4 Experimental Observations on 8-lead TWA ECG signals

In this section, experimental observations on TWA/CinC database are presented. Experiments are carried out with 8 independent leads.

5.4.1 Observations with MAS-HOSVD method

As mentioned earlier, the 'ABAB' pattern across beats of a lead is reflected in the row vectors of matrix **D** (5.6). Figure 5.7 shows the information in row vectors of matrix **D** for different leads. For better visualization, information of ten beats is concatenated and shown in this figure. These plots are for the T-waves of the same dataset as shown in Figure 5.1. Leads with high TWA or 'ABAB' pattern have high fluctuations and amplitude (Figures 5.7(c-f)). Consecutive beat amplitudes differ substantially. Unlike to this, leads with less TWA as in Lead-I and V1 (Figure 5.1) have low amplitude levels which indicates the absence of TWA in these leads. For the sake of comparison, all sub-panels of this figure are kept at the same scale, and the normalized amplitude of these vectors is in the range of ± 1 for all leads.

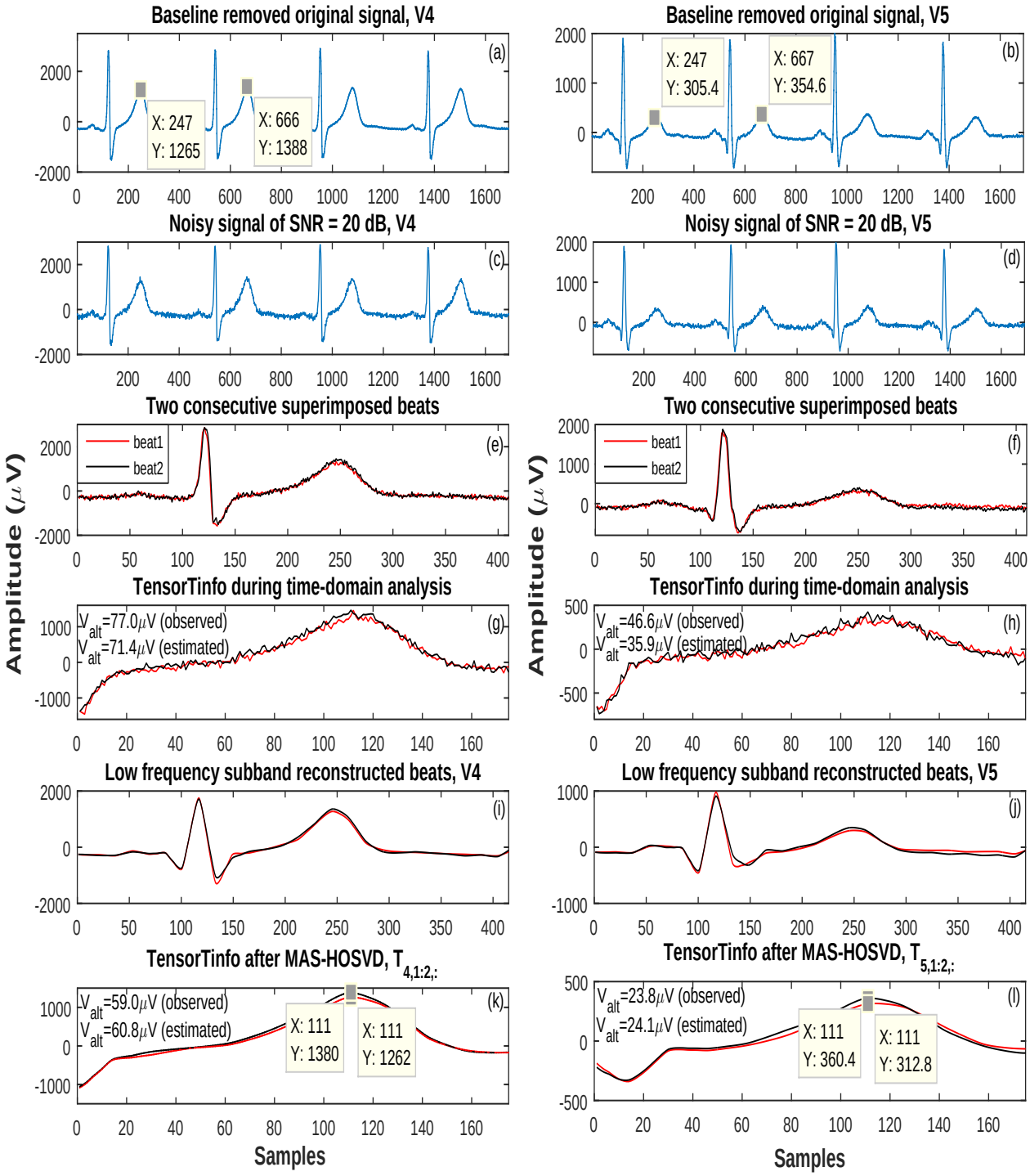

Figure 5.8: ECG fragments of two chest leads (V4 and V5). (a) and (b): baseline removed original ECG fragments, observed TWA amplitudes in V4 and V5 are 61.5 and 24.6 μV, respectively (c) and (d): ECG fragments of (a) and (b) with SNR of 20 dB, (e) and (f): two consecutive superimposed beats, (g) and (h): Plots showing the observed and estimated TWA amplitude during time-domain analysis, (i) and (j): reconstructed beats using multiscale synthesis of lower subband tensors $\mathcal{A}_6$, $\mathcal{D}_6$, and $\mathcal{D}_5$, (k) and (l): TWA detected beats in vectors $\mathbf{t}$ extracted from TensorTinfo. The observed and estimated TWA amplitudes are in accordance with each other. Dataset: twa66, TWA/CinC challenge database

The overall performance on two chest leads (V4 and V5) during different stages of the proposed algorithm is shown in Figure 5.8. Original ECG fragments are plotted in Figure 5.8 (a) and (b). T-wave

amplitude values of consecutive beats are shown with MATLAB data tips. Observed TWA amplitude levels in these two leads are 61.5 (= (1388−1265)/2)[1] and 24.6 μV in V4 and V5, respectively. These fragments are added with SNR of 20 dB, and resulting ECG fragments are shown in Figure 5.8 (c) and (d). TWAs are hardly observable to naked eye as TWA has a relatively small amplitude than signal noise. To appreciate the observed TWA amplitude difference, two consecutive beats from these two leads are superimposed and plotted in Figure 5.8 (e) and (f). Time-domain based results for TWA detection and estimation are pictured in Figure 5.8 (g) and (h). Neither the observed (77.0 and 46.6 μV) nor the estimated (62.7 and 25.9 μV) alternan amplitude levels in V4 and V5 are close to the original levels (61.5 and 24.6 μV). This is because of the presence of noise that alters these levels. However, the proposed MAS-HOSVD method is able to detect the presence of TWA and also helps quantify the TWA amplitude level. The TensorTinfo information of leads V4 and V5, after applying MAS-HOSVD, are shown in Figure 5.8 (k) and (l), respectively. Both observed (59.0 and 23.8 μV) and estimated (60.8 and 24.1 μV) levels are nearly same and in well accordance with the original levels. Note that the estimated values shown in subplots (Fig. 5.8 (g), (h), (k) and (l)) are not the maximum instantaneous difference between even and odd beats rather these are the maximum values occurring at the same location from the global estimation distribution (5.8).

5.4.2 Comparison using Kendall rank correlation coefficient

As discussed in Chapter 2, a number of methods were proposed for TWA analysis in the PhysioNet /CinC Challenge 2008. Records were ranked according to their estimated TWA amplitudes. Then the rankings from different methods were compared using the Kendall rank correlation coefficient. In this work also, records were sorted according to the estimated TWA amplitudes of the MMA, wavelet-based, multi-PCA and MAS-HOSVD methods. Also, records were sorted according to their true TWA content. Then, each resulting ranking by each method was compared with the actual ranking. The Kendall rank correlation coefficients between the estimated and true rankings are 0.774, 0.739, 0.758, and 0.812 for the MMA, wavelet-based, multi-PCA and MAS-HOSVD methods, respectively.

5.5 Study of MI Progression using TWA Analysis

After validating TWA analysis with synthetic and real ECG signals, in this section, we study the TWA progression in different leads over a period of time, in patients with prior MI. In MI or other cardiac patients, TWA analysis is in great care attention to check their progression towards lethal cardiac

[1] Data recorded with the resolution of 0.5 μV/LSB or 2000 A/D units per mV

arrhythmia. In [121], authors have mentioned that the μ-TWAs are risk factors for SCD after MI. A prospective study for prediction of SCD in patients after acute MI using TWA was carried out in [85, 87, 175, 176]. However, there is no quantitative study reported in the literature on how the TWA amplitude progresses in different leads over a period of time.

For evaluation purpose, datasets are considered from the PTB database (2.5). However, to study the TWA progression in MI cases over period of time, it is required to have the records of a subject which are recorded in different days. The subjects (MI and HC) with multiple records of this database are chosen, as it has information about the date of acute infarction, date of recording, and types of MI. This database contains MI (148) and HC (52) subjects, and each subject is represented by one to five records. Exclusion criteria are as follows: (1) subjects with no acute MI in MI subjects, (2) subjects with single record only, (3) subjects with multiple records but recorded on same day, (4) age 80 years or greater [87]. Records available on consecutive weeks with deviation of 3 to 4 days, after acute MI, are considered, while records with a lag of two weeks or more are not considered. Moreover, the MI subjects are having different types of acute MIs, namely anterior (AMI), antero-septal (ASMI), antero-lateral (ALMI), inferior (IMI), lateral (LMI), infero-lateral (ILMI), and infero-postero-lateral (IPLMI). Number of subjects for these HC and MI types are: HC – 6, AMI – 12, ALMI – 9, ASMI – 18, ASLMI – 1, IMI – 22, LMI – 1, ILMI – 9, and IPLMI – 6. A total of 286 records from 82 subjects are finally selected for this study, and number of records varied among the subjects.

TWA analysis is carried out in all leads (I, II, V1 – V6) of HC and MI subjects using the MAS-HOSVD method. Figure 5.9 shows the bar plots of TWA amplitudes for different leads. The mean V_{alt}s in consecutive weeks are stacked for a particular lead. Subplot in Figure 5.9(a) corresponds to HC case, whereas other subplots correspond to different types of MIs. The 1.9 μV cutpoint was established in previous studies for positive TWA. However, the V_{alt}s of HC suggest that leads V3 and V4 have TWA amplitudes > 1.9 μV. Hence, in this study, $V_{alt} = 4.91$ μV and $V_{alt} = 4.62$ μV are considered as the cutpoints for these two leads, respectively. Some salient observations regarding TWA progression in different MI cases noticed from this figure are as follows:

- In case of AMI (Figure 5.9(b)), positive TWA is found to be appear in anterior leads V3 ($V_{alt} = 5.48$ μV) and V4 ($V_{alt} = 8.24$ μV) initially, and it increases over time with mean TWA amplitude levels of 24.9 and 28.2 μV in these leads. There is no sign of TWA in lateral leads (V5) during first two weeks, and it starts appearing from the 3rd week onwards. This happens probably due to the gradual occlusion of blood flow, starting from the anterior portion of the heart to the lateral portion.

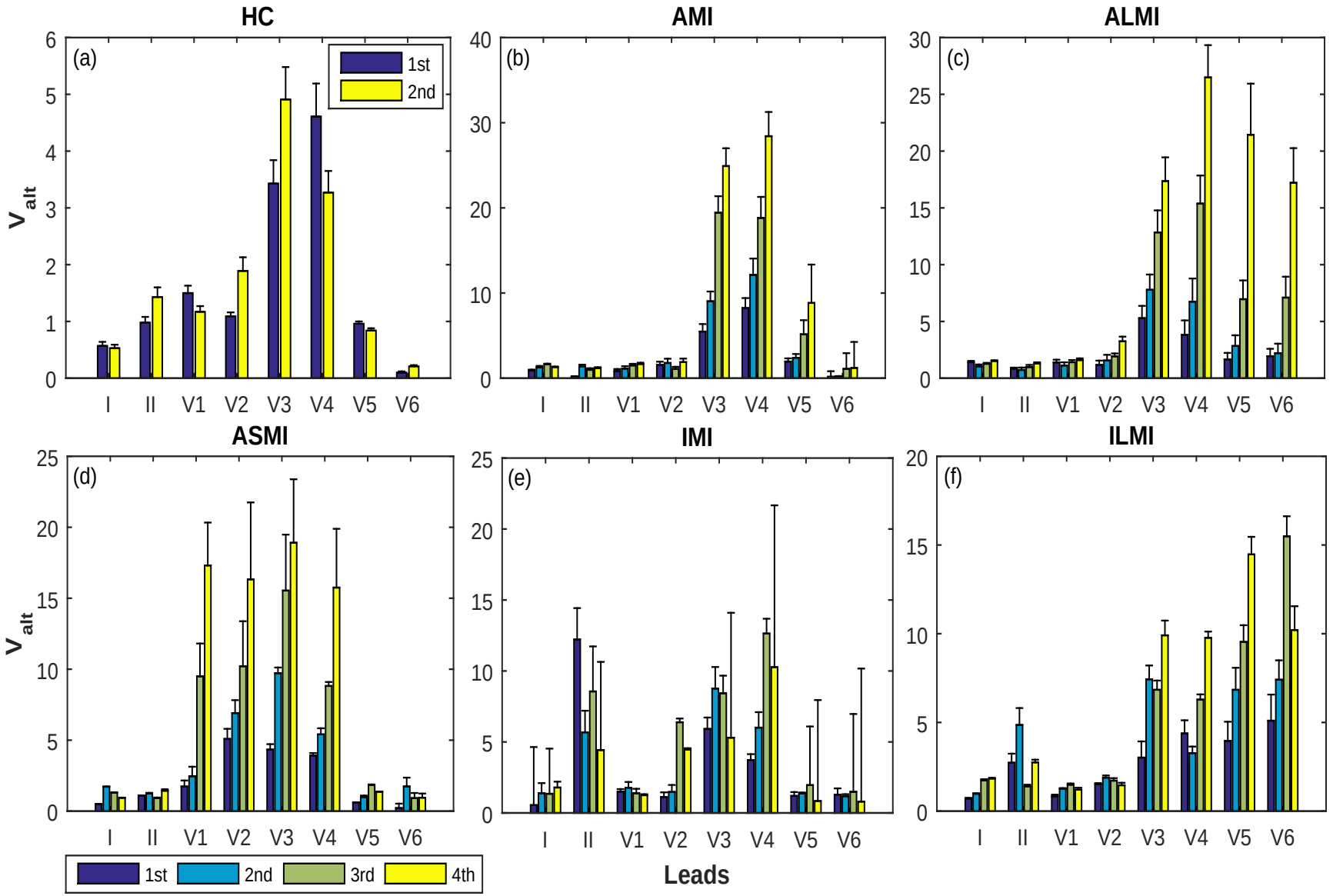

Figure 5.9: Variation of TWA amplitude in leads I, II, V1 – V6 for (a) HC, (b) AMI, (c) ALMI, (d) ASMI, (e) IMI, and (f) ILMI cases, respectively. Mean and standard deviation values in consecutive weeks are shown here.

- In case of ALMI (Figure 5.9(c)), sign of positive TWA appears initially in anterior (V3, $5.29\ \mu V$) lead, and it gradually increases over time with TWA amplitude levels of 12.84 and 15.38 μV in V3 and V4, respectively. Later, significant TWAs are observed in lateral leads (V5 and V6) after two weeks. Then prominent TWA amplitudes are observed in these leads after 3rd week. Similarly, in case of ASMI (Figure 5.9(d)), TWA amplitudes are seen in anterior and septal (V1 and V2) leads. The first positive sign of TWA appears in V2 (5.09 μV). Over time, TWA amplitudes are visible in septal and anterior leads. Compared to septal leads, high amount of TWA is observed in anterior leads. The high standard deviation in V4 and V5 of ALMI case and V2, V3 and V4 of ASMI case is due to the presence of prominent TWA amplitude ($V_{alt} > 47\ \mu V$) in some subjects. The $47\ \mu V$ cutpoint was established in previous study [176] for SCD, and this may be an indication of SCD in those subjects.

- In case of IMI (Figure 5.9(e)), sign of positive TWA is observed in limb lead II. Also it is observed in anterior chest leads, V3 and V4. One thing can be noticed that, the TWA amplitude is very high in some subjects during initial stages ($V_{alt} = 12.22\ \mu V$), and then it gets lower down after four days, and again increases in a week. This may be due to absence of sustained TWA. In case of another subject, we observed that TWA amount gets increase till one week and remains almost same during the second week. Meanwhile, TWA appears in leads V3 and V4. These type of behavior can be noticed from the mean and standard deviations of TWA amplitudes during couple of weeks. The high standard deviations in V5 and V6 indicate that positive sign of TWA appears in some subjects after 12-14 days. In case of ILMI (Figure 5.9(f)), sign of positive TWA is observed in limb lead II and chest leads V5 and V6. This is also observed in anterior lead V3 and V4 after a week. Unlike to IMI case, sustained TWA is experienced in some subjects due to the infarction in lateral wall of the ventricle.

Some of the insights which are deduced from the above observations are as follows:

- The presence of TWA (change in amplitude) is more prominent in different chest leads depending on the type of acute MI. This may be due to different viewing angles of chest leads.

- In either of anterior associated MI cases (AMI, ALMI, or ASMI), the TWA amplitude increases rapidly after second week, which is reflected in V3 and V4 leads. This may be due to the presence of sustained TWA in these patients.

- Different subplots in this figure suggest that MI progresses rapidly after 10-14 days. Also, acute MI appearing in anterior wall of the ventricles affect the lateral wall of left ventricle within two

weeks.

- Also we have observed that subjects with infarction in the anterior or in the lateral wall have high amount of sustained TWA than subjects with infarction in the inferior or in the septal wall (non-sustained TWA). There is no sight of TWA in limb lead I except in IMI case.

5.6 Summary

TWA detection still remains a challenging task because of its small amplitude (which might sometime suppressed in the presence of noise). In this chapter, an initial step for detection and estimation of TWA from the third-order MECG tensor was proposed. MAS was employed to reconstruct the T-wave from lower frequency subbands. Then, the HOSVD was applied on the T-wave tensor to extract the TensorTinfo and TWA detecting vector. The MAS-HOSVD method outperformed the temporal and MAS scheme during TWA detection.

After TWA detection with synthetic and real ECG signals, a study on TWA progression with few subjects having MI was carried out. The algorithm preformed well with these subjects. It detected and quantified correct TWA amplitudes in different leads. The TWA measure can help identify the type of MI in a subject during on-set of acute MI.

6

Conclusions

Contents

In this thesis, some of the MECG data processing methodologies using SVD and HOSVD in multiscale domain are investigated. These methods are designed for three interconnected topics, viz. dimensionality reduction, feature extraction from reduced MECG volume for MI classification (both detection and localization), and a study on progression of MI in different leads over period of time using TWA analysis, all by exploiting *spatio-temporal correlations* of MECG data. Solutions proposed in this work were shown to provide appreciable improvements in various MECG processing applications.

Chapter 1 presents a general introduction to single and multilead ECG signals, significance of ECG diagnostic features, and various data processing applications. Literature surveys on three topics, viz. correlation exploitation, feature extraction for MI classification, and TWA analysis methods are discussed. Chapter 2 presents the reviews on above three topics along with on multiscale analysis. It is difficult to present a review on these topics altogether, hence, these have been reviewed separately. Correlation exploitation methods using data dependent transforms like PCA or SVD are reviewed in the light of the three-stage unified framework. MI classification methods have been reviewed and discussed in view of features being extracted whether in time- or transform-domain and dimension of feature set. Some salient points are observed from these two chapters: proper arrangement of ECG/MECG data helps exploit one or two types of correlations, wavelet coefficients of multileads at each scale are also spatially and temporally correlated, SVD or its higher-derivative can be combined with multiscale analysis and synthesis signals to process the MECG data.

The low complex *MSVD* method is proposed in Chapter 3 for MECG dimensionality reduction by exploiting both *intra-beat* and *inter-lead* correlations. For fast and effective computation, MECG data is represented in a 2-D array. After decomposing the MECG data into different subbands, subband matrices are constructed by considering *wavelet coefficients* as matrix elements. The proposed MSVD method is applied on these subband matrices, and it exploits the correlations present in the wavelet coefficients. The MRFEC, a multiscale energy-based thresholding technique, is applied to select SVs of subband matrices. An effective value of the threshold parameter, $\nu = 5$ is chosen after performing subjective and objective distortion measures. Subjective evaluation is accomplished by taking opinions from experts (doctors and researchers) and measuring the MOS. Based on the MOS error criteria, the reconstructed ECG segments and signals (Table 3.5) falls under 'very good' category. The compression performance and objective distortion measures of the proposed method are evaluated by measuring average CR, PRD, WEDD, and WDD. The results are compared with the state-of-the-art techniques. Some clear advantages of the proposed method are its fast processing nature and storage efficiency. The proposed MSVD method achieves an average SRR and CR of 6.22:1 and 19.34:1,

respectively, for $\nu = 5$ with an average PRD value of 3.05%. This high dimensionality reduction is possible because of exploitation of both types of correlations. Also this method executes at least 2.7 times faster than the existing techniques. One of the limitation in this work is that inter-beat correlation present in MECG data, which is a huge source of redundancy, has not been exploited.

The *MHOSVD* method was proposed in Chapter 4 for dimensionality reduction and MI classification by exploiting all three types, viz. *intra-* and *inter-beat* and *inter-lead* of correlations. The MECG data is laid out in a third-order tensor form (leads$\times$beats$\times$samples). The 1-D DWT is applied to the mode-3 fibers of the tensor, and subband tensors are formed by considering wavelet coefficients as array elements. The MHOSVD method is applied to each subband tensors. An energy-based thresholding technique is suggested to truncate the dimensions along different modes of subband tensors. The dimensionality reduction performance and distortion measures of the proposed method are evaluated by measuring average CR, PRD and WEDD. Exploitation of all three types of correlations results an outstanding CR of approximately 45:1, which is the highest till date, with acceptable distortion levels.

A set of new discriminant mode (MSV- and NMWE-based) features is extracted for the automatic detection and localization of MI. The selected feature set dimension for detection (35) and localization (51) has been reduced compared to the state-of-the-art techniques, and this helps the algorithm compute faster. Another thing that has been followed in this work is that the training and the testing datasets are not over-fitted. The extracted set of features is shown to lead to a significant improvement in both detection and localization, while its performance is comparable to other methods with over-fitting the training and the testing datasets. It is also observed that SVM classifier with the chi-square kernel function has better accuracy compared to the polynomial and RBF kernel function based classifiers. The method achieves the detection Acc, Sen and Spe levels of 95.3, 94.6, and 96.0%, respectively, without over-fitting the dataset, while its localization Acc is 98.1%. Results show that the proposed tensor-based method performs better in terms of both dimension reduction and MI classification than the existing vector- or matrix-based methods.

In Chapter 5, a new method based on *MAS* and *HOSVD* is proposed for detection and estimation of TWA from the third-order MECG tensor. The MAS is employed to reconstruct the T-wave by synthesizing the lower frequency subbands. Then, the HOSVD is applied on the T-wave tensor to extract the TensorTinfo and a TWA detecting vector. The MAS-HOSVD method outperforms the temporal and MAS scheme during TWA detection. Then, presence of TWA is estimated by evaluating TWAR. To validate the proposed MAS-HOSVD method, experiments are conducted with both synthetic and real datasets, by adding different TWA amplitude levels at different SNRs. The MAS-HOSVD method

detects TWA and estimates its amplitude in all leads simultaneously. Also this method is tested to be accurate in TWA analysis of MECG data. A clear advantage of the proposed approach is its robustness to different types of noise added. Detection accuracy is 100% when TWA amplitude level is 50 μV or more, and it is still more than 95% when TWA amplitude level is less than 50 μV.

After TWA detection with synthetic and real ECG signals, a study on TWA progression with few subjects having MI has been carried out. From this study, we conclude that infarction in the anterior or lateral wall show sustained TWA than infarction in the inferior or septal wall (non-sustained TWA). The algorithm performed well with these subjects. It detects and quantifies correct TWA amplitudes in different leads, and in the future, the proposed algorithm can be extended with other subjects having MI of the PTB database for further analysis.

The major contributions of the work reported in this thesis include,

1. Exploitation of both intra-beat and inter-lead correlations using multiscale SVD.
2. Thresholding technique that accounts variation of relative energy across subbands.
3. Novel representation of MECG data in a 3-dimensional tensor structure
4. Exploiting all three types of correlations using multiscale HOSVD.
5. A set of discriminant features (MSVs and NMWE) is extracted for detection and localization of MI.
6. Validating TWA analysis using MAS-HOSVD with semi-synthetic and real ECG signals.
7. Study on acute MI progression in different leads over period of time using TWA analysis.

6.1 Scope for the Future Work

The thesis points to some interesting future work.

- Study and compare other tensor decomposition methods, and evaluating comparison performance with regard to accuracy and error.
- μ-volt TWAs have been proposed as a risk factor for SCD after MI. But there is no study that analyzes this problem. The present study is limited to few datasets. A detailed progression of MI towards SCD remains still an interesting study where it can be explored.

- The MAS-HOSVD-based TWA analysis method can be extended for cases with variable QRS-duration. The present study (Chapter 5) assumed a fixed width for the QRS complex. This can lead to error when the QRS-duration is longer in patients with high cardiac risk.
- The joint analysis of QT-interval and TWA may increase the prognostication value of TWA test.
- Combining PPG and HRV study with ECG to get better analysis on cardiac health. TWA analysis can be extended for shape variation during heart-rate variability and for amplitude transition during respiration.

A

ECG Morphology Segmentation in Different Subbands

ECG is a low frequency containing signal. The most significant information lies in the frequency range 0.05−60 Hz, and it may be up to approximately 100 Hz in pathological cases. From the study of cardiac electrical activity, QRS complex is the most significant component, and is characterized by sharp slopes in ECG signal. Spectral distribution ranges between 1 and 40 Hz, and even more if these waves have very sharp morphologies. The P and T waves have significant proportion of their energy only up to 10 Hz [96]. Frequency distribution of T wave is below 6 Hz. There is an overlapping problem of the P and T waves' spectral components. Figure A.1 shows this overlapping problem for L = 5. Details are to be followed. Due to multiresolution decomposition of an ECG signal (with sampling frequency F_s), morphological PQRST features are segmented into $L+1$ subbands. The level j = 1, 2 $\cdots$ L is associated with frequency band, ΔF, is given by

$$2^{-j-1}F_s \leq \Delta F \leq 2^{-j}F_s \tag{A.1}$$

Depending on frequency span of these features, Al-Fahoum [104] heuristically determined the formula $L = \lfloor log_2 F_s - 2.96 \rfloor$ for decomposition level. The maximum frequency content of different subbands is reported in Table 1 for F_s =500 Hz in our manuscript.

For an example, an ECG signal sampled with F_s =500 Hz and L = 6, subband A_6 includes most of the T-wave contribution and some of the P-wave contribution. Subband D_6 includes most of the P-wave contribution and part of the T-wave contribution. It will be difficult to segment P-wave and T-wave information if the value of L is small. To have a better resolution of these waves, it is essential to have high value of L i.e. L = 6 is most appropriate. Going beyond sixth level decomposition is not necessary. Figure A.1 shows the information in different subbands for different values of L of an ECG signal sampled with F_s = 500 Hz. It is clear that with L = 5, information in P and T-wave is not able to segment properly.

Let us discuss about the factor 2.96 and flooring operation that is used in this formula [104]. Generally, ECG signals are sampled with 250 Hz or more. Values of L for different factors are given as below:

$$\begin{array}{lll} L = \lfloor \log_2(250) - 2.95 \rfloor = 5 & L = \lfloor \log_2(250) - 2.96 \rfloor = 5 & L = \lfloor \log_2(250) - 2.97 \rfloor = 4 \\ L = \lfloor \log_2(500) - 2.95 \rfloor = 6 & L = \lfloor \log_2(500) - 2.96 \rfloor = 6 & L = \lfloor \log_2(500) - 2.97 \rfloor = 5 \\ L = \lfloor \log_2(1000) - 2.95 \rfloor = 7 & L = \lfloor \log_2(1000) - 2.96 \rfloor = 7 & L = \lfloor \log_2(1000) - 2.97 \rfloor = 6 \end{array}$$

We can observe that the value of L gets decrease by 1 when this negative factor becomes more than 2.96. It is worth necessary to decompose the signal with proper and smaller values of L. Perhaps the factor 2.96 and flooring operation help for the same. Selecting a smaller value L than the value

obtained using this formula may not be able to segment P-wave and T-wave information properly as discussed earlier. This may be the reason why the factor 2.96 has been used.

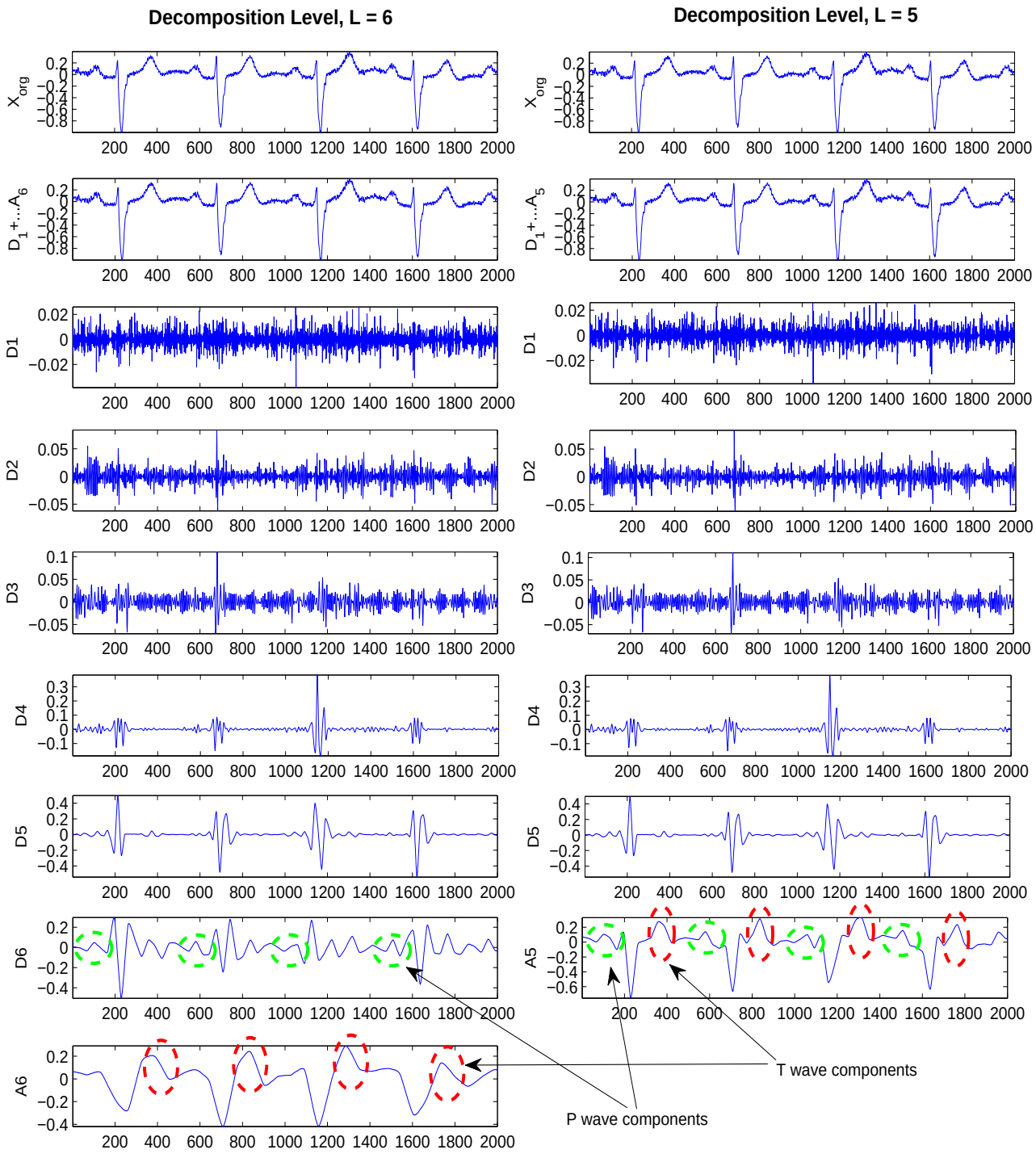

Figure A.1: Subband decomposition of an ECG

Bibliography

[1] [Online]. Available: http://lifeinthefastlane.com/ecg-library/basics/ecg-anatomy/

[2] B. Surawicz and T. K. Knilans, *CHOU'S ELECTROCARDIOGRAPHY IN CLINICAL PRACTICE*, 6th ed. Elsevier, 2008.

[3] A. B. Luna, M. Fiol-Sala, and E. M. Antman, "The 12 lead ECG in st elevation myocardial infarction: A practical approach for clinicians," *Wiley-Blackwell*, 2006.

[4] A. L. Goldberger, Z. D. Goldberger, and A. S. Shvilkin, *Goldberger's Clinical Electrocardiography A Simplifid Approach*. Elsevier Saunders, 2013.

[5] J. C. Huhta and J. G. Webster, "60-Hz interference in electrocardiography," *IEEE Trans. on Biomed. Eng.*, vol. 43, pp. 91–101, 1976.

[6] N. V. Thakor and Y. S. Zhu, "Applications of adaptive filtering to ECG analysis: Noise cancellation and arrhythmia detection," *IEEE Trans. on Biomed. Eng.*, vol. 38, pp. 785–794, August 1991.

[7] D. L. Donoho, "De-noising by soft thresholding," *IEEE Trans. on Info. Theory*, vol. 41, pp. 613–627, May 1995.

[8] S. Olmos, J. García, R. Jané, and P. Laguna, "ECG signal compression plus noise filtering with truncated orthogonal expansions," *Signal Processing*, vol. 79, no. 1, pp. 97 – 115, 1999. [Online]. Available: http://www.sciencedirect.com/science/article/pii/S0165168499000833

[9] Y. D. Lin and Y. H. Hu, "Power-line interference detection and suppression in ECG signal processing," *IEEE Trans. on Biomed. Eng.*, vol. 55, no. 1, pp. 354–357, Jan 2008.

[10] S. Jalaleddine, C. Hutchens, R. Stratran, and W. Coberly, "ECG data compression techniques – a unified approach," *IEEE Trans. on Biomed. Eng.*, vol. 37, no. 4, pp. 329–343, 1990.

[11] P. P. Kanjilal, S. Palit, and G. Saha, "Fetal ECG extraction from single-channel maternal ECG using singular value decomposition," *IEEE Trans. on Biomed. Eng.*, vol. 44, no. 1, pp. 51–59, Jan 1997.

[12] R. Sameni and G. D. Clifford, "A review of fetal ecg signal processing: Issues and promising directions," *The open pacing, electrophysiology & therapy journal*, vol. 3, pp. 4–20, 2010.

[13] J. Pan and W. J. Tompkins, "A real-time qrs detection algorithm," *IEEE Trans. on Biomed. Eng.*, vol. BME-32, no. 3, pp. 230–236, March 1985.

[14] J. Martinez, R. Almeida, S. Olmos, A. Rocha, and P. Laguna, "A wavelet-based ECG delineator: evaluation on standard databases," *IEEE Trans. on Biomed. Eng.*, vol. 51, no. 4, pp. 570–581, April 2004.

[15] J. S. Paul, M. Reddy, and V. J. Kumar, "Data processing of stress ECGs using discrete cosine transform," *Computers in Biology and Medicine*, vol. 28, no. 6, pp. 639 – 658, 1998. [Online]. Available: http://www.sciencedirect.com/science/article/pii/S0010482598000420

[16] L. N. Sharma, S. Dandapat, and A. Mahanta, "Multichannel ECG data compression based on multiscale principal component analysis," *IEEE Trans. on Info. Tech. in Biomed.*, vol. 16, no. 4, pp. 730–736, July 2012.

[17] M. Blanco-Velasco, B. Weng, and K. E. Barner, "ECG signal denoising and baseline wander correction based on the empirical mode decomposition," *Computers in Biology and Medicine*, vol. 38, no. 1, pp. 1 – 13, 2008. [Online]. Available: http://www.sciencedirect.com/science/article/pii/S0010482507001114

[18] B. A. Rajoub, "An efficient coding algorithm for the compression of ECG signals using the wavelet transform," *IEEE Trans. on Biomed. Eng.*, vol. 49, no. 4, pp. 355–362, Apr 2002.

[19] H. Lee and K. M. Buckley, “ECG data compression using cut and align beats approach and 2-D transforms,” *IEEE Trans. on Biomed. Eng.*, vol. 46, no. 5, pp. 556–564, May 1999.

[20] S. M. Ahmed, Q. Al-Zoubi, and M. Abo-Zahhad, “A hybrid ECG compression algorithm based on singular value decomposition and discrete wavelet transform,” *J. of Medical Engineering and Technology*, vol. 31, no. 1, pp. 54–61, Feb 2007.

[21] J. Wei, C. Chang, N. Chou, and G. Jan, “ECG data compression using truncated singular value decomposition,” *IEEE Trans. on Info. Tech. in Biomedicine*, vol. 5, no. 4, pp. 290–299, Dec 2001.

[22] F. Castells, P. Laguna, L. Sornmo, A. Bollmann, and J. M. Roig, “Principal component analysis in ECG signal processing,” *EURASIP J. on Advances in Signal Processing*, Feb 2007.

[23] J. R. Cox, F. M. Nolle, H. A. Fozzard, and G. C. Oliver, “AZTEC: A preprocessing scheme for real-time ECG rhythm analysis,” *IEEE Trans. on Biomed. Eng.*, vol. BME-15, pp. 128–129, April 1968.

[24] J. R. Cox, F. M. Nolle, and R. M. Arthur, “Digital analysis of the electroencephalogram, the blood pressure wave, and the electrocardiogram,” *IEEE Proceedings*, vol. 60, no. 10, pp. 1137–1164, Oct 1972.

[25] W. Mueller, “Arrhythmia detection program for an ambulatory ECG monitor,” *Biomedical sciences instrumentation*, vol. 14, pp. 81–85, 1978. [Online]. Available: http://europepmc.org/abstract/MED/687739

[26] J. P. Abenstein and W. J. Tompkins, “A new data-reduction algorithm for real-time ECG analysis,” *IEEE Trans. on Biomed. Eng.*, vol. BME-29, no. 1, pp. 43–48, Jan 1982.

[27] M. Ishijima, S. B. Shin, G. H. Hostetter, and J. Sklansky, “Scan-along polygonal approximation for data compression of electrocardiograms,” *IEEE Trans. on Biomed. Eng.*, vol. BME-30, no. 11, pp. 723–729, Nov 1983.

[28] B. Furht and A. Perez, “An adaptive real-time ECG compression algorithm with variable threshold,” *IEEE Trans. on Biomed. Eng.*, vol. 35, no. 6, pp. 489–494, June 1988.

[29] V. Kumar, S. Saxena, V. Giri, and D. Singh, “Improved modified AZTEC technique for ECG data compression: Effect of length of parabolic filter on reconstructed signal,” *Computers & Electrical Engineering*, vol. 31, no. 4-5, pp. 334 – 344, 2005. [Online]. Available: http://www.sciencedirect.com/science/article/pii/S0045790605000625

[30] H. Al-Nashash, “A dynamic fourier series for the compression of ECG using FFT and adaptive coefficient estimation,” *Medical Engineering & Physics*, vol. 17, no. 3, pp. 197 – 203, 1995. [Online]. Available: http://www.sciencedirect.com/science/article/pii/135045339595710R

[31] E. Berti, F. Chiaraluce, N. E. Evans, and J. J. McKee, “Double logarithmic quantisation of the walsh spectrum: application to real ECGs,” *Electronics Letters*, vol. 33, no. 18, pp. 1513–1515, Aug 1997.

[32] ——, “Reduction of walsh-transformed electrocardiograms by double logarithmic coding,” *IEEE Trans. on Biomed. Eng.*, vol. 47, no. 11, pp. 1543–1547, Nov 2000.

[33] R. Benzid, A. Messaoudi, and A. Boussaad, “Constrained ECG compression algorithm using the block-based discrete cosine transform,” *Digital Signal Processing*, vol. 18, no. 1, pp. 56 – 64, 2008. [Online]. Available: http://www.sciencedirect.com/science/article/pii/S1051200407001133

[34] S. Lee, J. Kim, and M. Lee, “A real-time ECG data compression and transmission algorithm for an e-health device,” *IEEE Trans. on Biomed. Eng.*, vol. 58, no. 9, pp. 2448–2455, Sept 2011.

[35] A. Bendifallah, R. Benzid, and M. Boulemden, “Improved ECG compression method using discrete cosine transform,” *Electronics Letters*, vol. 47, no. 2, pp. 87–89, January 2011.

[36] I. Daubechies, “Ten lectures on wavelets,” *SIAM CBMS-NSF Regional Conf*, 1992.

[37] S. G. Mallat, “A theory for multiresolution signal decomposition: the wavelet representation,” *IEEE Trans. on Pattern Analysis and Machine Intelligence*, vol. 11, no. 7, pp. 674–693, Jul 1989.

[38] S. Mallat, *A Wavelet Tour of Signal Processing: The Sparse Way*, 3rd ed., Elsevier, Ed. Academic Press, Dec 2008.

[39] Z. Lu, D. Y. Kim, and W. A. Pearlman, “Wavelet compression of ECG signals by the set partitioning in hierarchical trees algorithm,” *IEEE Trans. on Biomed. Eng.*, vol. 47, no. 7, pp. 849–856, July 2000.

[40] A. G. Ramakrishnan and S. Saha, “ECG coding by wavelet-based linear prediction,” *IEEE Trans. on Biomed. Eng.*, vol. 44, no. 12, pp. 1253–1261, Dec 1997.

[41] S. M. Ahmeda and M. Abo-Zahhad, "A new hybrid algorithm for ECG signal compression based on the wavelet transformation of the linearly predicted error," *Medical Engineering & Physics*, vol. 23, no. 2, pp. 117 – 126, 2001. [Online]. Available: http://www.sciencedirect.com/science/article/pii/S1350453301000261

[42] A. Alesanco, S. Olmos, R. S. H. Istepanian, and J. Garcia, "Enhanced real-time ECG coder for packetized telecardiology applications," *IEEE Trans. on Info. Tech. in Biomed.*, vol. 10, no. 2, pp. 229–236, April 2006.

[43] R. Benzid, F. Marir, A. Boussaad, M. Benyoucef, and D. Arar, "Fixed percentage of wavelet coefficients to be zeroed for ECG compression," *Electronics Letters*, vol. 39, no. 11, pp. 830–831, May 2003.

[44] M. Blanco-Velasco, F. Cruz-Roldan, J. I. Godino-Llorente, and K. E. Barner, "Wavelet packets feasibility study for the design of an ECG compressor," *IEEE Trans. on Biomed. Eng.*, vol. 54, no. 4, pp. 766–769, April 2007.

[45] S.-C. Tai, C. Sun, and W.-C. Yan, "A 2-D ECG compression method based on wavelet transform and modified SPIHT," *IEEE Trans. on Biomed. Eng.*, vol. 52, no. 6, pp. 999–1008, June 2005.

[46] T. Y. Young and W. H. Huggins, "The intrinsic component theory of electrocardiography," *IRE Trans. on Bio-Medical Electronics*, vol. 9, no. 4, pp. 214–221, Oct 1962.

[47] N. Ahmed, P. J. Milne, and S. G. Harris, "Electrocardiographic data compression via orthogonal transforms," *IEEE Trans. on Biomed. Eng.*, vol. BME-22, no. 6, pp. 484–487, Nov 1975.

[48] A. E. Cetin, H. Koymen, and M. C. Aydin, "Multichannel ECG data compression by multirate signal processing and transform domain coding techniques," *IEEE Trans. on Biomed. Eng.*, vol. 40, no. 5, pp. 495–499, May 1993.

[49] T. Blanchett, G. C. Kember, and G. A. Fenton, "KLT-based quality controlled compression of single-lead ECG," *IEEE Trans. on Biomed. Eng.*, vol. 45, no. 7, pp. 942–945, July 1998.

[50] M. Kotas, "Application of projection pursuit based robust principal component analysis to ECG enhancement," *Biomedical Signal Processing and Control, Elsevier*, vol. 1, no. 4, pp. 289 – 298, 2006. [Online]. Available: http://www.sciencedirect.com/science/article/pii/S174680940600053X

[51] G. Moody and R. Mark, "QRS morphology representation and noise estimation using the Karhunen-Loève transform," C. in Cardiology, Ed., vol. 16, 1989, pp. 269–272.

[52] P. Laguna, G. B. Moody, J. García, A. L. Goldberger, and R. G. Mark, "Analysis of the ST-T complex of the electrocardiogram using the Karhunen–Loeve transform: adaptive monitoring and alternans detection," *Medical & Biological Engineering & Computing*, vol. 37, no. 2, pp. 175–189, 1999. [Online]. Available: http://dx.doi.org/10.1007/BF02513285

[53] Y. C. Yeh, T. C. Chiang, and H. J. Lin, "Principal component analysis method for detection and classification of ECG beat," in *IEEE 11th International Conference on Bioinformatics and Bioengineering (BIBE)*, Oct 2011, pp. 318–322.

[54] R. J. Martis, U. R. Acharya, K. Mandana, A. Ray, and C. Chakraborty, "Application of principal component analysis to ECG signals for automated diagnosis of cardiac health," *Expert Systems with Applications*, vol. 39, no. 14, pp. 11 792 – 11 800, 2012. [Online]. Available: http://www.sciencedirect.com/science/article/pii/S0957417412006690

[55] R. Rodriguez, A. Mexicano, J. Bila, S. Cervantes, and R. Ponce, "Feature extraction of electrocardiogram signals by applying adaptive threshold and principal component analysis," *J. of Applied Research and Technology*, vol. 13, no. 2, pp. 261 – 269, 2015. [Online]. Available: http://www.sciencedirect.com/science/article/pii/S1665642315000103

[56] V. Kalpana, S. T. Hamde, and L. M. Waghmare, "ECG feature extraction using principal component analysis for studying the effect of diabetes," *Journal of Medical Engineering & Technology*, vol. 37, no. 2, pp. 116–126, 2013. [Online]. Available: http://dx.doi.org/10.3109/03091902.2012.753126

[57] R. Simoliuniene, A. Krisciukaitis, A. Macas, G. Baksyte, V. Saferis, and R. Zaliunas, "Principal component analysis based method for detection and evaluation of ECG T-wave alternans," in *Computers in Cardiology*, Sept 2008, pp. 757–760.

[58] V. Monasterio and J. P. Martinez, "Multilead T-wave alternans quantification based on spatial filtering and the laplacian likelihood ratio method," in *Computers in Cardiology*, Sept 2008, pp. 601–604.

[59] V. Monasterio, P. Laguna, and J. Martinez, "Multilead analysis of T-wave alternans in the ECG using principal component analysis," *IEEE Trans. on Biomed. Eng.*, vol. 56, no. 7, pp. 1880–1890, July 2009.

[60] P. Langley, E. J. Bowers, and A. Murray, "Principal component analysis as a tool for analyzing beat-to-beat changes in ECG features: Application to ECG-derived respiration," *IEEE Trans. on Biomed. Eng.*, vol. 57, no. 4, pp. 821–829, April 2010.

[61] B. Acar and H. Koymen, "SVD-based on-line exercise ECG signal orthogonalization," *IEEE Trans. on Biomed. Eng.*, vol. 46, no. 3, pp. 311–321, March 1999.

[62] R. Kumar, A. Kumar, and G. Singh, "Electrocardiogram signal compression based on singular value decomposition (SVD) and adaptive scanning wavelet difference reduction (ASWDR) technique," *AEU - International J. of Electronics and Communications*, vol. 69, no. 12, pp. 1810 – 1822, 2015. [Online]. Available: http://www.sciencedirect.com/science/article/pii/S1434841115002769

[63] ——, "Hybrid method based on singular value decomposition and embedded zero tree wavelet technique for {ECG} signal compression," *Computer Methods and Programs in Biomedicine*, vol. 129, pp. 135 – 148, 2016. [Online]. Available: http://www.sciencedirect.com/science/article/pii/S016926071530119X

[64] K. Thygesen, J. S. Alpert, A. S. Jaffe, M. L. Simoons, B. R. Chaitman, and H. D. White, "Third universal definition of myocardial infarction," *Circulation*, vol. 126, no. 16, pp. 2020–2035, Oct. 2012.

[65] C. D. Nugent, J. A. Webb, and N. D. Black, "Feature and classifier fusion for 12-lead ECG classification," *Med Inform Internet Med.*, vol. 25, no. 3, pp. 225–235, Jul-Sep 2000.

[66] M. Arif, I. Malagore, and F. Afsar, "Detection and localization of myocardial infarction using k-nearest neighbor classifier," *J. of Med. Syst.*, vol. 36, no. 1, pp. 279–289, 2012. [Online]. Available: http://dx.doi.org/10.1007/s10916-010-9474-3

[67] L. Sun, Y. Lu, K. Yang, and S. Li, "ECG analysis using multiple instance learning for myocardial infarction detection," *IEEE Trans. on Biomed. Eng.*, vol. 59, no. 12, pp. 3348–3356, Dec 2012.

[68] L. Sharma, R. Tripathy, and S. Dandapat, "Multiscale energy and eigenspace approach to detection and localization of myocardial infarction," *IEEE Trans. on Biomed. Eng.*, vol. 62, no. 7, pp. 1827–1837, July 2015.

[69] B. Liu, J. Liu, G. Wang, K. Huang, F. Li, Y. Zheng, Y. Luo, and F. Zhou, "A novel electrocardiogram parameterization algorithm and its application in myocardial infarction detection," *Computers in Biology and Medicine*, vol. 61, pp. 178 – 184, 2015. [Online]. Available: http://www.sciencedirect.com/science/article/pii/S0010482514002121

[70] M. R. S. Reddy, L. Edenbrandt, J. Svensson, W. K. Haisty, and O. Pahlm, "Neural network versus electrocardiographer and conventional computer criteria in diagnosing anterior infarct from the ECG," in *Computers in Cardiology*, Oct 1992, pp. 667–670.

[71] H. L. Lu, K. Ong, and P. Chia, "An automated ECG classification system based on a neuro-fuzzy system," in *Computers in Cardiology*, 2000, pp. 387–390.

[72] E. Jayachandran, P. Joseph K., and R. Acharya U., "Analysis of myocardial infarction using discrete wavelet transform," *J. of Med. Syst.*, vol. 34, no. 6, pp. 985–992, 2010. [Online]. Available: http://dx.doi.org/10.1007/s10916-009-9314-5

[73] S. Banerjee and M. Mitra, "Application of cross wavelet transform for ECG pattern analysis and classification," *IEEE Trans. on Inst. and Meas.*, vol. 63, no. 2, pp. 326–333, Feb 2014.

[74] J. Martinez and S. Olmos, "Methodological principles of T wave alternans analysis: a unified framework," *IEEE Trans. on Biomed. Eng.*, vol. 52, no. 4, pp. 599–613, April 2005.

[75] L. Burattini, S. Bini, and R. Burattini, "Comparative analysis of methods for automatic detection and quantification of microvolt T-wave alternans," *Medical Engineering & Physics*, vol. 31, no. 10, pp. 1290 – 1298, 2009.

[76] R. Goya-Esteban, O. Barquero-Perez, M. Blanco-Velasco, A. Caamano-Fernandez, A. Garcia-Alberola, and J. Rojo-Alvarez, "Nonparametric signal processing validation in T-wave alternans detection and estimation," *IEEE Trans. on Biomed. Eng.*, vol. 61, no. 4, pp. 1328–1338, April 2014.

[77] S. Bashir, A. D. Bakhshi, and M. A. Maud, "A template matched-filter based scheme for detection and estimation of T-wave alternans," *Biomedical Signal Processing and Control, Elsevier*, vol. 13, pp. 247 – 261, 2014.

[78] V. Monasterio, “Multilead analysis of T-wave alternans in the electrocardiogram,” Ph.D. dissertation, University of Zaragoza, June 2011.

[79] D. R. Adam, S. Akselrod, and R. J. Cohen, “Estimation of ventricular vulnerability to fibrillation through T-wave time series analysis,” in *Computers in Cardiology*, L. A. I. C. S. Press, Ed., 1981, pp. 307–310.

[80] S. M. Narayan, “T-wave alternans and the susceptibility to ventricular arrhythmias,” *J. of the American College of Cardiology*, vol. 47, no. 2, pp. 269 – 281, 2006.

[81] A. K. Gehi, R. H. Stein, L. D. Metz, and J. A. Gomes, “Microvolt T-wave alternans for the risk stratification of ventricular tachyarrhythmic events: A meta-analysis,” *Journal of the American College of Cardiology*, vol. 46, no. 1, pp. 75 – 82, 2005. [Online]. Available: http://www.sciencedirect.com/science/article/pii/S0735109705008715

[82] G. M. D. Ferrari and A. Sanzo, “T-wave alternans in risk stratification of patients with nonischemic dilated cardiomyopathy: Can it help to better select candidates for ICD implantation?” *Heart Rhythm*, vol. 6, no. 3, Supplement, pp. S29 – S35, 2009. [Online]. Available: http://www.sciencedirect.com/science/article/pii/S1547527108009752

[83] M. H. Hassan and E. S. Kaufman, “Prevalence of T wave alternans in the long qt syndrome population: A study involving 25 long QT syndrome families,” *Heart Rhythm*, vol. 2, no. 5, pp. 303–304, May 2005.

[84] O. Costantini, S. H. Hohnloser, M. M. Kirk, B. B. Lerman, J. H. B. II, B. Sethuraman, M. M. Dettmer, and D. S. Rosenbaum, “The ABCD (alternans before cardioverter defibrillator) trial: Strategies using T-wave alternans to improve efficiency of sudden cardiac death prevention,” *J. of the American College of Cardiology*, vol. 53, no. 6, pp. 471 – 479, 2009. [Online]. Available: http://www.sciencedirect.com/science/article/pii/S0735109708036747

[85] T. Ikeda, H. Saito, K. Tanno, H. Shimizu, J. Watanabe, Y. Ohnishi, Y. Kasamaki, and Y. Ozawa, “T-wave alternans as a predictor for sudden cardiac death after myocardial infarction,” *The American J. of Cardiology*, vol. 89, no. 1, pp. 79 – 82, 2002. [Online]. Available: http://www.sciencedirect.com/science/article/pii/S0002914901021713

[86] T. Ikeda, H. Yoshino, K. Sugi, K. Tanno, H. Shimizu, J. Watanabe, Y. Kasamaki, A. Yoshida, and T. Kato, “Predictive value of microvolt T-wave alternans for sudden cardiac death in patients with preserved cardiac function after acute myocardial infarction: Results of a collaborative cohort study,” *J. of the American College of Cardiology*, vol. 48, no. 11, pp. 2268 – 2274, 2006. [Online]. Available: http://www.sciencedirect.com/science/article/pii/S0735109706022066

[87] H. Yu, F. Pi-hua, W. Yuan, L. Xiao-feng, L. Jun, L. Zhi, L. Sen, and S. Zhang, “Prediction of sudden cardiac death in patients after acute myocardial infarction using t-wave alternans: a prospective study,” *J. of Electrocardiology*, vol. 45, no. 1, pp. 60 – 65, 2012.

[88] J. M. Smith, E. A. Clancy, C. R. Valeri, J. N. Ruskin, and R. J. Cohen, “Electrical alternans and cardiac electrical instability,” *Ciculation*, vol. 77, no. 1, pp. 110–121, 1988.

[89] B. D. Nearing and R. L. Verrier, “Modified moving average analysis of T-wave alternans to predict ventricular fibrillation with high accuracy,” *J. of Applied Physiology*, vol. 92, no. 2, pp. 541–549, 2002. [Online]. Available: http://jap.physiology.org/content/92/2/541

[90] J. P. Martinez and S. Olmos, “A robust T wave alternans detector based on the GLRT for Laplacian noise distribution,” in *Computers in Cardiology, 2002*, Sept 2002, pp. 677–680.

[91] J. P. Martinez, S. Olmos, G. Wagner, and P. Laguna, “Characterization of repolarization alternans during ischemia: time-course and spatial analysis,” *IEEE Trans. on Biomed. Eng.*, vol. 53, no. 4, pp. 701–711, April 2006.

[92] S. M. Narayan and J. M. Smith, “Spectral analysis of periodic fluctuations in electrocardiographic repolarization,” *IEEE Trans. on Biomed. Eng.*, vol. 46, no. 2, pp. 203–212, Feb 1999.

[93] G. Goovaerts, C. Varon, B. Vandenberk, R. Willems, and S. Van Huffel, “Tensor-based detection of T wave alternans in multilead ECG signals,” in *Computing in Cardiology Conference (CinC)*, Sept 2014, pp. 185–188.

[94] G. Bortolan and I. I. Christov, “Principal component analysis for detection and assessment of T-wave alternans,” in *Computers in Cardiology*, Sept 2008, pp. 521–524.

[95] V. Monasterio, G. D. Clifford, P. Laguna, and J. P. Martínez, "A multilead scheme based on periodic component analysis for T-wave alternans analysis in the ECG," *Annals of Biomed. Eng.*, vol. 38, no. 8, pp. 2532–2541, 2010. [Online]. Available: http://dx.doi.org/10.1007/s10439-010-0029-z

[96] M. S. Manikandan and S. Dandapat, "Wavelet energy based diagnostic distortion measure for ECG," *Biomedical Signal Processing and Control, Elsevier*, vol. 2, pp. 80–96, 2007.

[97] ——, "Multiscale entropy-based weighted distortion measure for ECG coding," *IEEE Sig. Process. Letters*, vol. 15, pp. 829–832, 2008.

[98] B. Bradie, "Wavelet packet-based compression of single lead ECG," *IEEE Trans. on Biomed. Eng.*, vol. 43, no. 5, pp. 493–501, May 1996.

[99] S. Padhy and S. Dandapat, "Exploiting multi-lead electrocardiogram correlations using robust third-order tensor decomposition," *Healthc. Technol. Lett.*, vol. 2, 2015. [Online]. Available: http://digital-library.theiet.org/content/journals/10.1049/htl.2015.0020

[100] S. Padhy, L. Sharma, and S. Dandapat, "Multilead ECG data compression using SVD in multiresolution domain," *Biomedical Signal Processing and Control, Elsevier*, vol. 23, pp. 10 – 18, 2016. [Online]. Available: http://www.sciencedirect.com/science/article/pii/S1746809415001147

[101] L. Polania, R. Carrillo, M. Blanco-Velasco, and K. Barner, "Exploiting prior knowledge in compressed sensing wireless ecg systems," *IEEE J. of Biomed. and Health Info.*, vol. PP, no. 99, pp. 1–1, 2014.

[102] M. S. Manikandan and S. Dandapat, "Wavelet-based electrocardiogram signal compression methods and their performances: A prospective review," *Biomedical Signal Processing and Control*, vol. 14, pp. 73 – 107, 2014. [Online]. Available: http://www.sciencedirect.com/science/article/pii/S1746809414000998

[103] L. J. Hadjileontiadis and S. M. Panas, "Separation of discontinuous adventitious sounds from vesicular sounds using a wavelet-based filter," *IEEE Trans. on Biomed. Eng.*, vol. 44, no. 12, pp. 1269–1281, Dec 1997.

[104] A. S. Al-Fahoum, "Quality assessment of ECG compression techniques using a wavelet-baseddiagnostic measure," *IEEE Trans. on Info. Tech. in Biomed.*, vol. 10, no. 1, pp. 182–191, Jan 2006.

[105] L. N. Sharma, S. Dandapat, and A. Mahanta, "ECG signal denoising using higher order statistics in wavelet subbands," *Biomedical Signal Processing and Control, Elsevier*, vol. 5, pp. 214–222, 2010.

[106] ——, "Kurtosis-based noise estimation and multiscale energy to denoise ECG signal," *Signal, Image and Video Processing*, 2011.

[107] L. N. Sharma, "Multiscale processing of multichannel electrocardiogram signals," Ph.D. dissertation, IIT Guwahati, India, July 2012.

[108] I. Jolliffe, *Principal Component Analysis*. Springer-Verlag New York, 2002.

[109] K. Pearson, "On lines and planes of closest fit to systems of points in space," *Philosophical Magazine*, vol. 2, no. 11, pp. 559–572, 1901.

[110] G. H. Golub and C. F. Van Loan, *Matrix Computations*, 3rd ed. Baltimore, MD, USA: Johns Hopkins University Press, 1996.

[111] D. S. Watkins, *Fundamentals of Matrix Computations*, 3rd ed. Wiley, June 2010.

[112] M. Vasilescu and D. Terzopoulos, "Multilinear (tensor) image synthesis, analysis, and recognition [exploratory dsp]," *IEEE Sig. Process. Mag.*, vol. 24, no. 6, pp. 118–123, Nov 2007.

[113] D. S. Watkins, *Fundamentals of Matrix Computations*, 2nd ed., ser. Wiley-Interscience. John Wiley & Sons, 2002.

[114] S. Olmos, M. Millan, J. Garcia, and P. Laguna, "ECG data compression with the Karhunen-Loeve transform," in *Computers in Cardiology*, Sept 1996, pp. 253–256.

[115] C. Cortes and V. Vapnik, "Support-vector networks," *Mach. Learn.*, vol. 20, no. 3, pp. 273–297, Sep. 1995. [Online]. Available: http://dx.doi.org/10.1023/A:1022627411411

[116] C.-C. Chang and C.-J. Lin, "LIBSVM: A library for support vector machines," *ACM Trans. Intell. Syst. Technol.*, vol. 2, no. 3, pp. 27:1–27:27, May 2011. [Online]. Available: http://doi.acm.org/10.1145/1961189.1961199

[117] C. J. C. Burges, "A tutorial on support vector machines for pattern recognition," *Data Mining and Knowledge Discovery*, vol. 2, no. 2, pp. 121–167, 1998.

[118] Y. Zigel, A. Cohen, and A. Katz, "The weighted diagnostic distortion (WDD) measure for ECG signal compression," *IEEE Trans. on Biomed. Eng.*, vol. 47, no. 11, pp. 1422–1430, Nov 2000.

[119] D. G. Altman and J. M. Bland, "Statistics notes: Diagnostic tests 1: sensitivity and specificity," *BMJ*, vol. 308, no. 6943, p. 1552, 1994.

[120] J.-c. Hsieh and M.-W. Hsu, "A cloud computing based 12-lead ECG telemedicine service," *BMC Medical Informatics and Decision Making*, vol. 12, no. 1, 2012. [Online]. Available: http://dx.doi.org/10.1186/1472-6947-12-77

[121] I. Romero, N. R. Grubb, G. R. Clegg, C. E. Robertson, P. S. Addison, and J. N. Watson, "T-wave alternans found in preventricular tachyarrhythmias in ccu patients using a wavelet transform-based methodology," *IEEE Trans. on Biomed. Eng.*, vol. 55, no. 11, pp. 2658–2665, Nov 2008.

[122] D. Ge and W. Zhou, "Discrimination of different myocardial infarction stages using wide band electrocardiogram," *Biomedical Signal Processing and Control, Elsevier*, vol. 25, pp. 143 – 149, 2016. [Online]. Available: http://www.sciencedirect.com/science/article/pii/S1746809415001937

[123] A. R. McIntosh and B. Mišić, "Multivariate statistical analyses for neuroimaging data," *Annual Review of Psychology*, vol. 64, pp. 499–525, Jan 2013.

[124] Y. Tuncer, M. M. Tanik, and D. B. Allison, "An overview of statistical decomposition techniques applied to complex systems," *Computational statistics & data analysis*, vol. 52, no. 5, pp. 2292–2310, 2008.

[125] J. C. Gomez and M.-F. Moens, "PCA document reconstruction for email classification," *Computational Statistics & Data Analysis*, vol. 56, no. 3, pp. 741 – 751, 2012. [Online]. Available: http://www.sciencedirect.com/science/article/pii/S0167947311003549

[126] F. Liang, "Use of SVD-based probit transformation in clustering gene expression profiles," *Computational Statistics and Data Analysis*, vol. 51, pp. 6355–6366, 2007.

[127] D. Yang, Z. Ma, and A. Buja, "A sparse singular value decomposition method for high-dimensional data," *J. of Computational and Graphical Statistics*, vol. 23, no. 4, pp. 923–942, 2014. [Online]. Available: http://dx.doi.org/10.1080/10618600.2013.858632

[128] L. De Lathauwer, B. De Moor, and J. Vandewalle, "A multilinear singular value decomposition," *SIAM Journal on Matrix Analysis and Applications*, vol. 21, no. 4, pp. 1253–1278, 2000. [Online]. Available: http://dx.doi.org/10.1137/S0895479896305696

[129] A. M. R. Dixon, E. G. Allstot, D. Gangopadhyay, and D. J. Allstot, "Compressed sensing system considerations for ECG and EMG wireless biosensors," *IEEE Trans. on Biomed. Circuits and Systems*, vol. 6, no. 2, pp. 156–166, April 2012.

[130] H. Mamaghanian, N. Khaled, D. Atienza, and P. Vandergheynst, "Compressed sensing for real-time energy-efficient ECG compression on wireless body sensor nodes," *IEEE Trans. on Biomed. Eng.*, vol. 58, no. 9, pp. 2456–2466, Sep 2011.

[131] Z. Zhang, T.-P. Jung, S. Makeig, and B. D. Rao, "Compressed sensing for energy-efficient wireless telemonitoring of noninvasive fetal ECG via block sparse bayesian learning," *IEEE Trans. on Biomed. Eng.*, vol. 60, no. 2, pp. 300–309, Feb 2013.

[132] G. D. Clifford, *Advanced Methods and Tools for ECG Data Analysis*, ser. Engineering in Medicine & Biology, G. D. Clifford, F. Azuaje, and P. E. McSharry, Eds. Artech House, 2006.

[133] [Online]. Available: http://wavelets.pybytes.com/wavelet/bior4.4/

[134] Y. Zigel, "ECG signal compression," Master's thesis, Ben-Gurion University, Beer-Sheva, Israel, Aug 1998.

[135] Y. Zigel, A. Cohen, and A. Katz, "The weighted diagnostic distortion (WDD) measure for ECG signal compression," *IEEE Trans. on Biomed. Eng.*, vol. 47, no. 11, pp. 1422–1430, Nov 2000.

[136] A. L. Goldberger, L. A. N. Amaral, L. Glass, J. M. Hausdorff, P. C. Ivanov, R. G. Mark, J. E. Mietus, G. B. Moody, C. K. Peng, and H. E. Stanley, "Physiobank, physiotoolkit, and physionet: Components of a new research resource for complex physiologic signals. circulation 101(23):e215-e220," [Circulation Electronic Pages; http://circ.ahajournals.org/cgi/content/full/101/23/e215], June 13, 2000.

[137] K. Luo, J. Li, and J. Wu, "A dynamic compression scheme for energy-efficient real-time wireless electrocardiogram biosensors," *IEEE Trans. on Inst. and Meas.*, vol. 63, no. 9, pp. 2160–2169, Sept 2014.

[138] M. R. Yuce, "Implementation of wireless body area networks for healthcare systems," *J. of Sensors and Actuators, Elsevier*, vol. 162, no. 1, pp. 116–129, July 2010.

[139] H. C. Keong, K. M. S. Thotahewa, and M. R. Yuce, "Transmit-only ultra wide band body sensor and collision analysis," *IEEE Sensors J.*, vol. 13, no. 5, pp. 1949–1958, May 2013.

[140] M. Ghavami, L. Michael, and R. Kohno, *Ultra Wideband Signals and Systems in Communication Engineering*, 2nd ed. Wiley, Feb 2007.

[141] M.-G. D. Benedetto and G. Giancola, *Understanding Ultra Wide Band Radio Fundamentals*. Pearson Education, 2008.

[142] T. K. Moon and W. C. Stirling, *Mathematical Methods and Algorithms for Signal Processig*. Prentice Hall, 2000.

[143] Q. Li, X. Shi, and D. Schonfeld, "Robust HOSVD-based higher-order data indexing and retrieval," *IEEE Signal Processing Letters*, vol. 20, no. 10, pp. 984–987, Oct 2013.

[144] L. Kuang, F. Hao, L. Yang, M. Lin, C. Luo, and G. Min, "A tensor-based approach for big data representation and dimensionality reduction," *IEEE Trans. on Emerging Topics in Computing*, vol. 2, no. 3, pp. 280–291, Sept 2014.

[145] B. Savas and L. Eldén, "Handwritten digit classification using higher order singular value decomposition," *Pattern Recognition, Elsevier*, vol. 40, no. 3, pp. 993–1003, 2007.

[146] R. Costantini, L. Sbaiz, and S. Susstrunk, "Higher order SVD analysis for dynamic texture synthesis," *IEEE Trans. on Image Proc.*, vol. 17, no. 1, pp. 42–52, Jan 2008.

[147] T. G. Kolda and B. W. Bader, "Tensor decompositions and applications," *SIAM REVIEW*, vol. 51, no. 3, pp. 455–500, 2009.

[148] S. Weiland and F. van Belzen, "Singular value decompositions and low rank approximations of tensors," *IEEE Trans. on Sig. Proc.*, vol. 58, no. 3, pp. 1171–1182, March 2010.

[149] J. Liang, Y. He, D. Liu, and X. Zeng, "Image fusion using higher order singular value decomposition," *IEEE Trans. on Image Proc.*, vol. 21, no. 5, pp. 2898–2909, May 2012.

[150] X. Geng, L. Ji, Y. Zhao, and F. Wang, "A small target detection method for the hyperspectral image based on higher order singular value decomposition (HOSVD)," *IEEE Geoscience and Remote Sensing Letters*, vol. 10, no. 6, pp. 1305–1308, Nov 2013.

[151] K. Srinivasan, J. Dauwels, and M. R. Reddy, "Multichannel EEG compression: Wavelet-based image and volumetric coding approach," *IEEE J. of Biomed. and Health Info.*, vol. 17, no. 1, pp. 113–120, Jan 2013.

[152] J. Dauwels, K. Srinivasan, M. R. Reddy, and A. Cichocki, "Near-lossless multichannel EEG compression based on matrix and tensor decompositions," *IEEE J. of Biomed. and Health Info.*, vol. 17, no. 3, pp. 708–714, May 2013.

[153] G. Bergqvist and E. G. Larsson, "The higher-order singular value decomposition: Theory and an application," *IEEE Sig. Process. Mag.*, vol. 27, no. 3, pp. 151–154, May 2010.

[154] J. Salmi, A. Richter, and V. Koivunen, "Sequential unfolding SVD for tensors with applications in array signal processing," *IEEE Trans. on Signal Proc.*, vol. 57, no. 12, pp. 4719–4733, Dec 2009.

[155] K. Huang and L. Zhang, "Cardiology knowledge free ECG feature extraction using generalized tensor rank one discriminant analysis," *EURASIP Journal on Advances in Signal Processing*, vol. 2014, no. 1, 2014. [Online]. Available: http://dx.doi.org/10.1186/1687-6180-2014-2

[156] L. N. Ribeiro, A. H.-M. noz, G. Favier, J. ao César Moura Mota, and A. L. F. D. Almeida, "A tensor decomposition approach to noninvasive atrial activity extraction in atrial fibrillation ecg," in *23rd European Signal Processing Conference (EUSIPCO-2015)*, Aug 2015, pp. 2576–2580.

[157] H. Akbari, M. B. Shamsollahi, and R. Phlypo, "Fetal ecg extraction using π tucker decomposition," in *2015 International Conference on Systems, Signals and Image Processing (IWSSIP)*, Sept 2015, pp. 174–178.

[158] A. A. S. León, G. Goovaerts, C. R. V. Seisdedos, and S. V. Huffel, "Irregular heartbeats detection using tensors and support vector machines," in *2016 Computing in Cardiology Conference (CinC)*, Sept 2016, pp. 1037–1040.

[159] M. A. Hall, “Correlation-based feature selection for machine learning,” Ph.D. dissertation, Department of Computer Science, The University of Waikato, 1999.

[160] C.-J. Huang, D.-X. Yang, and Y.-T. Chuang, “Application of wrapper approach and composite classifier to the stock trend prediction,” *Expert Systems with Applications*, vol. 34, no. 4, pp. 2870 – 2878, 2008. [Online]. Available: http://www.sciencedirect.com/science/article/pii/S0957417407001819

[161] M. S. Manikandan and S. Dandapat, “Wavelet threshold based ECG compression using USZZQ and Huffman coding of DSM,” *Biomedical Signal Processing and Control, Elsevier*, vol. 1, pp. 261–270, 2006.

[162] F. Lauer and Y. Guermeur, “MSVMpack: a multi-class support vector machine package,” *J. of Machine Learning Research*, vol. 12, pp. 2269–2272, 2011, http://www.loria.fr/~lauer/MSVMpack.

[163] E. Pasolli and F. Melgani, “Active learning methods for electrocardiographic signal classification,” *IEEE Trans. on Info. Tech. in Biomedicine*, vol. 14, no. 6, pp. 1405–1416, Nov 2010.

[164] B. Headen, H. Ohlin, R. Rittner, and L. Edenbrandt, “Acute myocardial infarction detected in the 12-lead ECG by artificial neural networks,” *Circulation*, vol. 96, no. 6, pp. 1798–1802, Sep 1997.

[165] R. L. Verrier, T. Klingenheben, M. Malik, N. El-Sherif, D. V. Exner, S. H. Hohnloser, T. Ikeda, J. P. Martinez, S. M. Narayan, T. Nieminen, and D. S. Rosenbaum, “Microvolt T-wave alternans: Physiological basis, methods of measurement, and clinical utility–consensus guideline by international society for holter and noninvasive electrocardiology,” *J. of the American College of Cardiology*, vol. 58, no. 13, pp. 1309–1324, 2011.

[166] L. Burattini, S. Bini, and R. Burattini, “Automatic microvolt T-wave alternans identification in relation to ECG interferences surviving preprocessing,” *Medical Engineering & Physics*, vol. 33, no. 1, pp. 17 – 30, 2011.

[167] L. Burattini, S. Man, R. Burattini, and C. A. Swenne, “Comparison of standard versus orthogonal ecg leads for t-wave alternans identification,” *Annals of Noninvasive Electrocardiology*, vol. 17, no. 2, pp. 130–140, 2012. [Online]. Available: http://dx.doi.org/10.1111/j.1542-474X.2012.00490.x

[168] L. Burattini, W. Zareba, and R. Burattini, “Automatic detection of microvolt T-wave alternans in holter recordings: Effect of baseline wandering,” *Biomedical Signal Processing and Control*, vol. 1, no. 2, pp. 162 – 168, 2006, voice Models and Analysis for Biomedical Applications.

[169] B. D. Hearing, P. H. Stone, and R. L. Verrier, “Frequency response characteristics required for detection of T-wave alternans during ambulatory ecg monitoring,” *Annals of Noninvasive Electrocardiology*, vol. 1, no. 2, pp. 103–112, 1996. [Online]. Available: http://dx.doi.org/10.1111/j.1542-474X.1996.tb00269.x

[170] A. A. Armoundas, G. F. Tomaselli, and H. D. Esperer, “Pathophysiological basis and clinical application of t-wave alternans,” *J. of the American College of Cardiology*, vol. 40, no. 2, pp. 207 – 217, 2002.

[171] A. L. Goldberger and *et al.*, “Physiobank, physiotoolkit, and physionet: Components of a new research resource for complex physiologic signals. circulation 101(23):e215-e220,” June 13, 2000.

[172] G. Moody, W. E. Muldrow, and R. G. Mark, “A noise stress test for arrhythmia detectors,” in *Computers in Cardiology*, no. 11, 1984, pp. 381–384.

[173] [Online]. Available: https://physionet.org/physiotools/wag/nst-1.htm

[174] A. Khaustov, S. Nemati, and G. D. Clifford, “An open-source standard T-wave alternans detector for benchmarking,” in *Computers in Cardiology*, Sept 2008, pp. 509–512.

[175] J. M. Tapanainen, A.-M. Still, K. J. Airaksinen, and H. V. Huikuri, “Prognostic significance of risk stratifiers of mortality, including T wave alternans, after acute myocardial infarction: Results of a prospective follow-up study,” *J. of Cardiovascular Electrophysiology*, vol. 12, no. 6, pp. 645–652, 2001. [Online]. Available: http://dx.doi.org/10.1046/j.1540-8167.2001.00645.x

[176] R. L. Verrier, B. D. Nearing, M. T. L. Rovere, G. D. Pinna, M. A. Mittleman, J. T. Bigger, P. J. Schwartz, and A. Investigators, “Ambulatory electrocardiogram-based tracking of T wave alternans in postmyocardial infarction patients to assess risk of cardiac arrest or arrhythmic death,” *J. of Cardiovascular Electrophysiology*, vol. 14, no. 7, pp. 705–711, 2003. [Online]. Available: http://dx.doi.org/10.1046/j.1540-8167.2003.03118.x

LIST OF PUBLICATIONS

Journals

1. **S. Padhy**, L. N. Sharma and S. Dandapat, “Multilead ECG Data Compression using SVD in Multiresolution Domain", Biomedical Signal Processing and Control (Elsevier), vol. 23, pp. 10-18, 2016. doi: http://dx.doi.org/10.1016/j.bspc.2015.06.012

2. **S. Padhy** and S. Dandapat, “Exploiting Multilead ECG Correlations using Robust 3-array Tensor Decomposition", IET-Healthcare Technology Letters, vol.2, Issue 5, pp. 112-117, 2015. doi: http://dx.doi.org/10.1049/htl.2015.0020

3. **S. Padhy** and S. Dandapat, “Third-order Tensor based Analysis of Multilead ECG for Classification of Myocardial Infarction", Biomedical Signal Processing and Control (Elsevier), vol. 31, pp. 71-78, 2017. doi: http://dx.doi.org/10.1016/j.bspc.2016.07.007.

Manuscripts under review

1. **[Submitted]** S. Padhy and S. Dandapat, “Enhancing Multilead T-Wave Alternans Analysis using Multiscale Analysis-by-Synthesis and HOSVD", Journal of Medical Systems, Springer

Conferences

1. **S. Padhy**, L. N. Sharma, and S. Dandapat, “Multilead ECG Data Transmission in Wireless Body Area Network (WBAN)," 5th International Conference on Computer Applications in Electrical Engineering Recent Advances, Oct 2013.

2. **S. Padhy** and S. Dandapat, “A New Multilead ECG Data Compression Method Using Higher-Order Singular Value Decomposition," Twentieth National Conference on Communications (NCC), 2014.

3. **S. Padhy** and S. Dandapat, “Synthesis of 12-Lead ECG from a Reduced Lead Set using Singuar Value Decomposition", PCITC, Oct 2015.

Book chapter

1. **S. Padhy** and S. Dandapat, “SVD Analysis on Reduced 3-Lead ECG Data", Lecture Notes in Electrical Engineering-Springer